

1 Cenozoic deformation in the Tauern Window (Eastern Alps) constrained
2 by in-situ Th-Pb dating of fissure monazite

3 Emmanuelle Ricchi¹, Christian A. Bergemann², Edwin Gnos³, Alfons Berger⁴, Daniela Rubatto^{4,5},
4 Martin J. Whitehouse⁶, Franz Walter⁷

5 ¹*Department of Earth Sciences, University of Geneva, Rue des Maraîchers 13, 1205 Geneva, Switzerland*

6 ²*Institute of Geosciences, Heidelberg University, Im Neuenheimer Feld 236, 69120 Heidelberg, Germany*

7 ³*Natural History Museum of Geneva, Route de Malagnou 1, 1208 Geneva, Switzerland*

8 ⁴*Institute of Geological Sciences, University of Bern, Baltzerstrasse 1+3, 3012 Bern, Switzerland*

9 ⁵*Institute of Earth Sciences, University of Lausanne, Geopolis, Lausanne, 1015 Switzerland*

10 ⁶*Swedish Museum of Natural History, Box 50007, SE104-05 Stockholm, Sweden*

11 ⁷*Institut für Erdwissenschaften, Karl-Franzens-Universität, Universitätsplatz 2, 8010 Graz, Austria*

12

13 Highlights:

- 14 • In-situ dating of hydrothermal monazite-(Ce)
- 15 • New constraints on the exhumation of the Tauern metamorphic dome
- 16 • Distinct tectonic pulses recorded from East to West

17

18 Keywords: Hydrothermal monazite; Alpine fissures; Th-Pb dating; Tauern Window; Protracted
19 deformation

20

21 **Abstract.** Thorium-Pb crystallization ages of hydrothermal monazites from the western, central
22 and eastern Tauern Window provide new insights into Cenozoic tectonic evolution of the Tauern
23 metamorphic dome. Growth domain crystallization ages range from 21.7 ± 0.4 Ma to 10.0 ± 0.2
24 Ma. Three major periods of monazite growth are recorded between $\sim 22 - 20$ (peak at 21 Ma), 19
25 $- 15$ (major peak at 17 Ma) and $14 - 10$ Ma (major peak around 12 Ma), respectively interpreted
26 to be related to prevailing N-S shortening, in association with E-W extension, beginning strike-
27 slip movements, and reactivation of strike-slip faulting. Fissure monazite ages largely overlap
28 with zircon and apatite fission tracks data. Besides tracking the thermal evolution of the Tauern
29 dome, monazite dates reflect episodic tectonic movement along major shear zones that took place
30 during the formation of the dome. Geochronological and structural data from the Pfitschtal area
31 in the western Tauern Window show the existence of two cleft generations separated in time by 4
32 Ma and related to strike-slip to oblique-slip faulting. Moreover, these two phases overprint earlier
33 phases of fissure formation.

34

35 **1 Introduction**

36 In-situ Th-Pb dating of hydrothermal fissure monazite-(Ce) (in the following simply monazite)
37 has recently been demonstrated to be a reliable method for dating tectonic activity under
38 retrograde metamorphic conditions (Bergemann et al., 2017, 2018, 2019, 2020; Berger et al.,
39 2013; Fitz-Diaz et al., 2019; Gasquet et al., 2010; Gnos et al., 2015; Grand'Homme et al., 2016a;
40 Janots et al., 2012; Ricchi et al., 2019). These studies conducted through the entire Alpine
41 orogenic belt allowed constraining tectonic activity in relation with exhumation and fault activity
42 under retrograde lower greenschist to sub-greenschist facies metamorphic conditions.
43 Hydrothermal fissure monazite, concentrating LREE, Th and U, generally crystallizes in Ca-poor

44 lithologies, outside the stability field of titanite or epidote/allanite. However, once formed,
45 hydrothermal processes may cause dissolution-reprecipitation events leading to resetting of the
46 monazite Th-Pb decay system in parts of the crystal. Chemically and isotopically homogeneous
47 crystals indicate a single, rapid growth episode (e.g., Grand'Homme et al., 2016a). However,
48 crystals showing different growth domains indicative of successive growth episodes are more
49 common. In other cases, parts of, or entire grains display a patchy zoning due to dissolution-
50 reprecipitation processes (e.g., Ayers et al., 1999; Grand'Homme et al., 2016b). These processes
51 involve element fractionation resulting in crystal zones with often distinct Th/U values (Seydoux-
52 Guillaume et al., 2012).

53 The advantage of using hydrothermal monazite for dating tectonic activity is related to the high
54 closure temperature of monazite of $>800^{\circ}\text{C}$, implying that diffusion in monazite is negligible
55 (Cherniak et al., 2004; Gardés et al., 2006, 2007) under P-T conditions at or below $450 - 500^{\circ}\text{C}$
56 and $0.3 - 0.4\text{ GPa}$ (e.g., Mullis et al., 1994; Mullis, 1996; Sharp et al., 2005) where hydrothermal
57 fissures form. Fissure monazites date crystallization following chemical disequilibrium within a
58 fissure. This causes a dissolution-precipitation cycle that may include dissolution or partial
59 dissolution of existing fissure monazite. This has the consequence that late
60 dissolution/precipitation steps may be well recorded, whereas earlier growth domains may be
61 completely destroyed. Thus, monazite crystallization due to chemical disequilibrium is
62 interpreted as being related to tectonic activity (e.g. volume change, fissure propagation,
63 exposure of fresh host-rock, delamination of fissure wall, seismic activity, fluid loss or gain).
64 Recent studies have shown that fissure monazite typically forms between generally lower to
65 higher $200 - 400^{\circ}\text{C}$ (Gnos et al., 2015; Janots et al., 2019). For this reason, fissure monazite ages
66 are generally interpreted as dating crystallization or re-crystallization. Monazite geochronology
67 can thus be utilized to constrain shear and damage zone activity under greenschist and very-low

68 grade metamorphic conditions at least down to 200°C (e.g. Bergemann et al., 2017, 2018; Gnos
69 et al., 2015).

70 Fissures and clefts develop close to the brittle-ductile transition (< 450°C, Mullis, 1996) and are
71 usually oriented perpendicular to the foliation and lineation of the host-rock (Gnos et al., 2015).

72 Fissures are generally straight when they form and either became enlarged by subsequent tectonic
73 activity to form fluid-filled dm- to m- sized clefts, displaying a more open shape with rounded
74 surfaces (e.g. Ricchi et al., 2019) when the stress field retains the same orientation, or became
75 completely filled to form mineral veins. However, they may show complex shape when the stress
76 field direction changes during deformation. Fluid inclusion studies (e.g. , Mullis, 1996) show that
77 clefts generally suffered several deformation episodes.

78 Interaction of the fluid that fills the fissures with the surrounding rock leads to dissolution of
79 minerals in the wall rock and mineral precipitation in the fissure. As long as deformation
80 continues, fluid-filled clefts will react to deformation via dissolution-precipitation cycles due to
81 disequilibrium between fluid, rock wall and mineral assemblage within the cleft (e.g. Putnis,
82 2009). Thus, hydrothermal minerals like monazite do not only grow following the initial fissure
83 formation but form, continue to grow, or dissolve during subsequent deformation stages. The
84 timing of these growth or alteration stages may not always be resolvable with the precision of
85 currently available geochronological methods, but different growth stages may be distinguishable
86 through differences in the chemical composition (Grand'Homme et al., 2018). In contrast to the
87 surrounding country rock, the fissures and clefts remain highly reactive at low temperature due to
88 the presence of fluids. For this reasons, deformation steps during brittle deformation may be
89 registered through mineral growth or recrystallization in clefts (e.g., Berger et al., 2013) down to
90 conditions where clay minerals form in fault gauges.

91 The Tauern window (TW) is a thermal and structural dome of the eastern Alps (Fig. 1) exhumed
92 over a period of about 30 Ma starting from the Early Oligocene (e.g. Rosenberg et al., 2018;
93 Schmid et al., 2013). Previous monazite crystallization ages obtained in the eastern sub-dome of
94 the TW record tectonic activity between 19.0 ± 0.5 and 15.0 ± 0.5 Ma (Gnos et al., 2015). In the
95 current study, monazite geochronology is extended to the entire TW, in order to investigate its
96 Cenozoic deformation history. We particularly aim to establish a chronological record for the
97 younger exhumation history recorded by fissure monazite crystallization, to be compared with
98 known deformation phases.

99 A total of 23 monazite grains together with provenance data, and in some cases host-rock
100 information were dated (Table 1). Seven grains come from the western limb of the TW (INNB1
101 ZE11, SCHR1, MAYR4, PFIT1, BURG2 and PLAN1; samples 1 to 7; Fig. 1), another seven
102 grains come from the eastern border of the western sub-dome (central TW; SCHE11, HOPF2,
103 GART1, NOWA3, GART3, STEI2 and KNOR1; samples 8 to 14; Fig. 1) and nine grains were
104 collected in the eastern sub-dome (KAIS6, SALZ18, LOHN4, ORT1, EUKL2, HOAR1,
105 MOKR1, SAND1 and REIS1; samples 15 to 25; Fig. 1, Table 1). In order to capture at best the
106 tectonic activity during the exhumation of the TW, the investigated samples were selected in a
107 way that gives priority to sample localities in regions affected by major fault zones and at
108 lithological boundaries. In the following we will discuss the ages in term of sample ID numbers
109 (1-25) provided by Table 1.

110

111 **2 Geologic settings**

112 In the largest tectonic window of the Austroalpine nappe stack, the TW, Penninic (Glockner
113 Nappe System and Matri Zone; Fig. 1) and Subpenninic nappes (mainly the Venediger Duplex)

114 are exposed (e.g. Schmid et al., 2013; Fig. 1). The TW metamorphic and structural dome consists
115 of two sub-domes, with E-W striking upright folds in the internal parts and bordered by two
116 major normal faults, the Katschberg Normal Fault (KNF) in the East and the Brenner Normal
117 Fault (BNF) in the West (Fig. 1). The western sub-dome is dissected by numerous sinistral shear
118 zones (Ahorn Shear Zone (ASZ), Olperer Shear Zone (OSZ), Tuxer Shear Zones (TSZ), Greiner
119 Shear Zone (GSZ) and Ahrntal Shear Zone (AhSZ)) and is bordered by the Salzach-Ennstal-
120 Mariazell-Puchberg fault (SEMP) in the north (Fig.1). The eastern sub-dome is bordered to the
121 east by the Katschberg Normal Fault (KNF), continuing to the north into the dextral Katschberg
122 Shear Zone System (KSZS), and to the south into an unnamed sinistral shear zone and oriented
123 parallel to the Mölltal Fault (MöF). The deformation history of these fault complexes will be
124 discussed later.

125 The Alpine evolution of the TW started in the Early Paleocene with the accretion and subduction
126 of the Piemont-Liguria Ocean (Matrei Zone; Fig. 1) under the Apulian margin (Austroalpine
127 nappe stack; e.g. Schmid et al., 2004, 2013; D1 deformation of Schmid et al., 2013; Fig.1, Table
128 2). In the Middle Eocene, the Valais Ocean and parts of the distal European margin (Glockner
129 Nappe System, Eclogite Zone and parts of the Modereck Nappe System; Fig. 1) were equally
130 subducted below the Austroalpine nappe stack and the Matrei Zone accreted during D1
131 deformation (D2 deformation of Schmid et al. 2013; Table 2). In the Late Eocene, exhumation
132 was achieved by extrusion of the high-pressure units that went together with major folding of the
133 D2 thrust formed between the subducted Glockner Nappe System and Modereck Nappe System
134 (D3 deformation of Schmid et al. 2013; Table 2). In the Early Oligocene, nearly
135 contemporaneous break off of the subducting European slab and formation of the Venediger
136 Duplex (crustal-scale duplex structure) occurred, followed by the “Tauernkristallisation”
137 (reheating of the whole nappe stack to amphibolite-facies conditions) (D4 deformation of Schmid

138 et al. 2013; Table 2). This was followed by an inversion of subduction polarity at ~23 to 21 Ma
139 (e.g., Rosenberg et al., 2018; Scharf et al., 2013; Schmid et al., 2013; Table 2). The following
140 exhumation of the TW started in the Early to Middle Miocene by Alpine N-S collisional
141 shortening and E-W orogen-parallel extension leading to folding, erosion and lateral extrusion
142 through shear zone development (e.g. Luth and Willingshofer, 2008; Rosenberg and Berger,
143 2009; Rosenberg and Garcia, 2011; Schmid et al., 2004, 2013; Selverstone, 1988; D5
144 deformation of Schmid et al., 2013). Previous shear zone age dating in the TW was achieved
145 using different geochronometers: Rb–Sr whole-rock–phengite dating (20 Ma; Blanckenburg et
146 al., 1989), Rb – Sr whole-rock–white mica dating (39 – 16 Ma; Glodny et al., 2008), Sm – Nd
147 dating on garnet (27.5 – 20 Ma; Pollington and Baxter, 2010, 2011) and $^{40}\text{Ar}/^{39}\text{Ar}$ dating on mica
148 (35 – 28 Ma; Urbanek et al., 2002). A recent detailed study by Schneider et al. (2013) using
149 texturally-controlled in-situ $^{40}\text{Ar}/^{39}\text{Ar}$ dating of syn-kinematic phengite and K-feldspar returned
150 ages between 33 – 15, 24 – 12 and 20 – 7 Ma. They were interpreted as recording deformation
151 along three major shear zones (ASZ, TSZ and GSZ respectively) of the western sub-dome.

152

153 **Sample location**

154 Fissure monazite is rare and difficult to find, meaning that this study could not have been
155 conducted without the help of crystal searchers who provided samples. Fissure monazites were
156 selected to cover all parts of the TW areas with known shear zones within it. It was, however,
157 unfortunately not possible to obtain exact coordinates for all of the samples (Table 1). This is due
158 to the rarity of fissure monazite, so that some samples were obtained from old finds or
159 collections. In other cases, the crystal searcher could not anymore precisely identify the fissure in
160 which the monazite was found. These samples are marked with “approx.” in Table 1. We could

161 therefore only revisit some of the sample locations in order to add structural information.
162 Experience from other parts of the Alps (e.g. Bergemann et al., 2017, 2019; Ricchi et al., 2019)
163 shows that fissure monazite sampled within the damage or central zones of a shear zone generally
164 records shear zone activity well. Information on the source localities, host-rocks, degree of alpine
165 metamorphism and mineral associations is in Table 1.

166

167 **3 Methods**

168 The crystals were polished individually on a lapidary disk and embedded in epoxy together with
169 the monazite standard “44069” (425 Ma, Aleinikoff et al., 2006), following the same procedure
170 as Bergemann et al. (2017). Backscatter electron (BSE) images were acquired in order to
171 investigate the internal textural features of each grain (e.g. zoning, evidences of alteration, etc.)
172 using an EDS-equipped JEOL JSM7001F and a Zeiss DSM940A electron microscope at the
173 University of Geneva with a beam current of 3.5 nA and acceleration voltage of 15kV. BSE
174 images helped in the selection of Secondary-Ion Mass Spectrometry (SIMS) spot analysis points,
175 carefully placed in chemically distinct domains.

176 Ion probe U-Th-Pb analyses of 15 monazite crystals were conducted at the SwissSIMS Ion
177 microprobe facility, University of Lausanne, Switzerland and analyses of another 8 crystals were
178 performed at the Nordsim facility, Swedish Museum of Natural History, Stockholm (Tables 1 and
179 3). Both laboratories are equipped with a Cameca IMS 1280-HR instrument. The instruments
180 were run following the procedure of Janots et al. (2012), applying a -13 kV O²⁻ primary beam, an
181 intensity of ~3 and 6 nA focused on the sample (SwissSIMS and Nordsim respectively) to
182 produce a spot of 15 – 20 micron in diameter. A mass resolution of 4300 – 5000 (M/ΔM,
183 ²⁰⁸Pb/²³²Th at 10% peak height) and an energy window 40 eV were applied, with data collection

184 in peak hopping mode using an ion-counting electron multiplier. All the unknowns were
185 standardised to 44069 (425 Ma; Aleinikoff et al., 2006) monazite and the uncertainty on the
186 standard $^{208}\text{Pb}/^{232}\text{Th}$ – ThO/Th calibration in each session was 1.7% on average.

187 A ^{207}Pb and ^{204}Pb common lead (Pbc) correction calculated at time zero was applied to the data
188 acquired at the SwissSIMS and Nordsim (Table 3), using the terrestrial Pb evolution model of
189 Stacey and Kramers (1975). The Cameca Customisable Ion Probe Software (CIPS) was used for
190 data reduction. ^{204}Pb - and ^{207}Pb -corrected ages agree within uncertainty (Table 3), but we
191 preferred to discuss ^{207}Pb -corrected ages because they are more robust and consistent (better
192 statistics and less scatter in the data). Calculation of weighted mean ages, based on ^{207}Pb -
193 correction, and plotting was carried out using the program IsoPlot Ex 4.1 (Ludwig, 2003). Single
194 and weighted mean ages (or average ages) are quoted at the 1 sigma and at 95% confidence level
195 in the text, respectively.

196 Weighted mean $^{208}\text{Pb}/^{232}\text{Th}$ ages were calculated for each growth domain following the approach
197 of Bergemann et al. (2017, 2018, 2019, 2020) and Ricchi et al. (2019). Distinct chemical and
198 textural domains were carefully defined in each grain based on Th concentrations as function of
199 U concentrations and BSE image information. Since fissure monazite is dissolved and re-
200 precipitated under changing chemical conditions (e.g. Grand'Homme et al., 2018), spot analyses
201 affected by Pbc (resulting in older dates directly related to higher Pbc, i.e. positive Age-f 208
202 correlation), inclusions or with high uncertainty ($1\sigma > 1$ abs.) were removed from the dataset and
203 marked in italic in Table 3. However, spot dates located on dissolution trails, generally providing
204 younger dates, were considered in the age ranges because they likely record a later phase of
205 monazite crystallization.

206

207 4 Results

208 4.1 Field observations

209 An example of deformed fissures and different stages of fissure formation is well exposed in
210 outcrops along the road leading to Pfitscherjoch (in vicinity to the PFIT1 sample locality 5,
211 Western TW; Table 1), where two fissure generations are present (Fig. 2a and b). In this outcrop
212 an earlier fissure generation (C_2 , green ellipses) is partly deformed during subsequent
213 deformation, and a younger generation of fissures (C_3 , blue ellipses) is also present. Sub-
214 horizontal fissures (C_3) seem linked to a strongly inclined lineation (L_3 , blue arrows), whereas
215 older sub-vertical fissures (C_2) seem related to a weakly-inclined strike-slip lineation (L_2 , green
216 arrows). The older fissures are wider and sigmoidal in shape and contain muscovite which is not
217 found in the younger fissures. In some cases younger fissures crosscut older ones (Fig. 2b).
218 Moreover, the orientation of the foliation ($S_{2,3}$, Fig. 2c) of these two fissure generations (C_2 and
219 C_3) is different from the foliation (S_1 , Fig. 2c) of early fissure formation mainly observed in the
220 eastern part of the TW (C_1 , Fig. 2c, discussed below). This suggests that in the Pfitscherjoch area,
221 early fissures C_1 were overprinted by younger tectonic movements.

222 The large majority of the fissures present in all the investigated localities are oriented sub-
223 vertically (C_1 and C_2 type in Fig. 2c), roughly striking NE-SW. For C_2 , this would indicate a
224 similar direction of extension for the development of this fissure type, which is in line with
225 paleostress orientations provided by Bertrand et al. (2015). However, even if all sub-vertical
226 fissures are sub-parallel, at least two generations exist. (i) Early sub-vertical fissures (C_1 , Fig. 2c)
227 are related to flat foliation (S_1) and E-W stretching lineation (L_1), these are oriented perpendicular
228 to the main fold axes (and lineation) of the TW and are associated with E-W extension (e.g. Gnos
229 et al., 2015; Rosenberg et al., 2018; Schneider et al., 2013). (ii) Younger sub-vertical fissures (C_2 ,

230 Fig. 2c) are associated with sub-vertical E-W oriented foliation (S_2) and flat to inclined lineation
231 (L_2), and are oriented perpendicular to strike-slip faults (mainly in the western part of the TW;
232 Fig. 2c). At Pfitscherjoch, the shape of C_2 fissures, indicating overprinting by sinistral sense of
233 shear, is in agreement with the larger scale sinistral shearing of the GSZ shear zone. (iii) A third
234 generation of fissures (C_3 , Fig. 2c) is locally observed, for example, in the Pfitscherjoch locality
235 (Fig. 2a and b) and is at high angle with C_1 and C_2 fissures. This third fissure generation observed
236 in the Pfitscherjoch locality is associated with a subvertical E-W striking foliation (S_3). Stretching
237 lineation related to the BNF activity is sub-parallel to C_3 lineation, however its foliation is
238 striking N-S (Fig. 2c). We suggest that C_3 fissures are related to oblique-slip movements in line
239 with the observed E-W striking foliation and not to the BNF activity.

240

241 **4.2 Monazite dating and composition**

242 The monazite grains selected for in-situ Th-Pb dating are mm-sized and, when BSE zoning is
243 visible, it shows two distinct textures: regular and patchy (Figs. 3, 4 and 5; Table 4). The term
244 regular refers to crystals showing growth-zonation, whereas a patchy texture is interpreted as
245 replacement by secondary dissolution/precipitation processes (e.g. Ayers et al., 1999;
246 Bergemann et al., 2018, 2019, 2020; Gnos et al., 2015). Thorium and U contents of the dated
247 fissure monazites display a large variability, ranging between ~200 to 63,000 ppm Th and ~2 to
248 2000 ppm U, with variations in Th/U ratio from 1 up to ~7000 (Figs. 3, 4 and 5; Table 3). ^{232}Th -
249 ^{208}Pb ages presented on the right-hand panel of figures 3, 4 and 5 are arranged according to the
250 order established in Table 3. A detailed description of each monazite grain is provided in the
251 Supplementary Information. Average ages are reported for group of dates on texturally and/or
252 chemically similar domains. In order to ensure that a group of dates from a domain is internally

253 consistent, rare outliers have been excluded to bring the MSWD within acceptable values
254 (MSWD < 3; Spencer et al., 2016). In a few cases the dates for specific monazite domains have a
255 scatter above analytical uncertainty (e.g. grain 6, 9, 24), which probably reflects the complex
256 formation process of fissure monazite.

257
258 The investigated grains from the western part of the western TW sub-dome come from the
259 Venediger Duplex, with the exception of sample 6, which comes from the Glockner Nappe
260 System (Fig. 1; Table 1). The samples 2, 4 and 6 were collected near to the major Brenner normal
261 fault, which delimits the TW to the west, and samples 1, 3, 5 and 7 were collected in the vicinity
262 of sinistral strike-slip faults (Fig. 1). Average growth domain ages range from 20.9 ± 0.6 to $10.0 \pm$
263 0.2 Ma (samples 3 and 2) with the youngest ages recorded in the western TW (Figs. 1, 3 and 6a;
264 Tables 3 and 4).

265 The central part of the TW displays growth domain ages between 18.3 ± 1.1 and 10.4 ± 0.2
266 (samples 8 and 14; Figs. 1 and 4; Tables 3 and 4), but the majority of the dated crystals in this
267 area record ages around 17 Ma (Fig. 6b). Samples 8, 9 and 10 were collected between the eastern
268 and western termination of the ASZ and the SEMP fault (Fig. 1). Another three samples (11, 12
269 and 13; Table 1) were collected in the northern prolongation of the AhSZ and a seventh monazite
270 (grain 14) was sampled near the southern border of the eastern part of the western sub-dome (Fig.
271 1).

272 The oldest ages are principally recorded in the eastern part of the TW at around 21 Ma (Fig. 6c).
273 Average ages of growth domains range from 21.7 ± 0.4 to 13.6 ± 0.6 Ma (samples 19a and 25;
274 Figs. 1, 4 and 6c; Tables 3 and 4). The samples were mainly collected at the western border of the
275 eastern sub-dome, in the Venediger Duplex or near the boundary with the Glockner/ Modereck

276 Nappe Systems (Fig. 1). Sample 25 was taken at some distance from the other samples, near the
277 south-eastern border of the eastern sub-dome (Fig. 1).

278

279 **5 Discussion**

280 **5.1 Fissure monazite ages**

281 The oldest monazite ages of 21.7 ± 0.4 to 19.9 ± 0.3 Ma (found in samples 19a and 20; Figs. 1, 6c
282 and 7a and d) are common in the eastern TW, but can also be found in the western area (Fig. 7a, c
283 and d, red symbols). This in line with regional fault activity recorded at ~ 21 Ma based on Pleuger
284 et al. (2012) (Fig. 8a) which corresponds to the main indentation phase (Favaro et al., 2017). We
285 interpret these as a first monazite crystallization event during E-W extension in association with
286 the dome formation (N-S shortening) when the existing clefts reached P-T conditions at which
287 fissure monazite starts to grow (phase 1, red symbols in Fig. 7). When comparing an assumed
288 fissure formation temperature of 450°C (typically obtained in quartz fluid inclusion studies on
289 early alpine fissures, (e.g., Mullis, 1996) with thermochronological data of the eastern TW
290 (compiled in Wölfler et al. 2012), the onset of fissure formation, predating primary monazite
291 crystallization, is estimated at around 25 Ma. Based on a comparison with thermochronological
292 data, monazite crystallization recorded between 19 – 15 Ma was estimated to have occurred at
293 $\sim 200 - 300^\circ\text{C}$ in the eastern TW (Gnos et al., 2015). New monazite ages from this study in the
294 eastern TW are up to ~ 22 Ma (sample 19 in Fig. 1), suggesting that early monazite crystallization
295 in the area may have occurred at higher temperatures of $350 - 400^\circ\text{C}$.

296 While early fissure formation is related to E-W extension (leading to flat foliation and E-W
297 mineral lineations; Fig. 2c), we suggest that monazite formation also occurred along the sinistral

298 strike-slip to oblique-slip movements (vertical foliation and flat to inclined lineation; Fig. 2),
299 particularly developed in the central and western part of the TW (e.g. Rosenberg et al., 2018;
300 Schneider et al., 2013). These shear zones developed as a result of bending of the E-W oriented
301 upright folds around a vertical axis (leading edge of the Dolomite indenter) (Fig. 1). This
302 occurred when N-S shortening could no longer be accommodated by folding and doming within
303 the TW. Associated with these movements is the formation of a younger generation of fissures
304 (see Pfitscherjoch example above), the peak activity of which is recorded at ~17 Ma (phase (2),
305 green symbols on figure 7). This fissure generation is associated with a steep foliation and a flat
306 lineation (Fig. 2), but sub-parallel in orientation to the earlier fissure formation. The monazite
307 ages at ~17 Ma found in the western and central TW (Figs. 1, 6 and 7; samples 5, 8, 13; Table 4)
308 are in association with sinistral fault zones, as in the Pfitscherjoch region or near the eastern
309 termination of the ASZ and AhSZ faults (see above). Unfortunately, we do not have structural
310 information on the westernmost and easternmost analysed samples (6 and 25; Figs 1, 6 and 7),
311 but they can be speculated to also have formed in association with a strike slip shear zone or the
312 BNF and KNF in the case of samples 6 and 25 respectively. At larger scale, these movements
313 seem to have been associated with the development of the sinistral Giudicarie Fault (GF, located
314 at the southwestern corner of the TW), offsetting the Periadriatic Fault (PF; Fig. 8b, e.g., Pleuger
315 et al., 2012). Ages of ~17 Ma are also recorded in the eastern part of the TW, likely linked to the
316 KNF and Mölltal Fault (MöF) activity (samples 16, 21, 24 and 25; Fig. 7a and d; e.g. Favaro et
317 al., 2017). In grains located in the western part of the eastern sub-dome, in the prolongation of the
318 MöF (e.g. Kurz and Neubauer, 1996) (Fig. 1), numerous monazite growth domains yield ages
319 between 15.6 ± 0.7 and 15.0 ± 0.5 Ma (bracketed by samples 22 and 21 from Gnos et al., 2015;
320 Figs 1, 6c, 7a and d; green circles on figure 7d; Table 4). These ages date the latest known
321 activity of this shear zone to ~15 Ma. Whereas younger ages, associated with reactivation of fault

322 zones are widespread in the central and western TW, tectonic movements seem to cease in the
323 eastern TW after this time (Fig. 8c).

324 The youngest monazite growth domain ages, principally recorded in the western sub-dome, range
325 from 13.2 ± 0.3 to 10.0 ± 0.2 Ma (samples 5 and 2; Table 4), indicate steps of reactivation of the
326 different sinistral strike-slip to oblique-slip movements along different faults (phase (3) and blue
327 symbols on figure 7). Based on our monazite crystallization data, the oldest activities of this
328 younger phase are recorded near the GSZ (sample 5) and in the prolongation of the AhSZ
329 (samples 7 and 9). The youngest activities are recorded in association with the ASZ, OSZ and
330 TSZ on figure 7a-c; samples 1, 2 and 4), and in the central TW in an area located south of the
331 main fault systems (sample 14, Figure 7a). In addition to faults activity at ~ 12 Ma (Fig. 8), coeval
332 strike-slip activity has also been documented in many areas of the central and western Alps (e.g.,
333 Bergemann et al., 2017, 2019; Berger et al., 2013; Gasquet et al., 2010; Grand'Homme et al.,
334 2016a; Pleuger et al., 2012; Ricchi et al., 2019).

335 In summary, in the western TW, monazite ages (Fig. 1) constrain the activities of the ASZ (18 –
336 12 Ma, samples 8 and 9), AhSZ (17 – 12 Ma, samples 13 and 7), TSZ/OSZ (11.5 – 10 Ma,
337 samples 1 and 2; older ages of sample 3 are probably related to extensional unroofing) and GSZ
338 (17 – 13 Ma). In the eastern part, the M6F is active between 19 and 15 Ma.

339

340 **5.2 Comparison with shear zone dating**

341 A number of attempts to date shear zone activity in the TW using Ar-Ar, Rb-Sr and Sm-Nd
342 techniques have been made in the past, which were, however, based on mineral separation
343 techniques without a clear structural control on the dated grains (e.g., Blanckenburg et al., 1989;

344 Glodny et al., 2008; Pollington and Baxter, 2010, 2011; Urbanek et al., 2002). An exception to
345 this is the $^{40}\text{Ar}/^{39}\text{Ar}$ study of Schneider et al. (2013) on syn-kinematic phengite and K-feldspar
346 which will be used in the following as a comparison (Table 2). Fissure monazite ages largely
347 corroborate this work, similarly showing the longevity of different shear zones in the TW. The
348 ages confirm that even though most of the dated monazite samples are only located in the damage
349 zone in the vicinity of the core of the shear zones, fluid-filled fissures provide a sensitive system
350 where tectonic activity triggers fluid-enhanced dissolution/precipitation reactions at lower
351 greenschist to sub-greenschist facies conditions.

352 While Schneider et al. (2013) obtained crystallization age ranges of 33 – 15 Ma for the ASZ, 24 –
353 12 Ma for the TSZ and 20 – 7 Ma for the GSZ (Table 2), our data confirms fluid activity, and thus
354 possible tectonic activity, at 18 – 12, 11.5 – 10 and 17 – 13 Ma respectively (Fig. 7). However,
355 the oldest dates from Schneider et al. (2013) might also be interpreted as older grains that have
356 been aligned in the new foliation (Fig. 8). The data presented here indicate that all of the shear
357 zones were potentially active at least until ~13 – 12 Ma, and the Tuxer and/or Olperer shear
358 zones even until ~7 Ma as suggested by younger dates observed in grain 2 (Figs. 3b, 6a and 7,
359 Tables 3 and 4). However, the fissure monazite data does not date the initiation of the GSZ
360 (Selverstone et al., 1991), nor the earliest activity of the TSZ (greenschist to amphibolite facies;
361 Selverstone et al., 1984, 1991) or the ASZ (greenschist facies; Cole et al., 2007), since their
362 formation already started at amphibolite facies conditions. As Alpine fissures only form under
363 greenschist facies conditions, the oldest monazite crystallization ages are younger than the data
364 obtained by Schneider et al. (2013). This indicates that shear zone activity started earlier than the
365 fissure monazite record. As the monazite age range of the younger fault activity is comparable to
366 the data of Schneider et al. (2013), but is not the same for individual shear zones, it seems likely
367 that all shear zones of the western TW were active as recently as 8 - 7 Ma.

369 **5.3 Comparison with fission track data**

370 There is a wealth of zircon fission track (ZFT) data that can assist in describing the exhumation
371 and low grade tectonic activity in the TW (Bertrand, 2014; Bertrand et al., 2017; Dunkl et al.,
372 2003; Fügenschuh et al., 1997; Mancktelow et al., 2001; Most, 2003; Pomella et al., 2011;
373 Steenken et al., 2002; Stöckhert et al., 1999; Viola et al., 2001; Wölfler et al., 2008) and apatite
374 fission track (AFT) data (Bertrand, 2014; Bertrand et al., 2017; Coyle, 1994; Di Fiore, 2013;
375 Foeken et al., 2007; Fügenschuh et al., 1997; Grundmann and Morteani, 1985; Hejl, 1997;
376 Mancktelow et al., 2001; Most, 2003; Pomella et al., 2011; Staufenberg, 1987; Steenken et al.,
377 2002; Viola et al., 2001; Wölfler et al., 2008, 2012).

378 Three cross sections, DD' (perpendicular to the BNF), AA' (perpendicular to the western limb of
379 the western sub-dome) and EE' (parallel to the main axial plane of the TW) are presented in
380 figure 7, redrawn after Bertrand et al. (2017) and Schmid et al. (2013). Zircon and apatite fission
381 track data compiled by Bertrand et al. (2017) are displayed in the lower part of figure 7b-d and
382 compared to fissure monazite ages. As described in Bertrand et al. (2017) (first model), fission
383 tracks data along AA' cross section (Fig. 7c) nicely display a dome-like shape with younger ages
384 recorded near the sub-dome axial plane, where cooling was slower. By contrast, along the EE'
385 longitudinal cross section (Fig. 7d), ZFT and AFT are younger in the western and eastern border
386 of the TW where the two major extensional faults, the BNF and KNF, are respectively located.
387 Perpendicular to the BNF (DD' cross section, Fig. 7b), the fission tracks record cooling ages
388 younging from the footwall toward the plane of the normal fault (from 10 to 4 Ma for AFT;
389 second model of Bertrand et al. 2017). Along EE' cross section, the youngest monazite ages (15 –
390 10 Ma) lie between zircon and apatite fission track data (grey and blue symbols), whereas the

391 older ages (>17 Ma) do not follow the cooling trend and are equal to or older than the ZFT data.
392 This means that at least the fissure monazites recording older ages crystallized somewhere above
393 ZFT closure temperatures of ~240 – 280 °C (Bernet, 2009; Bernet and Garver, 2005; Reiners,
394 2005; Yamada et al., 1995) (Fig. 7d).

395

396 **5.4 Monazite Th/U as monitor of oxidizing and reducing conditions**

397 Extreme low and high Th/U ratios described in fissure monazite by Gnos et al. 2015 (T1, T2 and
398 T3 sample in figure 9) are also observed in some grains from this study (red and blue labels on
399 figure 9). Hydrothermal monazite from the TW associated with hematite in fissure typically
400 displays very high Th/U ratios of around 1200 (Fig. 9, red labels; Table 1), whereas grains
401 obtained from graphite-bearing host rocks show very low Th/U ratios around 8 (Fig. 9, blue
402 labels; Table 1). This attests for oxidizing and reducing fluid conditions in the fissure
403 environment, respectively.

404 The Th/U in monazite grains PFIT1 and MOKR1 would instead record a dynamic oxidation
405 environment due to variable fluid conditions. In PFIT1 monazite the Th/U decreases from core to
406 rim, whereas within MOKR1 the opposite evolution is observed (Fig. 9). Thus in the first case the
407 fissure environment evolves toward reducing conditions whereas in the second case there is an
408 evolution towards more oxidizing conditions. Many of the other grains indicate intermediate
409 oxidizing conditions and they could not be assigned to one of the two categories defined above,
410 as the presence of either hematite or graphite is uncertain (Fig. 9; grey labels).

411

412 **6 Conclusions**

413 Th-Pb ages of fissure monazite provides an extended record of exhumation of the TW during the
414 Miocene. The investigated monazites crystallized at temperatures $<400^{\circ}\text{C}$ in the presence of
415 hydrothermal fluids that circulated in open fissures formed through tectonic movements. The Th-
416 Pb ages recorded by fissure monazites are in general agreement with previously published
417 geochronological data and range between 21.7 ± 0.4 Ma to 10.0 ± 0.2 Ma. Spot dates suggests
418 that monazite crystallization in the metamorphic and structural TW dome occurred over a period
419 of ~ 16 Ma. The combination of structural and geochronological information allows relating
420 monazite growth with tectonic movements that affected the TW. The three major growth episodes
421 identified in this study, by dating monazite growth domains, are interpreted to be associated with
422 N-S shortening associated to E-W extension (22 – 20 Ma), contemporaneous N-S shortening and
423 sinistral strike-slip movements (19 – 15 Ma) and reactivation of strike-slips/normal faulting (14 –
424 10 Ma). Overall, fissure monazite age recording indicates that in the TW Cenozoic faults show
425 increased activity at ~ 21 , ~ 17 and ~ 12 Ma, probably due to reorganization of plate movements
426 occurring at those times. Comparison of Th-Pb fissure monazite crystallization ages with existing
427 crystallization and cooling ages (e.g. AFT, ZFT, white mica from fault zones) show that the latest
428 stages of monazite crystallisation occurred at temperatures between apatite and zircon fission
429 track “closure” temperatures. This enlarged dataset also supports previous observations on fissure
430 monazites chemistry displaying extremely high Th/U ratios (~ 1200) under oxidizing conditions
431 in association with hematite.

432

433 *Data availability.* The data used in this study are available in Tables 3 and 4.

434 *Author contributions.* Fissure monazite samples were organized by EG and FW. Monazite for
435 dating were selected by ER, CAB, EG and AB according to tectonic settings and fault activity of

436 the study area. ER prepared the manuscript during her PhD project under the supervision of EG,
437 with contributions from all co-authors. Sample preparation and BSE imaging was performed by
438 ER and CAB. Data acquisition and reduction at the SwissSIMS and NordSim facility was
439 respectively carried out by ER and CAB under the supervision of DR and MJW.

440 *Competing interests.* The authors declare that they have no conflict of interest.

441 *Acknowledgments.* We thank Sepp Brugger, Kurt Novak, Franz Gartner, Peter Hellweger, Adolf
442 Meyer, Sebastian Plankensteiner, Johann Rappold, Josef Rathgeb, Alexandre Salzmann, Maria
443 Schaffhauser, Andreas Steiner and Ermin Welzl for having provided samples for this study. This
444 study was financed by the SNF grant number 200020-165513. Urs Klötzli and Jan Pleuger are
445 thanked for their helpful comments.

446

447 **References**

448 Aleinikoff, J. N., Schenck, W. S., Plank, M. O., Srogi, L. A., Fanning, C. M., Kamo, S. L. and
449 Bosbyshell, H.: Deciphering igneous and metamorphic events in high-grade rocks of the
450 Wilmington complex, Delaware: Morphology, cathodoluminescence and backscattered electron
451 zoning, and SHRIMP U-Pb geochronology of zircon and monazite, Bull. Geol. Soc. Am., 118(1–
452 2), 39–64, doi:10.1130/B25659.1, 2006.

453 Ayers, J. C., Miller, C., Gorisch, B. and Milleman, J.: Textural development of monazite during
454 high-grade metamorphism: Hydrothermal growth kinetics, with implications for U,Th-Pb
455 geochronology, Am. Mineral., 84(11–12), 1766–1780, doi:10.2138/am-1999-11-1206, 1999.

456 Bergemann, C. A., Gnos, E., Berger, A., Whitehouse, M., Mullis, J., Wehrens, P., Pettke, T. and

457 Janots, E.: Th-Pb ion probe dating of zoned hydrothermal monazite and its implications for
458 repeated shear zone activity: An example from the Central Alps, Switzerland, *Tectonics*, 36(4),
459 671–689, doi:10.1002/2016TC004407, 2017.

460 Bergemann, C. A., Gnos, E., Berger, A., Whitehouse, M. J., Mullis, J., Walter, F. and Bojar, H. P.:
461 Constraining long-term fault activity in the brittle domain through in situ dating of hydrothermal
462 monazite, *Terra Nov.*, 30(6), 440–446, doi:10.1111/ter.12360, 2018.

463 Bergemann, C. A., Gnos, E. and Whitehouse, M. J.: Insights into the tectonic history of the
464 Western Alps through dating of fissure monazite in the Mont Blanc and Aiguilles Rouges
465 Massifs, *Tectonophysics*, 750(May 2018), 203–212, doi:10.1016/j.tecto.2018.11.013, 2019.

466 Bergemann, C. A., Gnos, E., Berger, A., Janots, E. and Whitehouse, M. J.: Dating tectonic
467 activity in the Lepontine Dome and Rhone-Simplon Fault regions through hydrothermal
468 monazite-(Ce), *Solid Earth*, 199–222, 2020.

469 Berger, A., Gnos, E., Janots, E., Whitehouse, M., Soom, M., Frei, R. and Waight, T. E.: Dating
470 brittle tectonic movements with cleft monazite: Fluid-rock interaction and formation of REE
471 minerals, *Tectonics*, 32(5), 1176–1189, doi:10.1002/tect.20071, 2013.

472 Bernet, M.: A field-based estimate of the zircon fission-track closure temperature, *Chem. Geol.*,
473 259(3–4), 181–189, doi:10.1016/j.chemgeo.2008.10.043, 2009.

474 Bernet, M. and Garver, J. I.: Fission-track analysis of detrital zircon, *Rev. Mineral. Geochemistry*,
475 58.1, 205–237, 2005.

476 Bertrand, A.: Exhuming the core of collisional orogens, the Tauern Window (Eastern-Alps). A
477 geochronological, modelling and structural study, PhD thesis, Freie Univ. Berlin, 2014.

478 Bertrand, A., Rosenberg, C. and Garcia, S.: Fault slip analysis and late exhumation of the Tauern
479 Window, Eastern Alps, *Tectonophysics*, 649, 1–17, doi:10.1016/j.tecto.2015.01.002, 2015.

480 Bertrand, A., Rosenberg, C., Rabaute, A., Herman, F. and Fügenschuh, B.: Exhumation
481 mechanisms of the Tauern Window (Eastern Alps) inferred from apatite and zircon fission track
482 thermochronology, *Tectonics*, 36(2), 207–228, doi:10.1002/2016TC004133, 2017.

483 Blanckenburg, F. v., Villa, I. M., Baur, H., Morteani, G. and Steiger, R. H.: Time calibration of a
484 PT-path from the Western Tauern Window, Eastern Alps: the problem of closure temperatures,
485 *Contrib. to Mineral. Petrol.*, 101(1), 1–11, doi:10.1007/BF00387196, 1989.

486 Cherniak, D. J., Watson, E. B., Grove, M. and Harrison, T. M.: Pb diffusion in monazite: A
487 combined RBS/SIMS study, *Geochim. Cosmochim. Acta*, 68(4), 829–840,
488 doi:10.1016/j.gca.2003.07.012, 2004.

489 Cole, J., Hacker, B., Ratschbacher, L., Dolan, J., Seward, G., Frost, E. and Frank, W.: Localized
490 ductile shear below the seismogenic zone: Structural analysis of an exhumed strike-slip fault,
491 Austrian Alps, *J. Geophys. Res. Solid Earth*, 112(12), 1–15, doi:10.1029/2007JB004975, 2007.

492 Coyle, D. A.: The application of apatite fission-track analysis to problem in tectonics, PhD thesis,
493 La Trobe Univ. Bundoora, Victoria, Australia., 1994.

494 Dunkl, I., Frisch, W. and Grundmann, G.: Zircon fission-track thermochronology of the south-
495 eastern part of the TW and the adjacent Austroalpine margin, Eastern Alps, *Eclogae Geol. Helv.*,
496 96, 209–217, doi:10.1007/s00015-003-1092-3, 2003.

497 Favaro, S., Handy, M. R., Scharf, A. and Schuster, R.: Changing patterns of exhumation and
498 denudation in front of an advancing crustal indenter, Tauern Window (Eastern Alps), *Tectonics*,
499 36(6), 1053–1071, doi:10.1002/2016TC004448, 2017.

500 Di Fiore, G.: Evoluzione Morfotettonica delle aree alpine “Sempione” e “Brennero” attraverso
501 studi termocronologici di bassa temperatura, PhD thesis, Università di Bologna., 2013.

502 Fitz-Diaz, E., Cottle, J. M., Vidal-Reyes, M. I. and van der Pluijm, B.: In situ Th/Pb dating of
503 monazite in fibrous veins: Direct dating of veins and deformation in the shallow upper crust of
504 the Mexican Orogen, *J. Struct. Geol.*, 124(April), 136–142, doi:10.1016/j.jsg.2019.04.004, 2019.

505 Foeken, J. P. T., Persano, C., Stuart, F. M. and ter Voorde, M.: Role of topography in isotherm
506 perturbation: Apatite (U-Th)/He and fission track results from the Malta tunnel, Tauern Window,
507 Austria, *Tectonics*, 26(3), doi:10.1029/2006TC002049, 2007.

508 Fügenschuh, B., Seward, D. and Mancktelow, N.: Exhumation in a convergent orogen: the
509 western Tauern Window, *Terra Nov.*, 9(5–6), 213–217, doi:10.1111/j.1365-3121.1997.tb00015.x,
510 1997.

511 Gardés, E., Jaoul, O., Montel, J. M., Seydoux-Guillaume, A. M. and Wirth, R.: Pb diffusion in
512 monazite: An experimental study of $Pb^{2+} + Th^{4+} \Leftrightarrow 2Nd^{3+}$ interdiffusion, *Geochim.*
513 *Cosmochim. Acta*, 70(9), 2325–2336, doi:10.1016/j.gca.2006.01.018, 2006.

514 Gardés, E., Montel, J. M., Seydoux-Guillaume, A. M. and Wirth, R.: Pb diffusion in monazite:
515 New constraints from the experimental study of $Pb^{2+} \Leftrightarrow Ca^{2+}$ interdiffusion, *Geochim.*
516 *Cosmochim. Acta*, 71(16), 4036–4043, doi:10.1016/j.gca.2007.06.036, 2007.

517 Gasquet, D., Bertrand, J. M., Paquette, J. L., Lehmann, J., Ratzov, G., Ascensão De Guedes, R.
518 A., Tiepolo, M., Boullier, A. M., Scaillet, S. and Nomade, S.: Miocene to Messinian deformation
519 and hydrothermal activity in a pre-Alpine basement massif of the French western Alps: New U-
520 Th-Pb and argon ages from the Lauzière massif, *Bull. la Soc. Geol. Fr.*, 181(3), 227–241,
521 doi:10.2113/gssgfbull.181.3.227, 2010.

522 Glodny, J., Ring, U. and Kühn, A.: Coeval high-pressure metamorphism, thrusting, strike-slip,
523 and extensional shearing in the Tauern Window, Eastern Alps, *Tectonics*, 27(4),
524 doi:10.1029/2007TC002193, 2008.

525 Glotzbach, C., Reinecker, J., Danišik, M., Rahn, M., Frisch, W. and Spiegel, C.: Thermal history
526 of the central Gotthard and Aar massifs, European Alps: Evidence for steady state, long-term
527 exhumation, *J. Geophys. Res. Earth Surf.*, 115(3), F03017, doi:10.1029/2009JF001304, 2010.

528 Gnos, E., Janots, E., Berger, A., Whitehouse, M., Walter, F., Pettke, T. and Bergemann, C. A.: Age
529 of cleft monazites in the eastern Tauern Window: constraints on crystallization conditions of
530 hydrothermal monazite, *Swiss J. Geosci.*, 108(1), 55–74, doi:10.1007/s00015-015-0178-z, 2015.

531 Grand’Homme, A., Janots, E., Bosse, V., Seydoux-Guillaume, A. M. and Ascensão De Guedes,
532 R. A.: Interpretation of U-Th-Pb in-situ ages of hydrothermal monazite-(Ce) and xenotime-(Y):
533 evidence from a large-scale regional study in clefts from the western alps, *Mineral. Petrol.*,
534 110(6), 787–807, doi:10.1007/s00710-016-0451-5, 2016a.

535 Grand’Homme, A., Janots, E., Seydoux-Guillaume, A. M., Guillaume, D., Bosse, V. and Magnin,
536 V.: Partial resetting of the U-Th-Pb systems in experimentally altered monazite: Nanoscale
537 evidence of incomplete replacement, *Geology*, 44(6), 431–434, doi:10.1130/G37770.1, 2016b.

538 Grand’Homme, A., Janots, E., Seydoux-Guillaume, A. M., Guillaume, D., Magnin, V.,
539 Hövelmann, J., Höschen, C. and Boiron, M. C.: Mass transport and fractionation during monazite
540 alteration by anisotropic replacement, *Chem. Geol.*, 484(October 2017), 51–68,
541 doi:10.1016/j.chemgeo.2017.10.008, 2018.

542 Grundmann, G. and Morteani, G.: The young uplift and thermal history of the central Eastern
543 Alps (Austria/Italy), evidence from apatite fission track ages, *Jahrb. Geol. Bundesanst*, 128, 197–

544 216, 1985.

545 Hejl, E.: “Cold spots” during the Cenozoic evolution of the Eastern Alps: Thermochronological
546 interpretation of apatite fission-track data, *Tectonophysics*, 272(2–4), 159–173,
547 doi:10.1016/S0040-1951(96)00256-9, 1997.

548 Janots, E., Berger, A., Gnos, E., Whitehouse, M., Lewin, E. and Pettke, T.: Constraints on fluid
549 evolution during metamorphism from U–Th–Pb systematics in Alpine hydrothermal monazite,
550 *Chem. Geol.*, 326, 61–71, 2012.

551 Janots, E., Grand’Homme, A., Bernet, M., Guillaume, D. and Gnos, E.: Geochronological and
552 thermometric evidence of unusually hot fluids in an Alpine fissure of Lauzière granite
553 (Belledonne, Western Alps), *Solid Earth*, 10.1, 211–223, 2019.

554 Kurz, W. and Neubauer, F.: Deformation partitioning during updoming of the Sonnblick area in
555 the Tauern Window (Eastern Alps, Austria), *J. Struct. Geol.*, 18(11), 1327–1337,
556 doi:10.1016/S0191-8141(96)00057-0, 1996.

557 Ludwig, K. R.: User’s manual for a geochronological toolkit for Microsoft Excel (Isoplot/Ex
558 version 3.0), *Berkeley Geochronol. Cent. Spec. Publ.*, 4, 1–70, 2003.

559 Luth, S. W. and Willingshofer, E.: Mapping of the post-collisional cooling history of the Eastern
560 Alps, *Swiss J. Geosci.*, 101(SUPPL. 1), doi:10.1007/s00015-008-1294-9, 2008.

561 Mancktelow, N. S., Stöckli, D. F., Grollmund, B., Müller, W., Fügenschuh, B., Viola, G.,
562 Seward, D. and Villa, I. M.: The DAV and Pediatric fault systems in the Eastern Alps South of
563 the Tauern window, *Int. J. Earth Sci.*, 90(3), 593–622, doi:10.1007/s005310000190, 2001.

564 Most, P.: Late Alpine cooling histories of tectonic blocks along the central part of the Transalp-

565 Traverse (Inntal-Gadertal): Constraints from geochronology, PhD thesis, p. 97, Univ. of
566 Tübingen., 2003.

567 Mullis, J.: P-T-t path of quartz formation in extensional veins of the Central Alps, Schweiz.
568 *Miner. Petrogr. Mitt*, 76, 159–164, doi:10.5169/seals-57694, 1996.

569 Pleuger, J., Mancktelow, N., Zwingmann, H. and Manser, M.: K-Ar dating of synkinematic clay
570 gouges from Nealpine faults of the Central, Western and Eastern Alps, *Tectonophysics*, 550–
571 553, 1–16, doi:10.1016/j.tecto.2012.05.001, 2012.

572 Pollington, A. D. and Baxter, E. F.: High resolution Sm-Nd garnet geochronology reveals the
573 uneven pace of tectonometamorphic processes, *Earth Planet. Sci. Lett.*, 293(1–2), 63–71,
574 doi:10.1016/j.epsl.2010.02.019, 2010.

575 Pollington, A. D. and Baxter, E. F.: High precision microsampling and preparation of zoned
576 garnet porphyroblasts for Sm-Nd geochronology, *Chem. Geol.*, 281(3–4), 270–282,
577 doi:10.1016/j.chemgeo.2010.12.014, 2011.

578 Pomella, H., Klötzli, U., Scholger, R., Stipp, M. and Fügenschuh, B.: The Northern Giudicarie
579 and the Meran-Mauls fault (Alps, Northern Italy) in the light of new paleomagnetic and
580 geochronological data from boudinaged Eo-/Oligocene tonalites, *Int. J. Earth Sci.*, 100(8), 1827–
581 1850, doi:10.1007/s00531-010-0612-4, 2011.

582 Putnis, A.: Mineral Replacement Reactions, *Rev. Miner. Geochem.*, 70.1, 87–124,
583 doi:10.2138/rmg.2009.70.3, 2009.

584 Reiners, P. W.: Zircon (U-Th)/He Thermochronometry, in *Reviews in Mineralogy and*
585 *Geochemistry*, vol. 58, edited by T. A. Reiners, P.W. and Ehlers, pp. 151–179., 2005.

586 Ricchi, E., Bergemann, C. A., Gnos, E., Berger, A., Rubatto, D. and Whitehouse, M. J.:
587 Constraining deformation phases in the Aar Massif and the Gotthard Nappe (Switzerland) using
588 Th-Pb crystallization ages of fissure monazite-(Ce), *Lithos*, 342–343, 223–238,
589 doi:10.1016/j.lithos.2019.04.014, 2019.

590 Rosenberg, C. L. and Berger, A.: On the causes and modes of exhumation and lateral growth of
591 the Alps, *Tectonics*, 28(6), doi:10.1029/2008TC002442, 2009.

592 Rosenberg, C. L. and Garcia, S.: Estimating displacement along the Brenner Fault and orogen-
593 parallel extension in the Eastern Alps, *Int. J. Earth Sci.*, 100(5), 1129–1145, doi:10.1007/s00531-
594 011-0645-3, 2011.

595 Rosenberg, C. L., Schneider, S., Scharf, A., Bertrand, A., Hammerschmidt, K., Rabaute, A. and
596 Brun, J. P.: Relating collisional kinematics to exhumation processes in the Eastern Alps, *Earth-
597 Science Rev.*, 176(March 2017), 311–344, doi:10.1016/j.earscirev.2017.10.013, 2018.

598 Scharf, A., Handy, M. R., Favaro, S., Schmid, S. M. and Bertrand, A.: Modes of orogen-parallel
599 stretching and extensional exhumation in response to microplate indentation and roll-back
600 subduction (Tauern Window, Eastern Alps), *Int. J. Earth Sci.*, 102(6), 1627–1654,
601 doi:10.1007/s00531-013-0894-4, 2013.

602 Schmid, S. M., Fügenschuh, B., Kissling, E. and Schuster, R.: Tectonic map and overall
603 architecture of the Alpine orogen, *Eclogae Geol. Helv.*, 97(1), 93–117, doi:10.1007/s00015-004-
604 1113-x, 2004.

605 Schmid, S. M., Scharf, A., Handy, M. R. and Rosenberg, C. L.: The Tauern Window (Eastern
606 Alps , Austria): a new tectonic map , with cross-sections and a tectonometamorphic synthesis,
607 *Swiss J. Geosci.*, (106), 1–32, doi:10.1007/s00015-013-0123-y, 2013.

608 Schneider, S., Hammerschmidt, K. and Rosenberg, C. L.: Dating the longevity of ductile shear
609 zones: Insight from $^{40}\text{Ar}/^{39}\text{Ar}$ in situ analyses, *Earth Planet. Sci. Lett.*, 369–370(May 2012), 43–
610 58, doi:10.1016/j.epsl.2013.03.002, 2013.

611 Selverstone, J.: Evidence for east-west crustal extension in the Eastern Alps: Implications for the
612 unroofing history of the Tauern Window, *Tectonics*, 7(1), 87–105, 1988.

613 Selverstone, J., Spear, F. S., Franz, G. and Morteani, G.: High-pressure metamorphism in the SW
614 tauern window, Austria: P-T paths from hornblende-kyanite-staurolite schists, *J. Petrol.*, 25(2),
615 501–531, doi:10.1093/petrology/25.2.501, 1984.

616 Selverstone, J., Morteani, G. and Staude J.-M: Fluid channelling during ductile shearing:
617 transformation of granodiorite into aluminous schist in the Tauern Window, Eastern Alps, *J.*
618 *Metamorph. Geol.*, 9(4), 419–431, 1991.

619 Seydoux-Guillaume, A. M., Montel, J. M., Bingen, B., Bosse, V., de Parseval, P., Paquette, J. L.,
620 Janots, E. and Wirth, R.: Low-temperature alteration of monazite: Fluid mediated coupled
621 dissolution-precipitation, irradiation damage, and disturbance of the U-Pb and Th-Pb
622 chronometers, *Chem. Geol.*, 330–331, 140–158, doi:10.1016/j.chemgeo.2012.07.031, 2012.

623 Spencer, C. J., Kirkland, C. L. and Taylor, R. J. M.: Geoscience Frontiers Strategies towards
624 statistically robust interpretations of in situ U e Pb zircon geochronology, *Geosci. Front.*, 7(4),
625 581–589, doi:10.1016/j.gsf.2015.11.006, 2016.

626 Stacey, J. S. and Kramers, J. D.: Approximation of terrestrial lead isotope evolution by a two-
627 staged model, *Earth Planet. Sci. Lett.*, 26, 207–221, 1975.

628 Staufenberg, H.: Apatite fission-track evidence for postmetamorphic uplift and cooling history of
629 the Eastern Tauern Window and the surrounding Austroalpine (Central Eastern Alps, Austria),

630 Jahrb. Geol. Bundesanst, 130(1985), 571–586, 1987.

631 Steenken, A., Siegesmund, S., Heinrichs, T. and Fügenschuh, B.: Cooling and exhumation of the
632 Rieserferner Pluton (Eastern Alps, Italy/Austria), *Int. J. Earth Sci.*, 91(5), 799–817,
633 doi:10.1007/s00531-002-0260-4, 2002.

634 Stöckhert, B., Brix, M. R., Kleinschrodt, R., Hurford, A. J. and Wirth, R.: Thermochronometry
635 and microstructures of quartz—a comparison with experimental flow laws and predictions on the
636 temperature of the brittle-plastic transition, *J. Struct. Geol.*, 21(3), 351–369, doi:10.1016/S0191-
637 8141(98)00114-X, 1999.

638 Urbanek, C., Frank, W., Grasemann, B. and Decker, K.: Eoalpine versus Tertiary deformation:
639 dating of heterogeneously partitioned strain (Tauern Window, Austria), in Abstract volume, edited
640 by PanGeo Austria., 2002.

641 Viola, G., Mancktelow, N. S. and Seward, D.: Late oligocene-neogene evolution of Europe-Adria
642 collision: New structural and geochronological evidence from the Giudicarie fault system (Italian
643 Eastern Alps), *Tectonics*, 20(6), 999–1020, doi:10.1029/2001TC900021, 2001.

644 Wölfler, A., Dekant, C., Danišík, M., Kurz, W., Dunkl, I., Putiš, M. and Frisch, W.: Late stage
645 differential exhumation of crustal blocks in the central Eastern Alps: Evidence from fission track
646 and (U-Th)/He thermochronology, *Terra Nov.*, 20(5), 378–384, doi:10.1111/j.1365-
647 3121.2008.00831.x, 2008.

648 Wölfler, A., Stüwe, K., Danišík, M. and Evans, N. J.: Low temperature thermochronology in the
649 Eastern Alps: Implications for structural and topographic evolution, *Tectonophysics*, 541–543, 1–
650 18, doi:10.1016/j.tecto.2012.03.016, 2012.

651 Yamada, R., Tagami, T., Nishimura, S. and Ito, H.: Annealing kinetics of fission tracks in zircon :

652 an experimental study, *Chem. Geol.*, 122(1–4), 249–258, 1995.

653 **Figures:**

654 **Fig. 1:** Tectonic map of the TW dome modified after Bertrand et al. (2017), Scharf et al. (2013), Schmid et
655 al. (2013) and Schneider et al. (2013). Yellow stars on the map represent samples locations and numbers
656 inside the stars refer to samples listed in Table 1. Range of weighted mean growth domain ages are
657 indicated for each grain from this study and Gnos et al. (2015), labelled in black and green respectively
658 on the map (see Table 4 for an exhaustive summary of all the ages). Only the spot date range is indicated
659 for grains 1, 4 and 6. Locations of AA', BB' and CC' cross sections are indicated by black lines and
660 individual cross sections are presented in figure 6 together with monazite crystallization ages. Two normal
661 faults delimit the western and eastern border of the TW, the Brenner Normal Fault (BNF) and the
662 Katschberg Normal Fault (KNF) respectively. Note that the KNF prolongation results in dextral and
663 sinistral strike-slips in the North and South respectively (KSZS: Katschberg Shear Zone System). Several
664 sinistral strike-slip faults (AhSZ: Ahrntal Shear Zone; ASZ: Ahorn Shear Zone; DAV: Deferegggen-Antholz-
665 Vals Fault; GSZ: Greiner Shear Zone; InF: Inntal Fault; MüF: Mur-Mürz Fault; NF: Niedere Tauern
666 Southern Fault; OSZ: Olperer Shear Zone; SEMP: Salzach-Ennstal-Mariazell-Puchberg Fault; SpSZ:
667 Speikboden Shear Zone; TSZ: Tuxer Shear Zones; ZWD: Zwischenbergen-Wöllatratten and Drautal
668 Faults), dextral shear zones (HoF: Hochstuhl Fault; IsF: Iseltal Fault; KLT: Königsee-Lammertal-
669 Traunsee Fault; Mölltal Fault (MöF); PF: Pustertal Fault) and a reverse fault (MM: Meran-Maules
670 Fault) are also visible in red on the map.

671 **Fig. 2:** a) Two generations of late fissures visible in a road outcrop located between monazite locality
672 ($46^{\circ}59.436'N/011^{\circ}39.240'E$) and Pfitscherjoch. Steeply oriented fissures (C_2 : $\sim 090/65$) are older and
673 deformed (green ellipses), and seem related to a flatter lineation (L_2 : $\sim 250/30$, green arrows) visible on
674 some of the foliation planes. Younger and flatter oriented fissures (C_3 : $\sim 085/30$) are straight (blue ellipses),
675 and seem related to a steeper lineation (L_3 : $270/70$, blue arrows). These observations indicate that a
676 fissure can be deformed during its existence. Lengths of hammer handle is 60 cm. b) Enlargement of a). c)

677 *Schematic illustration of the 3 fissure generations observed in this study (C_1 , C_2 and C_3), together with*
678 *respective orientation, foliation (S_1 , S_2 and S_3) and lineation (L_1 , L_2 and L_3). The first fissure generation*
679 *(C_1) is related to E-W extension, the second fissure generation (C_2) is linked to strike-slip movements and*
680 *the third fissure generation (C_3) is related to the oblique-slip movements.*

681 **Fig. 3:** *Chemical, textural and geochronological information of monazite grains from the western TW. On*
682 *BSE images, colour-filled circles correspond to ion probe spot locations. Note that the square-shape*
683 *shading in grain 4 is due to an artefact of composing BSE images with diverse contrast.*

684 **Fig. 4:** *Chemical, textural and geochronological information of monazite grains from the central TW. On*
685 *BSE images, colour-filled circles correspond to ion probe spot locations. Note that the square-shape*
686 *shading in grains 10 and 11 is due to an artefact of composing BSE images with diverse contrast.*

687 **Fig. 5:** *Chemical, textural and geochronological information of monazite grains from the eastern TW. On*
688 *BSE images, colour-filled circles correspond to ion probe spot locations. Note that the square-shape*
689 *shading in grains 15, 17, 18 and 20 is due to an artefact of composing BSE images with diverse contrast.*

690 **Fig. 6:** *Cross sections of (a) the western, (b) the central part of the western sub-dome and (c) western end*
691 *of the eastern sub-dome, modified after (Schmid et al., 2013). See figure 1 for locations and legend.*
692 *Sample locations are indicated by yellow stars and identified by sample numbers listed in Table 1.*
693 *Monazite crystallization ages are present in the lower part of the figure and are linked to each sample by*
694 *light-grey dashed lines. Weighted mean ages from this study and from Gnos et al. (2015) are presented by*
695 *yellow diamonds and yellow circles, respectively, and blue bars correspond to the range of single spot*
696 *dates.*

697 **Fig. 7:** *a) Map of the TW from figure 1 with sample locations colored as function of deformation episodes*
698 *(colored stars). See figure 1 for legend. b) DD' NE-SW cross section across the BNF, c) AA' NW-SE cross*
699 *section perpendicular to the axial plane of the western sub-dome and d) EE' longitudinal cross section*
700 *parallel to the main axial plane of the TW metamorphic dome, modified after Bertrand et al. (2017). In the*

701 upper part, colored and numbered stars correspond to samples locations and are linked to corresponding
702 Th-Pb monazite ages by dashed vertical lines. Sample numbers refer to Table 1. In the lower part,
703 monazite weighted mean ages from this study and from Gnos et al. (2015) are labelled by colored diamond
704 and circles, respectively, and the range of single spot dates is depicted by blue bars. The color code used
705 for diamonds and circles follow deformation episodes explained in the discussion. Note that most error
706 bars are smaller than the size of the diamonds and circles. Zircon and apatite fission track ages are from
707 the Bertrand et al. (2017) compilation, light- and dark- grey dots with error bars, are displayed for
708 comparison. Square brackets shown to the right delimit the main periods of monazite growth discussed in
709 the text: (1) Early record of N-S shortening and associated E-W extension, (2) Contemporaneous N-S
710 shortening and strike-slip, (3) Reactivation of strike-slip to oblique-slip.

711 **Fig. 8:** Tectonic map of the Alps based on Pleuger et al. (2012) showing active Cenozoic faults at ~21 (in
712 red), 17 (in green) and 12 Ma (in blue) respectively. Note that after 17 Ma the Giudicarie Fault (GF)
713 becomes active and hence the Periadriatic Fault (PF) and the Mölltal Fault (MöF, dextral fault at the
714 southeastern corner of the TW) become inactive. Sinistral strike-slip faulting starts at ~19 Ma and is
715 affecting the western and central parts of the TW until at least 8 Ma. Future active faults are depicted in
716 grey and inactive faults in black.

717 **Fig. 9:** Th as function of U content obtained for all the monazite grains analysed in this study. Samples
718 indicated by an asterisk are from Gnos et al. (2015). Fissure monazite grains associated to hematite
719 (oxidizing conditions) are labelled in red whereas grains hosted in graphite bearing rocks (reducing
720 conditions) are labelled in blue. Samples with intermediate composition and/or for which we have no
721 information on the presence of hematite or graphite in the fissure environment are labelled in grey.

722

723

724

725 **Tables:**

726 **Table 1:** *Summary of monazite samples investigated in this study and from Gnos et al. (2015). Samples*
727 *name, number, location, host-rock lithology, metamorphic degree and fissure mineral association are*
728 *provided. Samples with approximate finding location are marked with “approx.”.*

729 **Table 2:** *Summary of deformation phases in the Tauern metamorphic dome.*

730 **Table 3:** *Th-U-Pb analyses of monazite by ion microprobe (SwissSIMS and Nordsim). Analyses resulting*
731 *in unreliable dates (e.g. presence of cracks, affected by Pbc causing high uncertainty) were not considered*
732 *and are written in italic.*

733 **Table 4:** *Summary of weighted mean ages of monazite growth domains and spot age ranges of each grain*
734 *from the TW.*

Figure 1.

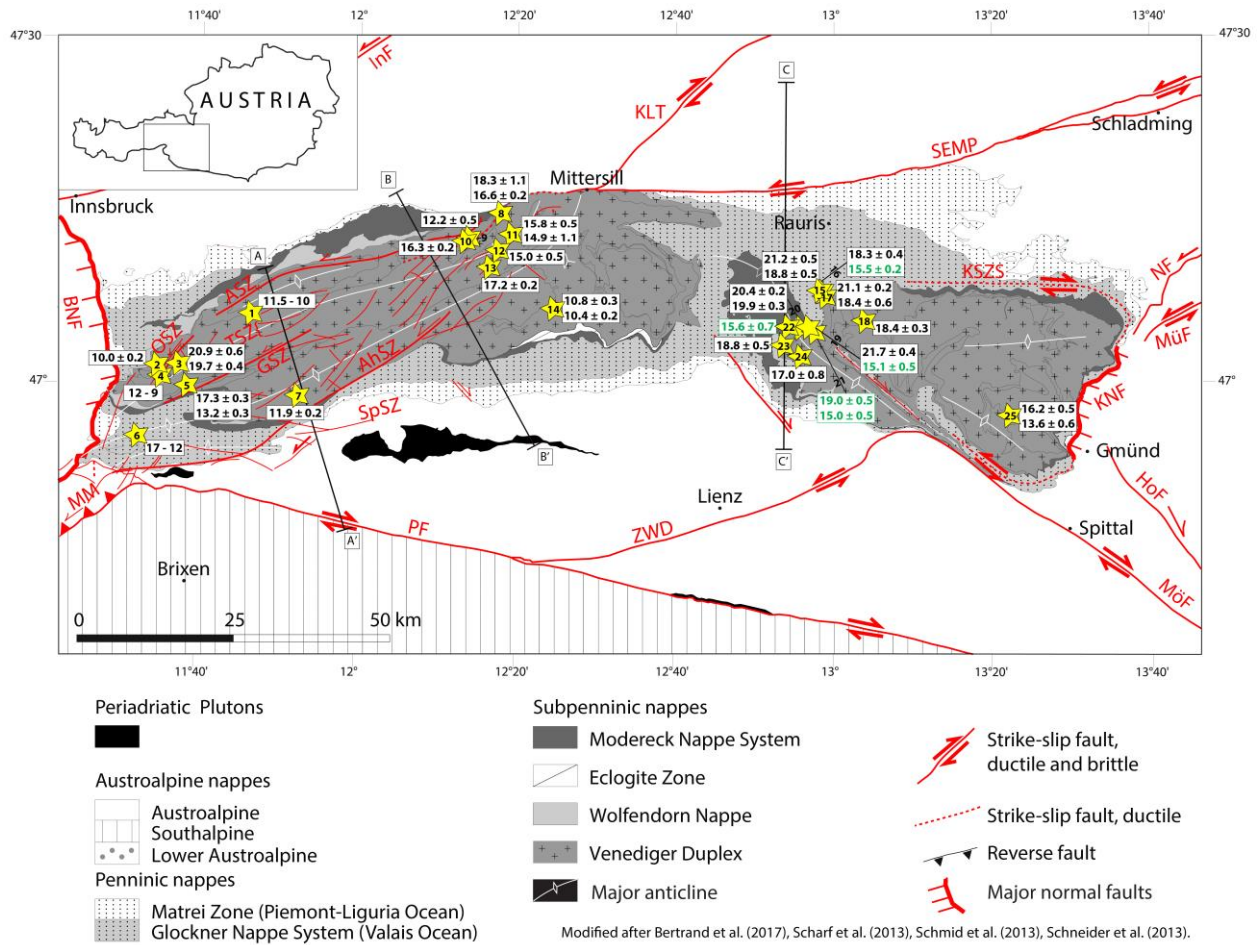
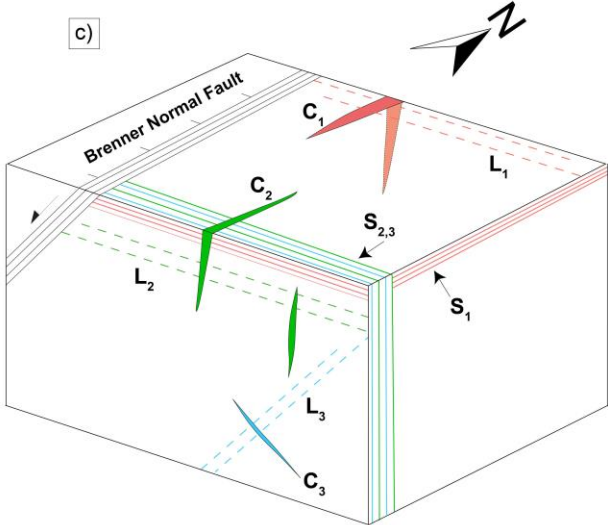
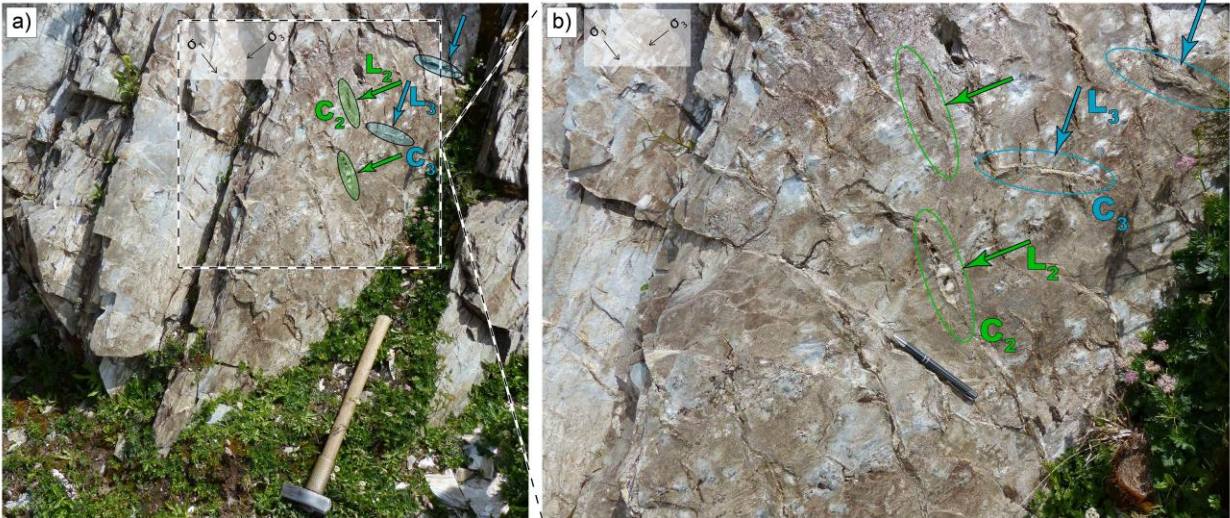


Figure 2.



C₁: Subvertical fissures
 Related to flat foliation (S₁)
 and to E-W lineation (L₁)

C₂: Subvertical fissures
 Related to vertical foliation (S₂)
 and flat to slightly inclined lineation (L₂)

C₃: Subhorizontal fissures
 Related to subvertical foliation (S₃)
 and steep lineation (L₃)

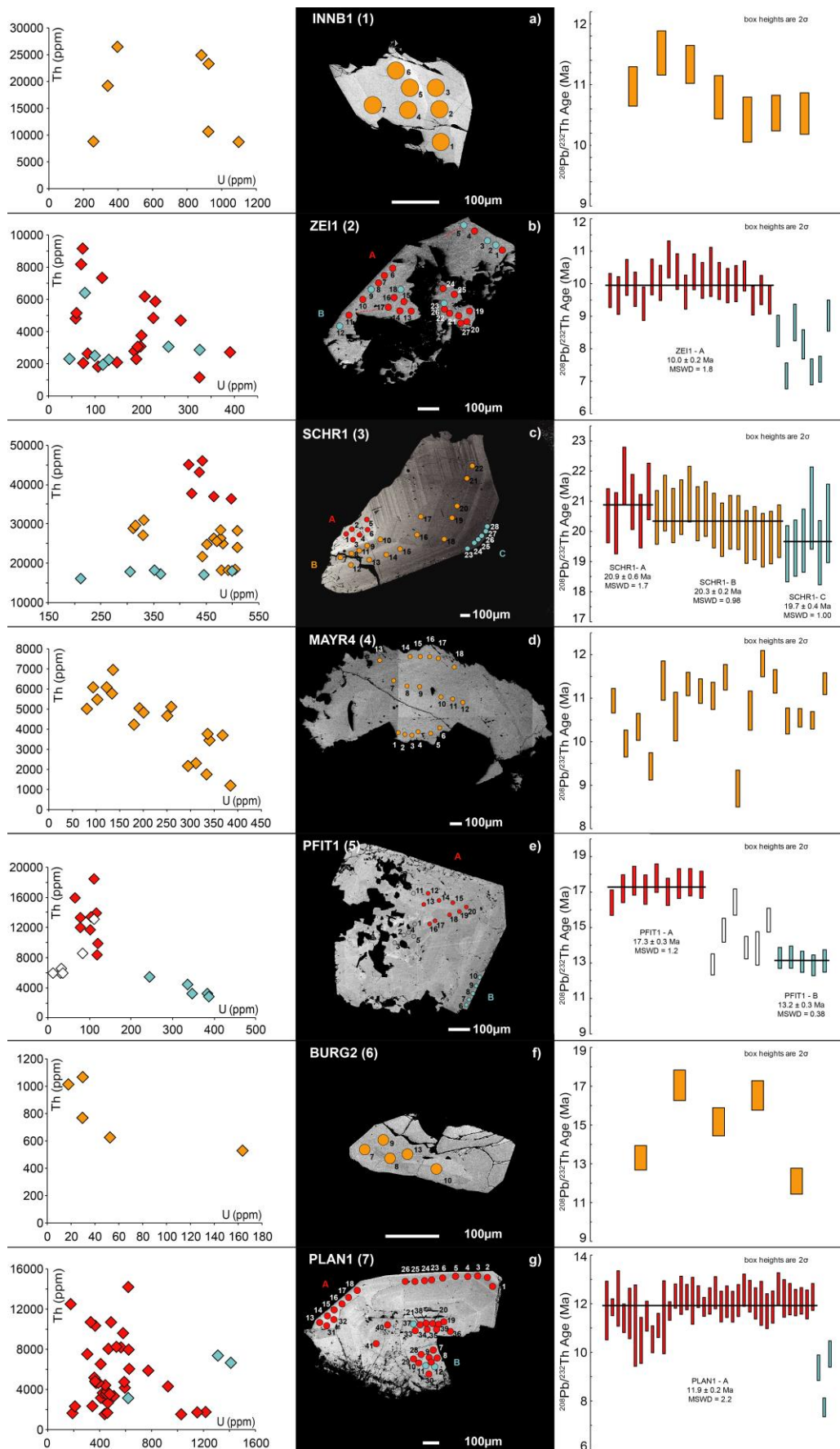


Figure 3.

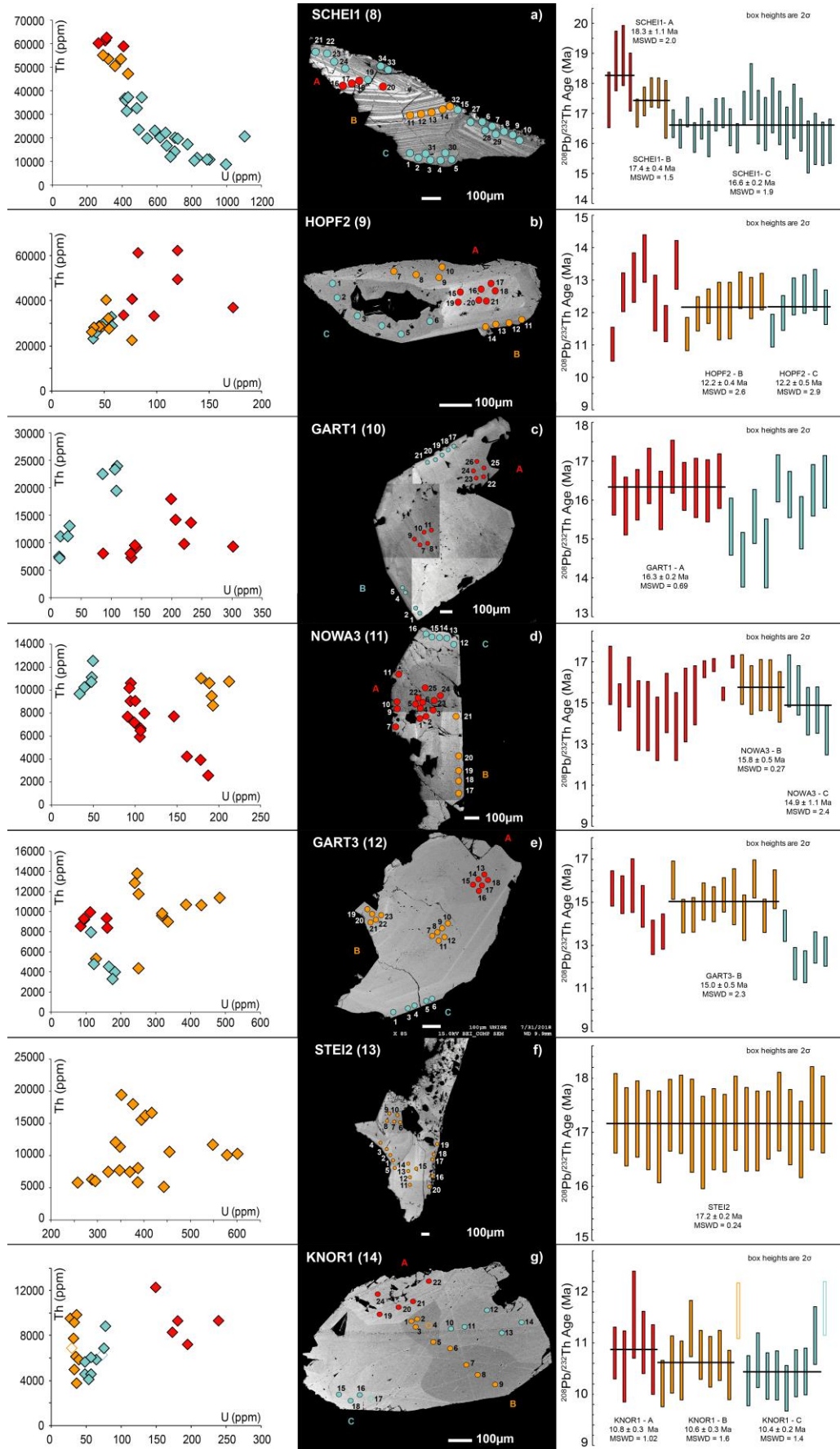


Figure 4.

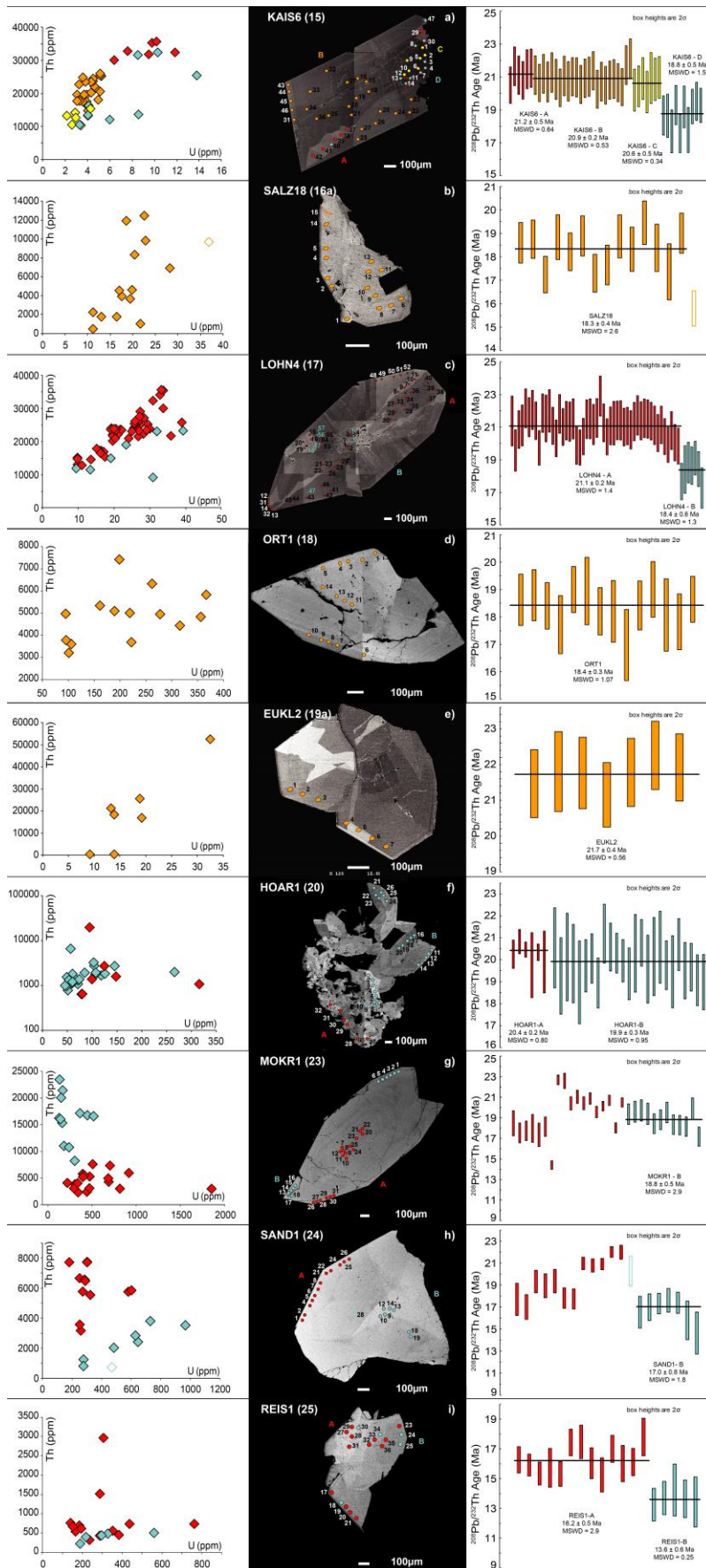


Figure 5.

Figure 6.

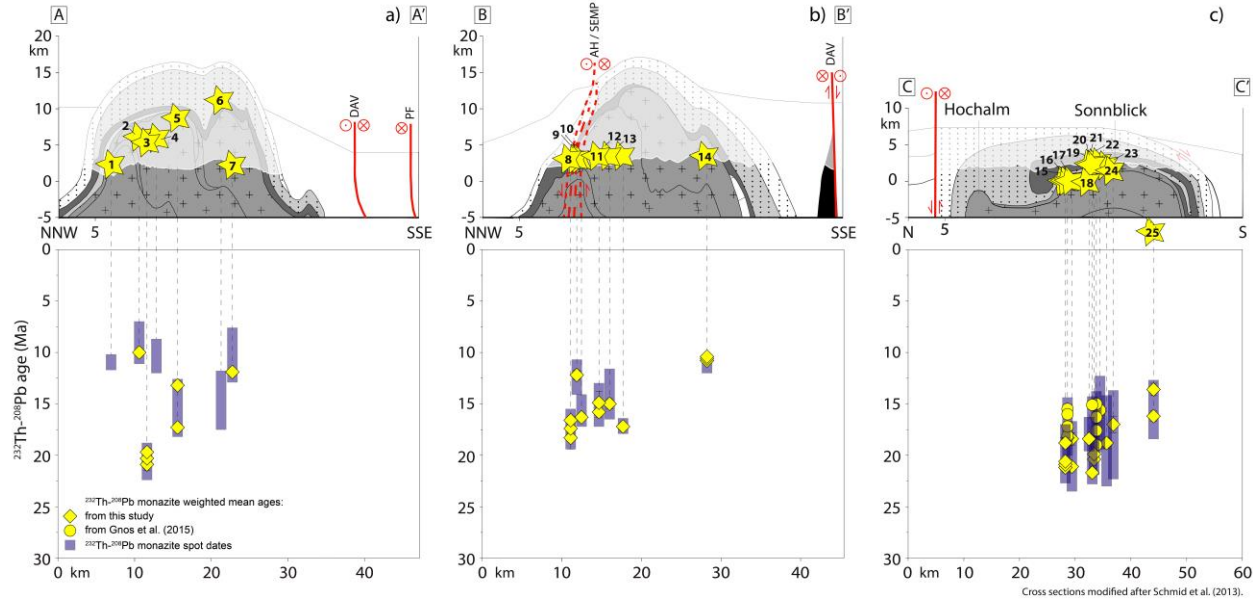
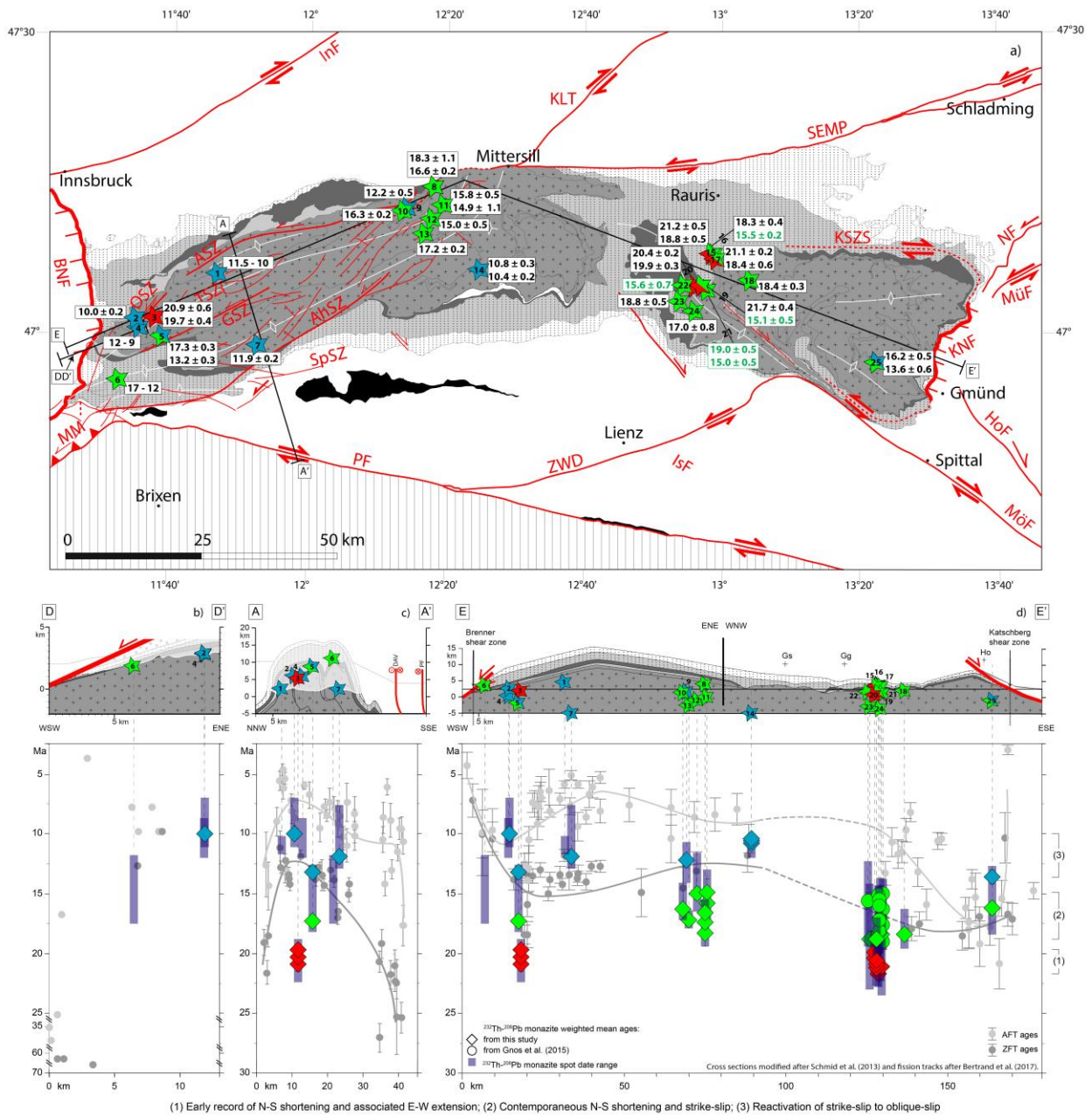


Figure 7.



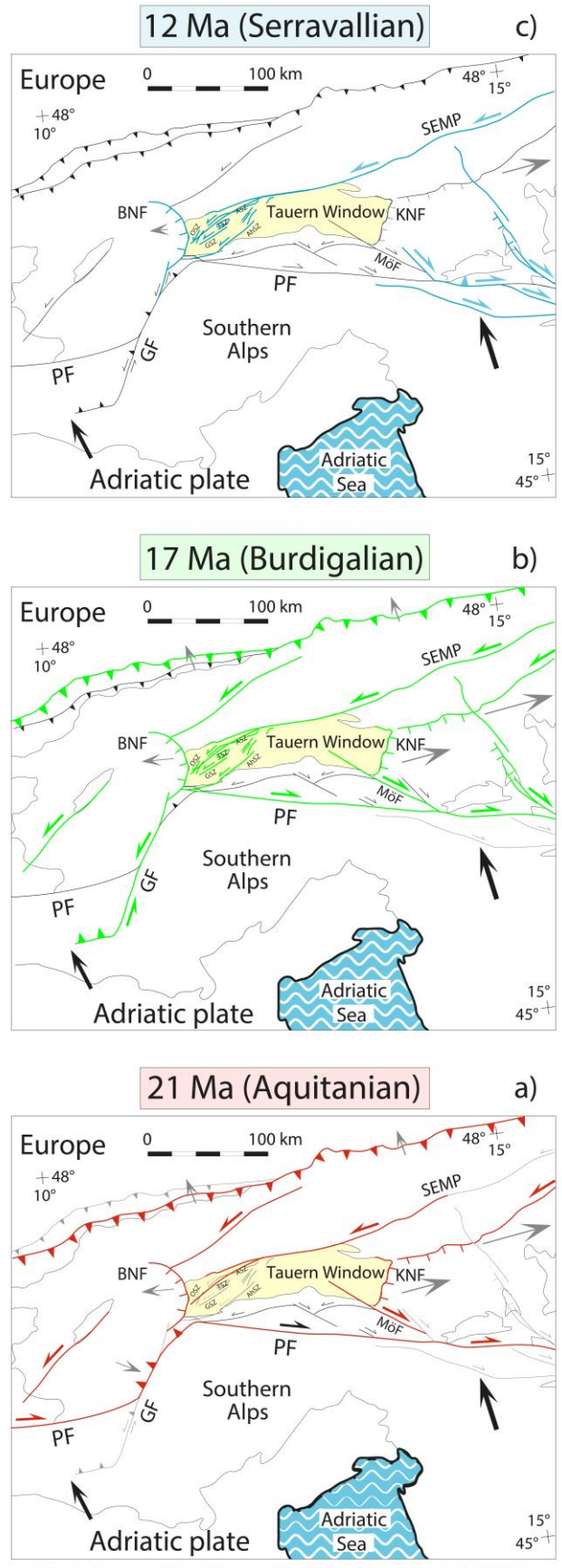


Figure 8. Tectonic map of the Alps modified after Pleuger et al. (2012)

Figure 9.

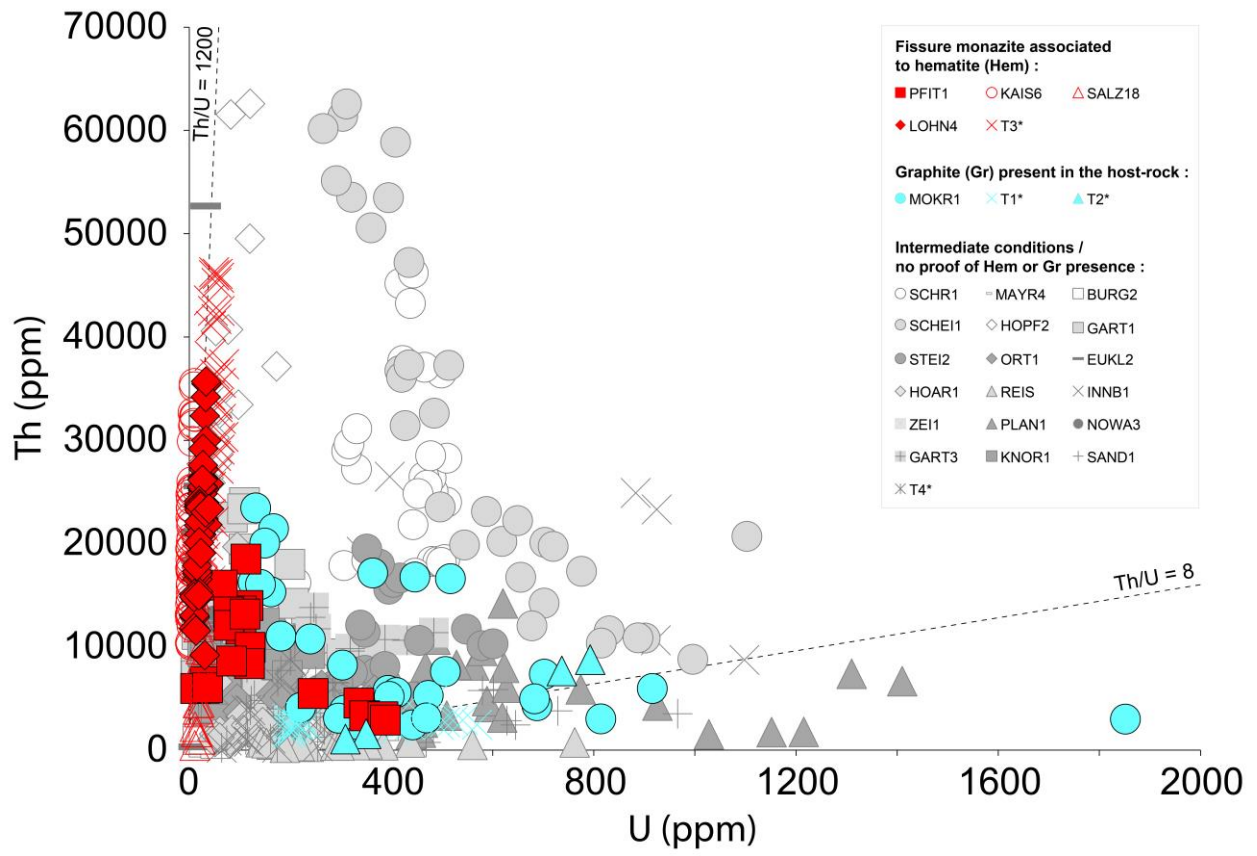


Table 1. Summary of monazite samples investigated in this study and by Gnos et al. (2015). Samples name, number, location, host-rock lithology, metamorphic degree and fissure mineral association are provided. Samples with approximate finding location are marked with "approx.".

Locality	Sample	N°	Latitude (°N)	Longitude (°E)	Remark	Host-rock	Host rock Alpine met.	Fissure mineral association	Reference	Ion probe
Western Tauern Window										
Innerböden, Zillertal, Tirol, Austria	INN1	1	47°05.850'	011°47.667'	approx.	gneiss	AM	Qtz, Adl, Chl	this study	SwissSIMS
Zeischalm, Valsertal, Tirol, Austria	ZEI1	2	47°01.400'	011°35.767'	approx.	gneiss	AM	Qtz, Adl, Chl	this study	SwissSIMS
Schrammacher, Zillertal, Tirol, Italy	SCHR1	3	47°01.47'	011°38.60'	approx.	gneiss	AM	Qtz, Chl, Adl, Rt, Snt	this study	NordSim
Kluppen, Pfitschtal, Südtirol, Italy	MAYR4	4	47°00.400'	011°36.217'	approx.	gneiss	AM	Qtz, Adl, Ant, Cc, Rt, Xnt	this study	SwissSIMS
Pfitscherjoch, Tirol, Austria	PFT1	5	46°59.65'	011°39.60'		mica schist	AM	Qtz, Hm, Adl, Trm, Rt, Brk, Ant, Syn, Asc	this study	NordSim
§ Burgumalpe, Pfitschtal, Südtirol, Italy	BURG2	6	46°55.217'	011°33.350'	approx.	serpentinite	GAT	Ilm, Rt, Cc	this study	SwissSIMS
Schwarzenbach, Ahrntal, Südtirol, Italy	PLAN1	7	46°58.641'	011°53.302'	approx.	gneiss	AM	Qtz, Adl	this study	SwissSIMS
Central Tauern Window										
Scheissgraben (Kotriesen), Habachtal, Salzburg, Austria	SCHE1	8	47°14.483'	012°18.667'		mica schist	UGS	Qtz, Ab, Ant, Ank, Rt	this study	SwissSIMS
Hopffeldboden, Oberzurbachtal, Salzburg, Austria	HOPF2	9	47°12.278'	012°14.844'		gneiss	GAT	Qtz, Ilm, Rt, Ant, Brk, Asc, Syn, Ap, Chl, Lm	this study	NordSim
Hopffeldgraben, Oberzurbachtal, Salzburg, Austria	GART1	10	47°12.100'	012°14.167'		gneiss	GAT	Qtz, Adl, Ant, Rtl, Asc + Bt and Chl from EDS analyses	this study	SwissSIMS
Wildenkarer-Wald, Habachtal, Salzburg, Austria	NOWA3	11	47°12.633'	012°20.000'	approx.	gneiss	GAT	Qtz, Ab, Adl	this study	SwissSIMS
Beryller, Untersulzbachtal, Salzburg, Austria	GART3	12	47°11.250'	012°18.517'	approx.	gneiss	AM	Qtz, Adl	this study	SwissSIMS
Sattelkar, Obersulzbachtal, Salzburg, Austria	STEI2	13	47°09.783'	012°17.250'	approx.	gneiss	AM	Qtz, Adl, Rt, Chl	this study	SwissSIMS
Innerer Knorrkogel, Osttirol, Austria	KNOR1	14	47°06.117'	012°25.183'		gneiss	AM	Adl, Qtz, Chl	this study	NordSim
Eastern Tauern Window										
* Kaiserer Steinbruch, Hüttwinkeltal, Rauris, Salzburg, Austria	KAIS6	15	47°07.787'	012°58.708'		meta-arenite	GAT	Qtz, Adl, Trm, Cc, Hm, Rt, Chl	this study	NordSim
* Lohninger Quarry, Hüttwinkeltal, Rauris, Salzburg, Austria	SALZ18	16a	47°07.20'	012°59.33'		meta-arenite	GAT	Qtz, Adl, Trm, Cc, Hm, Rt, Chl	this study	NordSim
* Lohninger Quarry, Hüttwinkeltal, Rauris, Salzburg, Austria	T3	16b	47°07.20'	012°59.33'		meta-arenite	GAT	Alb, Qtz, Trm, Hm, Rt	Gnos et al., 2015	NordSim
* Lohninger Quarry, Hüttwinkeltal, Rauris, Salzburg, Austria	LOHN4	17	47°07.20'	012°59.33'		meta-arenite	GAT	Qtz, Adl, Trm, Cc, Hm, Rt, Chl	this study	NordSim
Ortberg bei Böckstein, Salzburg, Austria	ORT1	18	47°05.150'	013°04.217'		granitic gneiss	GAT	Qtz, Adl, Rt, Chl, Ap	this study	SwissSIMS
Euklaskluft, Griesswies, Salzburg, Austria	EUKL2	19a	47°04.683'	012°57.250'		Bt-Mu schist	GAT	Alb, Pyr, Qtz, Rt, Chl, euclase, Xnt, goethite-todorokite-nordstrandite	this study	NordSim
Euklaskluft, Griesswies, Salzburg, Austria	T2	19b	47°04.683'	012°57.250'		Bt-Mu schist	GAT	Alb, Pyr, Qtz, Rt, Chl, euclase, Xnt, goethite-todorokite-nordstrandite	Gnos et al., 2015	NordSim
Hocharn, Kärnten, Austria	HOAR1	20	47°04.500'	012°56.083'		granitic gneiss	GAT	Qtz, Ab, Rt	this study	SwissSIMS
Erfurter Steig, Rauris, Salzburg	T1	21	47°04.133'	012°57.917'		Bt-Mu schist	GAT	Qtz, Ab, Adl, phenakite, Rt, Cc	Gnos et al., 2015	NordSim
Gjaidtroghöhe, Grosses Fleisstal, Kärnten	T4	22	47°03.783'	012°54.650'		gneiss	GAT	Qtz, Ab, Ant/Rt, Chl, Cc	Gnos et al., 2015	NordSim
Mokritzen, Kleines Fleisstal, Kärnten, Austria	MOKR1	23	47°03.033'	012°53.983'		graphite bearing schist	GAT	Qtz, Sid	this study	SwissSIMS
Sandkopf, Grosses Zirknitztal, Kärnten, Austria	SAND1	24	47°01.983'	012°56.05'		banded gneiss	GAT	Qtz, Adl, Chl, Sid, Ant	this study	SwissSIMS
Kleiner Reisseck, Reisseckgruppe, Kärnten, Austria	REIS1	25	46°56.950'	013°22.433'		banded gneiss	AM	Qtz, Ant, Ab, Chl	this study	SwissSIMS

Ab = albite; Adl = adularia; Ank = ankerite; Ant = anatase; Ap = fluorapatite; Asc = Aeschynite; Brk = brookite; Cc = calcite; Chl = chlorite; Cle = clinocllore; Hm = hematite; Ilm = ilmenite; Lm = limonite; Pyr = pyrite; Qtz = quartz; Rt = rutile; Sd = Siderite; Snt = senaite; Str = strontianite; Syn = synchisite; Trm = tourmaline; Xnt = xenotime; Alpine metamorphism: AM (Amphibolite facies), GAT (Greenschist-amphibolite transition), UGS (Upper greenschist facies). Bloc in glacial moraine : §. Bloc in rock slide : *.

Table 2. Summary of deformation phases in the Tauern metamorphic dome.

Age [Ma]	Phase	Fault	Domain	Characteristics	Ref.	Remarks
Estimated peaks of deformation						
~ 65	D1		Penninic nappes	Accretion and subduction of Piemont-Liguria Ocean	E	
~ 41	D2		Penninic and Subpenninic nappes	Subduction of Valais Ocean and parts of the distal European margin	E	
~ 35	D3		Central TW	Exhumation of high-pressure units	E	Folding of D2 thrust, decompression
~ 29	D4		Subpenninic nappes	European slab break off, Venediger Duplex formation and "Tauernkristallisation"	E	Contemporaneous intrusion of Periadriatic plutons and incipient NE-wards subduction of the Adriatic slab
~ 23 - 21			East of the Giudicarie Belt	Incipient indentation of the Southalpine Units in the Eastern Alps	D, E	
~ 17	D5		TW	Indentation, doming and lateral extrusion	E	
Faults motion						
33 - 15		ASZ	Western TW	Sinistral ductile shear	F, G	Ductile continuation of the SEMP fault
24 - 12		TSZ	Western TW	Sinistral ductile shear	B, F	
20 - 7		GSZ	Western TW	Sinistral ductile shear	F	
21 - 10		BNF	Western TW	Normal fault	C	
22 - 13		KNF	Eastern TW	Normal fault	C	

A: Bertrand et al., 2017, 2015; B: Blanckenburg et al., 1989; C: Favaro et al., 2017; D: Scharf et al. 2013; E: Schmid et al., 2013; F: Schneider et al., 2013; G: Rosenberg and Schneider, 2008. ASZ: Ahorn Shear Zone, BNF: Brenner Normal Fault, GSZ: Greiner Shear Zone, KNF: Katschberg Normal Fault, SEMP: Salzach-Ennstal-Mariazell-Puchberg fault, TSZ: Tuxer Shear Zones.

Table 3: Th-U-Pb analyses of monazite by ion microprobe (SwissSIMS and Nordsim). Analyses resulting in unreliable dates (e.g. presence of cracks, affected by Pbc causing high uncertainty) were not considered and are written in italic.

Groups	Analysis ID	U (ppm)	Th (ppm)	Th/U	²⁰⁸ Pb/ ²⁰⁴ Pb	1σ (%)	²⁰⁷ Pb/ ²⁰⁶ Pb	1σ (%)	²⁰⁸ Pb/ ²³² Th	1σ (%)	f ²⁰⁸ from 207 (%)	204-corr		204-corr spot ages		207-corr		207-corr spot ages		
												²⁰⁸ Pb/ ²³² Th	1σ (%)	²⁰⁸ Pb/ ²³² Th Age (Ma)	1σ (abs.)	²⁰⁸ Pb/ ²³² Th	1σ (%)	²⁰⁸ Pb/ ²³² Th Age (Ma)	1σ (abs.)	
<i>Western Tauern Window</i>																				
	INN1@01	258	8810	34	180	11	0.359	3.0	0.000621	1.4	13	0.000514	2.7	10.39	0.29	0.000543	1.5	10.97	0.16	
	INN1@02	397	26461	67	497	10	0.253	2.8	0.000592	1.6	4	0.000560	1.7	11.32	0.19	0.000570	1.6	11.52	0.18	
	INN1@03	341	19205	56	421	11	0.280	3.0	0.000589	1.4	5	0.000547	1.6	11.05	0.18	0.000561	1.4	11.34	0.16	
	INN1@04	1098	8717	8	202	12	0.158	2.7	0.000607	1.6	12	0.000536	2.8	10.83	0.31	0.000534	1.6	10.80	0.18	
	INN1@05	924	23297	25	421	10	0.216	2.3	0.000552	1.8	7	0.000518	1.9	10.47	0.20	0.000516	1.8	10.43	0.18	
	INN1@06	883	24902	28	364	9	0.215	2.3	0.000557	1.4	6	0.000514	1.7	10.39	0.17	0.000521	1.4	10.54	0.15	
	INN1@07	923	10635	12	200	11	0.194	2.6	0.000594	1.6	12	0.000508	2.6	10.26	0.27	0.000521	1.6	10.53	0.17	
	<i>INN1@08</i>	<i>1217</i>	<i>15622</i>	<i>13</i>	<i>283</i>	<i>13</i>	<i>0.228</i>	<i>2.7</i>	<i>0.000466</i>	<i>5.1</i>	<i>13</i>	<i>0.000433</i>	<i>5.1</i>	<i>8.74</i>	<i>0.45</i>	<i>0.000406</i>	<i>5.1</i>	<i>8.21</i>	<i>0.42</i>	
A	ZEI1@01	84	2630	31	393	21	0.202	5.2	0.000515	2.6	6	0.000465	3.1	9.39	0.29	0.000485	2.7	9.80	0.26	
	ZEI1@04	75	2041	27	408	25	0.196	5.8	0.000509	3.0	6	0.000475	3.8	9.60	0.36	0.000477	3.0	9.65	0.29	
	ZEI1@06	147	2086	14	251	18	0.185	4.2	0.000558	2.6	9	0.000485	3.6	9.79	0.36	0.000505	2.7	10.20	0.28	
	ZEI1@07	185	2785	15	547	24	0.159	4.4	0.000524	2.6	7	0.000503	3.2	10.16	0.32	0.000487	2.7	9.84	0.26	
	ZEI1@08	189	2292	12	316	21	0.185	4.2	0.000519	2.7	10	0.000456	3.5	9.21	0.32	0.000465	2.7	9.39	0.26	
	ZEI1@10	198	3078	16	421	20	0.143	4.0	0.000542	2.7	7	0.000493	3.0	9.96	0.30	0.000505	2.7	10.21	0.27	
	ZEI1@11	107	1820	17	298	20	0.180	4.6	0.000546	2.6	9	0.000475	3.5	9.60	0.34	0.000496	2.7	10.03	0.27	
	ZEI1@13	230	5870	26	559	15	0.163	3.2	0.000558	2.6	5	0.000519	2.6	10.49	0.28	0.000532	2.6	10.75	0.28	
	ZEI1@14	226	4846	21	532	18	0.153	3.8	0.000542	2.6	5	0.000509	2.8	10.29	0.29	0.000514	2.6	10.38	0.27	
	ZEI1@15	284	4694	16	412	16	0.204	3.4	0.000523	2.7	8	0.000474	2.8	9.58	0.27	0.000482	2.7	9.75	0.26	
	ZEI1@16	192	3057	16	422	18	0.158	3.7	0.000553	2.6	7	0.000506	2.9	10.23	0.30	0.000513	2.7	10.37	0.28	
ZEI1@17	200	3756	19	282	14	0.234	3.1	0.000561	2.7	11	0.000484	3.0	9.79	0.30	0.000500	2.7	10.11	0.28		
ZEI1@19	325	1152	4	188	22	0.114	3.8	0.000622	3.3	18	0.000495	5.2	10.00	0.52	0.000513	3.6	10.37	0.38		
ZEI1@20	391	2715	7	485	27	0.094	4.6	0.000533	2.8	6	0.000491	3.3	9.91	0.33	0.000499	2.8	10.09	0.28		

B	ZEI1@21	115	7335	64	555	15	0.219	4.3	0.000509	2.6	3	0.000476	2.7	9.62	0.26	0.000492	2.6	9.95	0.26
	ZEI1@22	74	9153	124	780	15	0.281	4.0	0.000509	2.8	3	0.000484	2.7	9.78	0.27	0.000495	2.8	10.01	0.28
	ZEI1@24	58	4809	82	617	19	0.235	4.7	0.000523	2.2	3	0.000491	2.4	9.91	0.24	0.000507	2.2	10.24	0.23
	ZEI1@25	60	5152	86	670	21	0.230	4.8	0.000485	2.3	3	0.000459	2.5	9.28	0.23	0.000470	2.3	9.49	0.22
	ZEI1@26	70	8182	117	609	18	0.255	4.8	0.000499	2.3	3	0.000468	2.4	9.45	0.23	0.000486	2.3	9.81	0.22
	ZEI1@27	207	6179	30	565	21	0.109	4.4	0.000485	2.3	3	0.000455	2.6	9.19	0.24	0.000471	2.3	9.52	0.22
	ZEI1@02	99	2499	25	352	23	0.194	6.0	0.000451	2.8	6	0.000402	3.6	8.12	0.29	0.000423	2.8	8.56	0.24
	ZEI1@03	130	2246	17	663	41	0.177	7.7	0.000378	2.7	6	0.000356	3.5	7.19	0.25	0.000355	2.8	7.18	0.20
	ZEI1@05	45	2301	51	447	26	0.286	5.9	0.000468	3.1	7	0.000434	3.7	8.78	0.33	0.000436	3.2	8.82	0.28
	ZEI1@09	325	2860	9	615	35	0.127	6.4	0.000429	2.7	6	0.000402	3.4	8.12	0.27	0.000403	2.8	8.15	0.22
	ZEI1@12	117	1943	17	312	24	0.139	5.4	0.000394	2.7	8	0.000352	3.9	7.12	0.28	0.000361	2.7	7.30	0.20
	ZEI1@18	258	3058	12	393	25	0.127	5.0	0.000398	2.6	8	0.000365	3.5	7.37	0.26	0.000365	2.7	7.38	0.20
	ZEI1@23	78	6403	82	744	20	0.307	4.7	0.000464	2.6	4	0.000440	2.7	8.89	0.24	0.000447	2.6	9.03	0.24
A	SCHR1@01	423	37708	89	1766	6	0.126	2.4	0.001025	2.19	1	0.001011	2.2	20.42	0.44	0.001016	2.2	20.53	0.45
	SCHR1@02	499	36495	73	2194	8	0.124	2.7	0.001012	2.51	1	0.001004	2.5	20.29	0.51	0.001004	2.5	20.28	0.51
	SCHR1@03	417	45163	108	1969	5	0.132	2.2	0.001090	2.18	1	0.001079	2.2	21.80	0.47	0.001082	2.2	21.85	0.48
	SCHR1@04	438	43245	99	1960	6	0.142	2.3	0.001048	2.18	1	0.001038	2.2	20.97	0.45	0.001039	2.2	20.98	0.46
	SCHR1@05	465	37059	80	2172	7	0.126	2.5	0.001016	2.18	1	0.001006	2.2	20.32	0.44	0.001007	2.2	20.35	0.44
	SCHR1@06	443	46170	104	1859	5	0.137	2.3	0.001064	2.20	1	0.001051	2.2	21.24	0.46	0.001056	2.2	21.33	0.47
	SCHR1@07	509	24001	47	1168	6	0.160	2.0	0.001037	2.18	2	0.001009	2.1	20.38	0.43	0.001013	2.2	20.47	0.45
	SCHR1@08	482	25025	52	1167	6	0.158	2.0	0.001060	2.20	2	0.001033	2.2	20.88	0.45	0.001037	2.2	20.95	0.46
	SCHR1@09	478	26320	55	1119	6	0.167	1.9	0.001040	2.19	2	0.001012	2.1	20.44	0.44	0.001016	2.2	20.54	0.45
	SCHR1@10	510	28255	55	1211	6	0.168	2.0	0.001051	2.17	2	0.001026	2.1	20.72	0.44	0.001030	2.2	20.81	0.45
	SCHR1@11	465	26453	57	1145	6	0.169	1.8	0.001076	2.18	2	0.001053	2.1	21.28	0.46	0.001052	2.2	21.25	0.46
	SCHR1@12	331	27180	82	1099	6	0.212	2.0	0.001043	2.18	2	0.001018	2.1	20.57	0.44	0.001020	2.2	20.60	0.45
	SCHR1@13	312	28957	93	1243	6	0.233	2.0	0.001052	2.19	2	0.001028	2.1	20.76	0.44	0.001027	2.2	20.75	0.45
	SCHR1@14	316	29632	94	1200	6	0.239	2.1	0.001031	2.22	2	0.001004	2.2	20.29	0.44	0.001008	2.2	20.37	0.45
	SCHR1@15	331	31105	94	1151	5	0.247	2.1	0.001016	2.21	2	0.000993	2.2	20.05	0.43	0.000993	2.2	20.07	0.44
	SCHR1@16	471	25641	54	1676	7	0.132	2.3	0.001020	2.19	1	0.001004	2.2	20.27	0.44	0.001005	2.2	20.31	0.44
	SCHR1@17	477	28482	60	1358	6	0.151	2.3	0.001020	2.20	2	0.001001	2.2	20.23	0.44	0.001005	2.2	20.30	0.45

C	SCHR1@18	480	18234	38	1599	9	0.119	2.5	0.000998	2.21	2	0.000976	2.2	19.72	0.43	0.000981	2.2	19.83	0.44
	SCHR1@19	492	18252	37	1339	8	0.116	2.5	0.001004	2.21	2	0.000981	2.2	19.81	0.43	0.000988	2.2	19.95	0.44
	SCHR1@20	506	18432	36	1461	8	0.117	2.5	0.000992	2.25	2	0.000973	2.2	19.66	0.44	0.000976	2.3	19.72	0.44
	SCHR1@21	443	21802	49	1500	8	0.134	2.4	0.000997	2.19	2	0.000979	2.2	19.78	0.43	0.000980	2.2	19.81	0.43
	SCHR1@22	453	24816	55	1475	7	0.149	2.4	0.001007	2.18	2	0.000991	2.2	20.03	0.43	0.000991	2.2	20.01	0.44
	SCHR1@23	211	16187	77	921	7	0.323	2.4	0.000994	2.42	4	0.000957	2.3	19.34	0.45	0.000954	2.4	19.27	0.47
	SCHR1@24	306	17861	58	513	5	0.371	2.0	0.001025	2.39	6	0.000960	2.3	19.39	0.44	0.000963	2.4	19.45	0.47
	SCHR1@25	363	17322	48	546	6	0.370	2.3	0.001036	2.65	6	0.000968	2.5	19.55	0.49	0.000975	2.7	19.70	0.52
	SCHR1@26	447	17105	38	1579	11	0.168	3.8	0.001047	3.28	2	0.001027	3.2	20.74	0.67	0.001029	3.3	20.78	0.68
	SCHR1@27	351	18354	52	1635	10	0.177	3.3	0.000973	2.75	2	0.000954	2.7	19.28	0.52	0.000955	2.8	19.30	0.53
SCHR1@28	499	18145	36	1394	11	0.215	3.5	0.001031	3.21	3	0.001006	3.1	20.33	0.64	0.001004	3.2	20.28	0.65	
	MAYR4@01	259	5113	20	514	18	0.127	3.3	0.000567	1.3	4	0.000527	1.8	10.65	0.19	0.000542	1.3	10.95	0.14
	MAYR4@02	340	3449	10	341	19	0.120	3.5	0.000527	1.5	6	0.000468	2.5	9.45	0.23	0.000493	1.5	9.96	0.15
	MAYR4@03	336	3763	11	305	17	0.109	3.6	0.000541	1.5	5	0.000476	2.5	9.62	0.24	0.000512	1.5	10.35	0.15
	MAYR4@04	368	3691	10	424	21	0.114	3.8	0.000496	1.6	6	0.000451	2.4	9.12	0.22	0.000467	1.7	9.44	0.16
	MAYR4@05	311	2301	7	246	17	0.135	3.0	0.000636	1.9	11	0.000536	3.1	10.84	0.34	0.000565	2.0	11.41	0.23
	MAYR4@06	385	1190	3	189	21	0.097	3.2	0.000618	2.3	15	0.000504	4.8	10.19	0.49	0.000524	2.6	10.58	0.28
	MAYR4@07	136	6949	51	411	13	0.294	2.8	0.000601	1.2	7	0.000544	1.6	10.99	0.18	0.000561	1.2	11.33	0.13
	MAYR4@08	192	5038	26	370	15	0.224	2.9	0.000599	1.2	8	0.000536	1.9	10.84	0.21	0.000553	1.3	11.17	0.14
	MAYR4@09	201	4829	24	293	13	0.233	2.7	0.000602	1.4	9	0.000522	2.1	10.55	0.22	0.000547	1.4	11.06	0.16
	MAYR4@10	251	4665	19	427	16	0.139	3.2	0.000600	1.2	5	0.000553	1.9	11.17	0.21	0.000568	1.3	11.48	0.15
	MAYR4@11	334	1748	5	300	24	0.103	3.4	0.000511	2.2	14	0.000446	3.7	9.00	0.33	0.000442	2.4	8.93	0.21
	MAYR4@12	295	2169	7	229	18	0.112	3.5	0.000582	2.0	9	0.000491	3.5	9.92	0.35	0.000531	2.1	10.72	0.22
	MAYR4@13	81	5010	62	404	16	0.335	3.4	0.000627	1.3	7	0.000574	1.9	11.60	0.23	0.000584	1.3	11.80	0.15
	MAYR4@14	103	5475	53	381	14	0.289	3.3	0.000602	1.2	6	0.000541	1.8	10.92	0.20	0.000564	1.2	11.39	0.13
	MAYR4@15	94	6085	65	457	15	0.274	3.6	0.000545	1.4	5	0.000499	1.8	10.09	0.18	0.000519	1.4	10.48	0.15
	MAYR4@16	122	6082	50	486	15	0.236	3.5	0.000546	1.0	4	0.000503	1.5	10.16	0.15	0.000522	1.0	10.56	0.11
	MAYR4@17	134	5776	43	381	14	0.270	3.1	0.000553	0.9	6	0.000497	1.6	10.04	0.16	0.000519	1.0	10.50	0.10
	MAYR4@18	180	4227	23	351	14	0.200	3.0	0.000603	1.1	7	0.000543	1.9	10.96	0.21	0.000561	1.1	11.34	0.12

A	PFIT1@12	103	11683	114	554	6	0.387	2.6	0.000852	2.19	5	0.000809	2.1	16.34	0.35	0.000813	2.2	16.42	0.36
	PFIT1@13	112	18466	165	580	5	0.450	2.4	0.000891	2.29	4	0.000845	2.2	17.06	0.38	0.000852	2.3	17.21	0.39
	PFIT1@14	117	13986	120	569	5	0.413	2.4	0.000918	2.31	5	0.000868	2.2	17.54	0.39	0.000874	2.3	17.66	0.41
	PFIT1@15	104	13449	130	473	5	0.430	2.3	0.000895	2.41	5	0.000835	2.3	16.87	0.39	0.000849	2.4	17.15	0.41
	PFIT1@16	65	15956	244	629	5	0.497	2.8	0.000913	2.26	4	0.000877	2.2	17.72	0.39	0.000881	2.3	17.80	0.40
	PFIT1@17	78	13368	171	586	7	0.506	3.3	0.000877	2.25	4	0.000833	2.2	16.82	0.37	0.000843	2.3	17.03	0.38
	PFIT1@18	79	12054	153	662	7	0.365	3.6	0.000892	2.40	3	0.000859	2.4	17.35	0.41	0.000866	2.4	17.49	0.42
	PFIT1@19	121	9937	82	697	10	0.328	4.6	0.000896	2.19	3	0.000856	2.2	17.29	0.38	0.000869	2.2	17.57	0.39
	PFIT1@20	119	8358	70	871	11	0.287	4.9	0.000885	2.19	3	0.000853	2.2	17.23	0.37	0.000862	2.2	17.42	0.38
	<i>PFIT1@01</i>	30	5962	199	808	12	0.360	5.4	0.000658	2.29	3	0.000631	2.3	12.74	0.29	0.000640	2.3	12.94	0.30
	<i>PFIT1@02</i>	32	6627	209	723	10	0.350	5.0	0.000754	2.25	2	0.000721	2.2	14.57	0.32	0.000736	2.3	14.86	0.34
<i>PFIT1@03</i>	13	5940	466	1033	11	0.414	6.9	0.000824	2.24	1	0.000808	2.2	16.33	0.37	0.000814	2.2	16.45	0.37	
<i>PFIT1@04</i>	36	6027	166	859	13	0.317	5.7	0.000705	2.28	3	0.000681	2.3	13.77	0.31	0.000687	2.3	13.88	0.32	
<i>PFIT1@05</i>	84	8610	102	1011	19	0.389	7.1	0.000710	3.39	4	0.000690	3.4	13.94	0.47	0.000685	3.4	13.84	0.47	
<i>PFIT1@11</i>	110	13146	119	548	6	0.428	2.7	0.000800	2.18	4	0.000756	2.1	15.28	0.32	0.000764	2.2	15.43	0.34	
B	PFIT1@06	245	5464	22	525	10	0.155	3.0	0.000697	2.20	6	0.000664	2.2	13.42	0.30	0.000658	2.2	13.30	0.29
	PFIT1@07	336	4523	13	381	11	0.161	3.6	0.000706	2.33	6	0.000642	2.4	12.98	0.31	0.000661	2.3	13.35	0.31
	PFIT1@08	347	3300	10	314	12	0.201	3.5	0.000728	2.21	11	0.000647	2.4	13.07	0.32	0.000648	2.3	13.09	0.30
	PFIT1@09	383	3220	8	343	13	0.170	3.9	0.000704	2.21	9	0.000636	2.5	12.86	0.32	0.000638	2.3	12.89	0.29
	PFIT1@10	388	2889	7	238	11	0.190	3.7	0.000740	2.33	12	0.000641	2.8	12.95	0.36	0.000650	2.4	13.13	0.32
	BURG2@07	30	769	26	193	20	0.165	4.7	0.000732	2.3	10	0.000585	4.4	11.83	0.53	0.000659	2.4	13.32	0.31
	BURG2@08	18	1014	57	219	16	0.306	3.6	0.000959	2.2	12	0.000790	3.4	15.97	0.54	0.000844	2.3	17.06	0.39
	BURG2@09	53	626	12	275	24	0.087	5.1	0.000797	2.3	6	0.000685	3.9	13.85	0.54	0.000751	2.4	15.17	0.36
	BURG2@10	30	1067	36	324	19	0.179	4.1	0.000878	2.3	7	0.000774	3.0	15.63	0.47	0.000818	2.3	16.53	0.38
	BURG2@13	164	529	3	403	55	0.112	7.5	0.000683	2.3	12	0.000660	6.5	13.35	0.86	0.000600	2.8	12.12	0.33
	<i>BURG2@12</i>	52	2273	44	69	18	0.415	3.7	0.001048	8.6	46	0.000462	10.7	9.34	1.00	0.000571	9.5	11.53	1.10
	PLAN1@01	190	1647	9	56	9	0.577	2.2	0.001582	3.1	63	0.000706	6.9	14.27	0.98	0.000580	5.1	11.73	0.60
	PLAN1@02	177	12498	71	284	11	0.361	2.9	0.000643	1.4	9	0.000585	2.1	11.81	0.25	0.000587	1.5	11.86	0.17
	PLAN1@03	209	2322	11	56	8	0.620	1.9	0.001634	3.3	63	0.000578	5.5	11.67	0.64	0.000605	4.7	12.23	0.57

A

PLAN1@04	410	3160	8	101	12	0.269	2.8	0.000788	2.2	28	0.000583	5.4	11.78	0.63	0.000565	2.6	11.41	0.29
PLAN1@05	438	1542	4	59	11	0.261	2.7	0.001043	3.3	45	0.000489	7.9	9.88	0.78	0.000574	4.5	11.61	0.52
PLAN1@06	458	1687	4	58	10	0.377	2.4	0.001231	6.5	55	0.000575	8.0	11.62	0.93	0.000550	7.5	11.11	0.84
PLAN1@07	462	2662	6	90	12	0.284	2.5	0.000864	4.0	40	0.000635	6.3	12.83	0.81	0.000520	4.5	10.50	0.47
PLAN1@08	509	3332	7	104	14	0.242	3.3	0.000751	2.3	24	0.000607	6.0	12.26	0.74	0.000569	2.7	11.50	0.31
PLAN1@09	594	4167	7	101	12	0.238	2.9	0.000690	2.4	24	0.000501	5.1	10.12	0.51	0.000522	2.6	10.55	0.28
PLAN1@10	774	5878	8	148	12	0.190	2.8	0.000661	2.1	17	0.000557	3.9	11.26	0.44	0.000550	2.2	11.11	0.25
PLAN1@13	1215	1759	1	68	12	0.136	2.5	0.000967	5.4	41	0.000576	8.2	11.65	0.96	0.000567	6.6	11.45	0.75
PLAN1@14	589	4750	8	176	14	0.167	3.2	0.000680	1.5	15	0.000581	3.7	11.73	0.43	0.000579	1.6	11.71	0.19
PLAN1@15	424	3653	9	98	11	0.233	2.9	0.000783	1.8	22	0.000624	5.1	12.61	0.65	0.000610	2.0	12.32	0.25
PLAN1@16	448	3567	8	86	10	0.288	2.4	0.000869	2.9	30	0.000596	5.2	12.04	0.63	0.000611	3.2	12.35	0.39
PLAN1@17	454	3815	8	108	11	0.198	3.0	0.000744	1.9	18	0.000566	4.7	11.44	0.54	0.000608	2.1	12.28	0.26
PLAN1@18	443	4422	10	161	13	0.250	2.7	0.000763	3.9	21	0.000670	4.9	13.53	0.67	0.000600	4.0	12.13	0.48
PLAN1@19	365	10351	28	214	10	0.305	2.7	0.000685	1.8	11	0.000596	2.5	12.04	0.31	0.000609	1.8	12.30	0.22
PLAN1@20	467	8041	17	153	9	0.359	2.1	0.000751	1.5	22	0.000606	2.8	12.25	0.34	0.000588	1.6	11.88	0.20
PLAN1@21	627	6050	10	103	9	0.322	2.0	0.000836	2.0	28	0.000577	3.7	11.66	0.43	0.000600	2.2	12.12	0.27
PLAN1@23	373	4646	12	715	17	0.102	2.9	0.000645	2.6	4	0.000611	2.7	12.34	0.33	0.000617	2.7	12.46	0.33
PLAN1@24	390	4664	12	677	18	0.090	3.5	0.000610	2.6	4	0.000576	2.7	11.63	0.31	0.000588	2.7	11.89	0.32
PLAN1@25	359	5180	14	519	17	0.121	3.0	0.000639	2.7	6	0.000591	2.8	11.94	0.33	0.000598	2.7	12.09	0.32
PLAN1@26	365	4817	13	401	15	0.116	3.0	0.000627	2.6	6	0.000570	2.8	11.52	0.32	0.000588	2.7	11.88	0.32
PLAN1@27	476	3538	7	541	19	0.101	2.9	0.000650	2.7	8	0.000603	2.8	12.19	0.35	0.000601	2.7	12.14	0.33
PLAN1@28	564	8192	15	460	11	0.125	2.3	0.000660	2.6	6	0.000604	2.6	12.21	0.32	0.000622	2.6	12.56	0.33
PLAN1@29	620	14199	23	619	10	0.130	2.1	0.000637	2.6	4	0.000598	2.6	12.09	0.31	0.000609	2.6	12.32	0.33
PLAN1@30	528	8241	16	420	13	0.127	2.7	0.000632	2.7	6	0.000574	2.7	11.60	0.31	0.000595	2.7	12.02	0.32
PLAN1@31	1028	1527	1	124	12	0.090	2.0	0.000802	3.1	26	0.000552	4.4	11.16	0.49	0.000595	3.8	12.02	0.45
PLAN1@32	1152	1721	1	227	19	0.066	2.7	0.000661	2.7	12	0.000548	4.0	11.08	0.44	0.000579	3.1	11.70	0.36
PLAN1@33	926	4303	5	361	14	0.085	2.2	0.000642	2.7	8	0.000573	2.8	11.57	0.33	0.000588	2.8	11.87	0.33
PLAN1@34	623	7966	13	483	12	0.125	2.3	0.000669	2.6	7	0.000615	2.6	12.43	0.32	0.000624	2.6	12.61	0.33
PLAN1@35	408	6529	16	185	8	0.307	1.7	0.000746	3.1	19	0.000592	3.0	11.97	0.36	0.000605	3.2	12.22	0.39
PLAN1@36	304	7521	25	427	13	0.182	2.7	0.000646	2.6	7	0.000587	2.7	11.87	0.31	0.000603	2.6	12.19	0.32
PLAN1@38	580	9607	17	525	14	0.112	2.4	0.000626	2.2	5	0.000580	2.3	11.73	0.27	0.000596	2.2	12.05	0.27

B	PLAN1@39	331	10707	32	497	13	0.164	2.7	0.000628	2.2	4	0.000581	2.3	11.74	0.27	0.000600	2.2	12.12	0.27
	PLAN1@40	344	2342	7	311	21	0.143	2.9	0.000698	2.3	15	0.000612	3.3	12.36	0.41	0.000593	2.5	11.98	0.30
	PLAN1@41	487	10698	22	360	11	0.172	2.1	0.000654	2.2	7	0.000584	2.3	11.80	0.27	0.000608	2.3	12.28	0.28
	PLAN1@11	1410	6659	5	175	20	0.204	4.3	0.000568	2.5	18	0.000578	6.4	11.69	0.74	0.000464	2.8	9.38	0.26
	PLAN1@12	1310	7371	6	160	23	0.206	5.3	0.000467	2.1	18	0.000509	7.9	10.28	0.81	0.000384	2.5	7.75	0.19
	PLAN1@37	619	3146	5	312	20	0.085	2.7	0.000555	2.6	11	0.000493	3.5	9.96	0.34	0.000492	2.7	9.94	0.27
	PLAN1@22	733	1514	2	52	9	0.291	2.1	0.001227	7.7	60	0.000544	8.3	10.99	0.92	0.000491	9.1	9.91	0.90

Central Tauern Window

A	SCHE11@16	408	58860	144	1205	6	0.181	1.8	0.000876	2.6	1	0.000849	2.6	17.14	0.44	0.000864	2.6	17.46	0.46
	SCHE11@17	304	61361	202	1483	7	0.210	1.9	0.000939	2.6	1	0.000915	2.6	18.49	0.48	0.000928	2.6	18.75	0.50
	SCHE11@18	265	60179	227	1432	6	0.235	1.9	0.000949	2.6	1	0.000924	2.6	18.66	0.48	0.000937	2.6	18.93	0.50
	SCHE11@20	311	62554	201	1416	7	0.222	2.0	0.000906	2.7	1	0.000881	2.6	17.81	0.46	0.000893	2.7	18.05	0.48
B	SCHE11@11	394	53473	136	780	7	0.309	2.0	0.000868	1.4	3	0.000829	1.4	16.75	0.23	0.000842	1.4	17.02	0.23
	SCHE11@12	434	47204	109	857	9	0.268	2.2	0.000886	1.4	3	0.000855	1.4	17.28	0.24	0.000862	1.4	17.41	0.24
	SCHE11@13	360	50556	140	639	8	0.349	2.1	0.000907	1.4	3	0.000861	1.4	17.39	0.24	0.000876	1.4	17.71	0.24
	SCHE11@14	321	53530	167	655	7	0.402	1.9	0.000911	1.4	4	0.000863	1.4	17.45	0.24	0.000876	1.4	17.69	0.25
C	SCHE11@32	291	55126	189	1026	6	0.303	1.5	0.000868	2.8	2	0.000836	2.7	16.88	0.46	0.000848	2.8	17.14	0.48
	SCHE11@01	776	17285	22	303	8	0.196	2.1	0.000888	1.4	7	0.000802	1.7	16.20	0.27	0.000825	1.4	16.67	0.23
	SCHE11@02	485	32602	67	655	11	0.283	2.6	0.000843	1.4	4	0.000808	1.5	16.33	0.25	0.000808	1.4	16.33	0.24
	SCHE11@03	496	23525	47	411	9	0.285	2.2	0.000899	1.4	6	0.000826	1.6	16.70	0.26	0.000844	1.4	17.05	0.25
	SCHE11@04	619	20187	33	312	10	0.254	2.5	0.000862	1.5	7	0.000797	1.9	16.10	0.31	0.000802	1.5	16.21	0.25
	SCHE11@05	702	14215	20	252	9	0.255	2.1	0.000929	1.5	11	0.000806	1.9	16.29	0.32	0.000825	1.5	16.66	0.25
	SCHE11@06	831	11524	14	190	8	0.274	1.7	0.000974	1.8	18	0.000810	2.3	16.36	0.37	0.000800	1.8	16.16	0.30
	SCHE11@07	545	19842	36	279	8	0.383	1.9	0.000949	1.6	12	0.000839	1.8	16.95	0.31	0.000840	1.6	16.97	0.27
	SCHE11@08	902	10829	12	216	9	0.220	2.0	0.000979	1.4	14	0.000843	2.1	17.04	0.36	0.000843	1.5	17.03	0.25
	SCHE11@09	888	10863	12	239	11	0.212	2.3	0.000942	1.8	13	0.000809	2.4	16.35	0.39	0.000819	1.8	16.55	0.31
	SCHE11@10	1103	20671	19	314	11	0.206	2.6	0.000864	1.5	7	0.000791	2.0	15.98	0.31	0.000801	1.5	16.18	0.24
	SCHE11@15	427	31409	74	280	6	0.426	1.7	0.000933	1.6	9	0.000818	1.7	16.53	0.28	0.000851	1.6	17.19	0.28
	SCHE11@19	650	22198	34	1132	11	0.093	2.6	0.000890	2.6	1	0.000860	2.6	17.37	0.45	0.000878	2.6	17.73	0.47

	SCHE1@21	704	20090	29	1036	10	0.086	2.2	0.000849	2.6	2	0.000818	2.6	16.52	0.42	0.000836	2.6	16.89	0.44
	SCHE1@22	815	10348	13	1078	15	0.078	2.3	0.000846	2.6	3	0.000818	2.6	16.52	0.43	0.000825	2.6	16.66	0.44
	SCHE1@23	417	36731	88	1703	12	0.133	2.8	0.000865	2.6	1	0.000847	2.6	17.11	0.44	0.000855	2.6	17.28	0.45
	SCHE1@24	656	16727	25	1183	11	0.083	2.3	0.000848	2.6	2	0.000821	2.6	16.59	0.43	0.000834	2.6	16.86	0.44
	SCHE1@27	720	19708	27	976	10	0.108	2.0	0.000831	2.6	3	0.000798	2.6	16.13	0.41	0.000809	2.6	16.35	0.43
	SCHE1@28	420	36082	86	1062	9	0.169	2.4	0.000860	2.6	2	0.000829	2.6	16.76	0.43	0.000846	2.6	17.08	0.45
	SCHE1@29	513	37241	73	665	9	0.231	2.2	0.000854	2.6	4	0.000804	2.5	16.25	0.41	0.000823	2.6	16.64	0.44
	SCHE1@30	588	23098	39	738	10	0.122	2.3	0.000808	2.7	3	0.000765	2.6	15.46	0.40	0.000787	2.7	15.89	0.43
	SCHE1@31	435	37275	86	945	8	0.176	2.0	0.000817	2.6	2	0.000784	2.5	15.84	0.40	0.000800	2.6	16.16	0.43
	SCHE1@33	678	12021	18	1406	18	0.060	2.6	0.000800	2.2	1	0.000778	2.2	15.73	0.35	0.000792	2.2	16.00	0.36
	SCHE1@34	996	8782	9	2159	31	0.056	3.1	0.000807	2.3	1	0.000793	2.3	16.02	0.37	0.000796	2.3	16.08	0.37

A	HOPF2@15	82	61530	749	720	4	0.611	2.2	0.000560	2.37	2	0.000542	2.3	10.94	0.25	0.000546	2.4	11.03	0.26
	HOPF2@16	69	33784	490	619	4	0.641	2.6	0.000647	2.36	3	0.000620	2.3	12.54	0.29	0.000625	2.4	12.63	0.30
	HOPF2@17	97	33439	343	972	7	0.571	3.6	0.000663	2.91	2	0.000643	2.8	13.00	0.37	0.000647	2.9	13.08	0.38
	HOPF2@18	77	40713	530	274	3	0.761	1.5	0.000762	2.67	11	0.000667	2.4	13.48	0.32	0.000677	2.7	13.67	0.37
	HOPF2@19	120	62586	520	840	5	0.572	2.8	0.000623	3.49	2	0.000605	3.4	12.23	0.42	0.000609	3.5	12.30	0.43
	HOPF2@20	120	49522	413	853	7	0.590	3.7	0.000594	2.39	3	0.000571	2.3	11.54	0.27	0.000577	2.4	11.67	0.28
	HOPF2@21	173	37157	215	1309	13	0.585	6.1	0.000683	2.78	2	0.000667	2.7	13.47	0.37	0.000667	2.8	13.47	0.38
B	HOPF2@07	49	28763	591	480	5	0.735	2.5	0.000600	2.26	6	0.000559	2.1	11.29	0.24	0.000561	2.3	11.35	0.26
	HOPF2@08	46	28779	627	495	5	0.740	2.3	0.000630	2.20	6	0.000593	2.1	11.98	0.25	0.000592	2.2	11.97	0.26
	HOPF2@09	55	32338	593	429	4	0.721	1.9	0.000649	2.17	7	0.000603	2.1	12.18	0.25	0.000604	2.2	12.20	0.27
	HOPF2@10	76	22645	296	595	9	0.714	4.1	0.000637	3.67	6	0.000597	3.5	12.06	0.42	0.000596	3.7	12.05	0.44
	HOPF2@11	40	28273	701	140	3	0.810	1.2	0.000782	3.59	24	0.000580	2.8	11.72	0.32	0.000597	3.6	12.07	0.43
	HOPF2@12	38	26357	689	346	4	0.780	2.1	0.000694	2.20	9	0.000628	2.1	12.68	0.26	0.000628	2.2	12.69	0.28
	HOPF2@13	52	40578	775	305	3	0.777	1.7	0.000688	2.54	10	0.000615	2.3	12.43	0.29	0.000616	2.5	12.45	0.32
C	HOPF2@14	55	27790	505	261	3	0.773	1.6	0.000708	2.22	12	0.000614	2.0	12.41	0.25	0.000626	2.2	12.65	0.28
	HOPF2@01	40	23096	582	683	6	0.646	3.0	0.000591	2.20	4	0.000565	2.1	11.43	0.24	0.000567	2.2	11.45	0.25
	HOPF2@02	42	25870	612	584	6	0.682	3.3	0.000619	2.23	4	0.000590	2.2	11.92	0.26	0.000594	2.2	11.99	0.27
	HOPF2@03	45	29023	642	538	5	0.659	2.6	0.000647	2.27	4	0.000617	2.2	12.46	0.27	0.000619	2.3	12.50	0.28
	HOPF2@04	50	30246	610	510	4	0.677	2.3	0.000656	2.35	5	0.000621	2.2	12.54	0.28	0.000622	2.3	12.58	0.30

	HOPF2@05	57	32908	577	451	4	0.690	2.1	0.000670	2.48	6	0.000627	2.4	12.67	0.30	0.000629	2.5	12.70	0.32
	HOPF2@06	58	28865	500	481	4	0.680	2.1	0.000642	2.18	6	0.000602	2.1	12.16	0.25	0.000602	2.2	12.17	0.27
A	GART1@07	232	13668	59	1022	10	0.175	2.0	0.000830	2.3	2	0.000799	2.3	16.14	0.36	0.000811	2.3	16.38	0.38
	GART1@08	302	9312	31	523	8	0.208	1.6	0.000831	2.3	6	0.000769	2.3	15.54	0.35	0.000785	2.3	15.85	0.37
	GART1@09	206	14195	69	1054	9	0.173	2.0	0.000815	2.0	2	0.000785	2.0	15.86	0.31	0.000799	2.0	16.14	0.32
	GART1@10	199	17962	90	716	7	0.192	2.1	0.000838	2.1	2	0.000793	2.1	16.01	0.33	0.000823	2.1	16.63	0.36
	GART1@11	221	9789	44	881	12	0.162	2.5	0.000813	2.3	3	0.000778	2.3	15.71	0.36	0.000792	2.3	16.00	0.38
	GART1@22	86	8047	93	412	8	0.321	1.8	0.000889	2.0	6	0.000806	2.0	16.29	0.32	0.000835	2.0	16.86	0.34
	GART1@23	142	9137	65	454	8	0.317	1.8	0.000858	1.9	6	0.000786	1.9	15.88	0.29	0.000810	1.9	16.36	0.31
	GART1@24	133	7292	55	371	8	0.322	1.8	0.000864	2.3	7	0.000774	2.2	15.64	0.35	0.000808	2.3	16.32	0.38
	GART1@25	132	8048	61	435	9	0.318	2.0	0.000855	2.4	6	0.000779	2.3	15.74	0.37	0.000804	2.5	16.24	0.40
	GART1@26	139	9550	69	512	8	0.328	1.8	0.000866	2.1	6	0.000800	2.1	16.17	0.33	0.000816	2.1	16.49	0.35
B	GART1@01	14	7467	551	446	9	0.626	2.3	0.000807	2.3	6	0.000737	2.3	14.89	0.34	0.000758	2.4	15.32	0.37
	GART1@02	16	11180	718	285	14	0.707	3.8	0.000774	2.3	7	0.000669	2.7	13.51	0.37	0.000716	2.4	14.47	0.35
	GART1@04	28	11198	401	967	11	0.299	3.0	0.000783	2.2	1	0.000752	2.2	15.19	0.33	0.000771	2.2	15.59	0.35
	GART1@05	31	13066	424	1149	11	0.232	3.4	0.000731	3.0	1	0.000707	2.9	14.28	0.42	0.000724	3.0	14.64	0.44
	GART1@17	86	22525	263	679	7	0.397	1.5	0.000854	1.8	4	0.000806	1.8	16.28	0.29	0.000820	1.8	16.56	0.30
	GART1@18	110	23948	218	894	7	0.307	1.7	0.000820	1.8	2	0.000784	1.8	15.84	0.28	0.000799	1.8	16.15	0.30
	GART1@19	14	7182	501	832	14	0.437	3.9	0.000778	2.2	2	0.000742	2.2	14.98	0.32	0.000763	2.2	15.42	0.34
	GART1@20	108	19460	180	740	7	0.321	1.8	0.000828	2.0	3	0.000785	2.0	15.86	0.31	0.000805	2.0	16.26	0.33
	GART1@21	106	23334	220	775	7	0.330	1.6	0.000839	2.0	3	0.000797	2.0	16.10	0.32	0.000816	2.0	16.48	0.34
	<i>GART1@03</i>	<i>16</i>	<i>15175</i>	<i>927</i>	<i>53</i>	<i>3</i>	<i>0.802</i>	<i>0.8</i>	<i>0.001916</i>	<i>11.9</i>	<i>62</i>	<i>0.000516</i>	<i>4.1</i>	<i>10.43</i>	<i>0.43</i>	<i>0.000729</i>	<i>17.7</i>	<i>14.72</i>	<i>2.61</i>
<i>GART1@04</i>	<i>19</i>	<i>13099</i>	<i>696</i>	<i>69</i>	<i>4</i>	<i>0.810</i>	<i>1.0</i>	<i>0.001303</i>	<i>7.8</i>	<i>48</i>	<i>0.000571</i>	<i>4.2</i>	<i>11.53</i>	<i>0.48</i>	<i>0.000679</i>	<i>12.9</i>	<i>13.72</i>	<i>1.76</i>	
<i>GART1@06</i>	<i>93</i>	<i>12315</i>	<i>133</i>	<i>2322</i>	<i>26</i>	<i>0.182</i>	<i>6.4</i>	<i>0.000453</i>	<i>4.0</i>	<i>1</i>	<i>0.000446</i>	<i>3.9</i>	<i>9.01</i>	<i>0.35</i>	<i>0.000450</i>	<i>4.0</i>	<i>9.09</i>	<i>0.36</i>	
	NOWA3@01	99	7183	73	397	10	0.433	2.1	0.000894	4.3	9	0.000807	4.0	16.31	0.65	0.000809	4.3	16.35	0.71
	NOWA3@02	111	7973	72	205	7	0.569	1.8	0.000864	3.8	15	0.000704	3.4	14.23	0.48	0.000733	3.8	14.80	0.57
	NOWA3@03	95	10612	112	506	9	0.474	2.1	0.000852	3.8	7	0.000787	3.6	15.90	0.57	0.000793	3.8	16.03	0.61
	NOWA3@04	93	10175	109	103	5	0.724	1.2	0.001132	5.8	37	0.000707	4.1	14.29	0.58	0.000713	5.9	14.40	0.84
	NOWA3@05	107	6658	62	94	5	0.695	1.4	0.001145	5.8	38	0.000674	4.1	13.62	0.56	0.000711	5.9	14.37	0.84

A	NOWA3@06	146	7715	53	176	9	0.606	2.0	0.000875	5.6	22	0.000683	4.8	13.80	0.66	0.000681	5.6	13.75	0.77
	NOWA3@07	162	4216	26	137	7	0.461	1.6	0.001023	4.8	27	0.000734	4.0	14.84	0.59	0.000743	4.8	15.01	0.72
	NOWA3@09	187	2571	14	81	7	0.445	1.7	0.001077	5.9	36	0.000565	4.4	11.42	0.50	0.000686	5.9	13.86	0.82
	NOWA3@10	178	3925	22	124	7	0.478	1.5	0.001053	6.0	30	0.000726	4.6	14.68	0.68	0.000738	6.0	14.91	0.89
	NOWA3@11	106	5924	56	188	7	0.477	1.8	0.000922	4.7	17	0.000732	4.0	14.80	0.59	0.000761	4.7	15.38	0.72
	NOWA3@22	106	6470	61	1230	19	0.133	3.9	0.000837	1.2	2	0.000811	1.3	16.38	0.22	0.000824	1.2	16.65	0.20
	NOWA3@23	94	9038	96	1036	14	0.300	2.7	0.000864	0.9	4	0.000832	1.0	16.81	0.18	0.000834	0.9	16.85	0.16
	NOWA3@24	100	9053	90	896	14	0.265	3.1	0.000786	1.0	3	0.000752	1.2	15.19	0.18	0.000765	1.1	15.45	0.16
	NOWA3@25	91	7689	84	1010	15	0.176	3.6	0.000857	0.9	2	0.000824	1.0	16.65	0.17	0.000842	0.9	17.01	0.15
B	NOWA3@17	192	9482	50	555	10	0.290	1.7	0.000859	3.7	7	0.000799	3.5	16.15	0.57	0.000799	3.7	16.15	0.61
	NOWA3@18	193	8656	45	388	8	0.288	1.7	0.000838	3.8	8	0.000755	3.5	15.24	0.53	0.000774	3.8	15.64	0.59
	NOWA3@19	179	11023	62	531	9	0.286	1.7	0.000832	3.9	6	0.000771	3.7	15.58	0.57	0.000786	3.9	15.87	0.62
	NOWA3@20	189	10600	56	451	8	0.278	1.7	0.000836	3.9	6	0.000765	3.6	15.45	0.56	0.000786	3.9	15.87	0.62
	NOWA3@21	212	10750	51	225	13	0.368	2.5	0.000907	4.0	17	0.000752	4.0	15.18	0.60	0.000757	4.0	15.30	0.61
C	NOWA3@12	50	12537	253	347	7	0.547	1.8	0.000868	3.9	8	0.000771	3.6	15.58	0.56	0.000796	3.9	16.08	0.63
	NOWA3@13	34	9676	287	371	8	0.556	1.9	0.000839	3.8	8	0.000751	3.5	15.18	0.54	0.000773	3.8	15.62	0.60
	NOWA3@14	39	10246	260	323	8	0.534	2.0	0.000783	3.9	8	0.000689	3.6	13.93	0.50	0.000723	3.9	14.61	0.58
	NOWA3@15	48	11123	231	498	10	0.504	2.1	0.000777	3.8	7	0.000717	3.6	14.48	0.52	0.000726	3.8	14.66	0.56
	NOWA3@16	48	10718	225	349	9	0.590	2.0	0.000745	4.4	9	0.000663	4.0	13.39	0.53	0.000677	4.4	13.68	0.60
	NOWA3@08	212	3097	15	123	8	0.375	1.7	0.001111	6.8	29	0.000763	5.3	15.41	0.81	0.000788	6.9	15.93	1.09
A	GART3@13	85	8547	101	226	9	0.537	2.1	0.000901	2.6	14	0.000747	2.7	15.09	0.41	0.000775	2.6	15.65	0.41
	GART3@14	112	9936	89	207	10	0.541	2.4	0.000879	2.8	14	0.000715	3.0	14.46	0.43	0.000760	2.9	15.36	0.44
	GART3@15	95	9197	97	184	10	0.595	2.1	0.000969	3.9	19	0.000769	3.7	15.54	0.58	0.000781	3.9	15.78	0.62
	GART3@16	94	9295	99	183	9	0.585	1.9	0.000917	3.2	20	0.000723	3.2	14.61	0.47	0.000733	3.3	14.82	0.48
	GART3@17	159	9327	59	179	13	0.621	2.6	0.000881	2.9	25	0.000691	3.7	13.95	0.51	0.000662	3.0	13.38	0.40
	GART3@18	161	8380	52	128	11	0.623	2.6	0.000904	2.9	25	0.000638	4.0	12.90	0.51	0.000676	3.0	13.65	0.41
	GART3@07	251	11739	47	318	10	0.312	2.1	0.000865	2.8	8	0.000760	2.7	15.36	0.41	0.000794	2.8	16.04	0.44
	GART3@08	318	9593	30	219	11	0.374	2.3	0.000836	2.7	15	0.000689	3.0	13.92	0.41	0.000711	2.7	14.37	0.39
	GART3@09	335	8995	27	220	11	0.379	2.2	0.000858	2.7	17	0.000711	3.0	14.37	0.44	0.000714	2.8	14.43	0.40
	GART3@10	318	9819	31	221	11	0.377	2.2	0.000875	2.8	15	0.000722	3.0	14.58	0.44	0.000745	2.9	15.05	0.43

B	GART3@11	387	10683	28	244	13	0.326	2.8	0.000829	2.7	11	0.000703	3.1	14.20	0.44	0.000738	2.7	14.92	0.41
	GART3@12	484	11366	24	210	13	0.388	3.1	0.000864	2.6	12	0.000712	3.3	14.38	0.47	0.000760	2.6	15.35	0.40
	GART3@19	129	5307	41	100	7	0.543	1.7	0.001103	4.2	31	0.000681	3.9	13.75	0.53	0.000756	4.3	15.27	0.65
	GART3@20	251	4358	17	122	10	0.408	2.1	0.000990	3.6	29	0.000676	4.1	13.65	0.56	0.000707	3.7	14.29	0.53
	GART3@21	247	13787	56	218	8	0.411	1.9	0.000901	2.7	12	0.000742	2.7	14.99	0.40	0.000797	2.7	16.09	0.44
	GART3@22	431	10631	25	215	13	0.466	2.5	0.000880	2.6	19	0.000734	3.3	14.83	0.49	0.000712	2.7	14.38	0.39
	GART3@23	240	12846	54	247	10	0.414	2.2	0.000879	2.9	12	0.000745	2.9	15.05	0.44	0.000773	2.9	15.61	0.45
C	GART3@01	114	7936	69	285	12	0.352	2.7	0.000762	2.6	10	0.000659	2.8	13.31	0.37	0.000689	2.6	13.92	0.36
	GART3@03	183	3983	22	100	13	0.392	3.3	0.000778	2.9	23	0.000477	5.4	9.65	0.52	0.000602	3.1	12.17	0.37
	GART3@04	176	3297	19	138	17	0.392	3.3	0.000802	2.9	26	0.000578	5.1	11.67	0.60	0.000595	3.1	12.02	0.37
	GART3@05	123	4784	39	191	14	0.393	2.9	0.000770	2.8	17	0.000614	3.6	12.41	0.44	0.000639	2.8	12.92	0.36
	GART3@06	166	4521	27	197	17	0.374	3.5	0.000763	2.6	17	0.000623	4.0	12.58	0.51	0.000630	2.7	12.72	0.34
	<i>GART3@02</i>	<i>161</i>	<i>3479</i>	<i>22</i>	<i>109</i>	<i>12</i>	<i>0.449</i>	<i>2.6</i>	<i>0.000824</i>	<i>8.0</i>	<i>32</i>	<i>0.000531</i>	<i>6.8</i>	<i>10.73</i>	<i>0.73</i>	<i>0.000558</i>	<i>8.1</i>	<i>11.28</i>	<i>0.91</i>
	STEL2@01	395	15567	39	1346	11	0.106	2.0	0.000873	2.12	2	0.000848	2.1	17.14	0.36	0.000859	2.1	17.36	0.37
STEL2@02	403	16229	40	1096	10	0.113	2.0	0.000862	2.11	2	0.000833	2.1	16.82	0.35	0.000847	2.1	17.11	0.36	
STEL2@03	417	16643	40	1022	9	0.115	1.9	0.000869	2.04	2	0.000836	2.0	16.89	0.34	0.000854	2.0	17.25	0.35	
STEL2@04	376	17989	48	1436	11	0.097	2.2	0.000854	2.15	1	0.000831	2.1	16.79	0.35	0.000844	2.1	17.05	0.37	
STEL2@05	348	7706	22	844	13	0.101	2.2	0.000860	2.50	3	0.000820	2.5	16.57	0.41	0.000837	2.5	16.92	0.42	
STEL2@06	288	6287	22	700	13	0.125	2.3	0.000892	1.90	4	0.000843	1.9	17.02	0.33	0.000857	1.9	17.32	0.33	
STEL2@07	257	5814	23	556	12	0.176	2.0	0.000915	2.06	6	0.000851	2.1	17.20	0.36	0.000858	2.1	17.34	0.36	
STEL2@08	387	5851	15	730	13	0.090	2.3	0.000874	2.49	3	0.000830	2.5	16.76	0.41	0.000848	2.5	17.13	0.43	
STEL2@09	443	5143	12	649	14	0.080	2.3	0.000859	2.51	3	0.000810	2.5	16.37	0.41	0.000832	2.5	16.82	0.43	
STEL2@10	295	6041	20	689	14	0.118	2.4	0.000875	2.18	3	0.000828	2.2	16.73	0.37	0.000844	2.2	17.06	0.37	
STEL2@11	370	7478	20	1151	15	0.088	2.4	0.000858	2.11	2	0.000829	2.1	16.76	0.35	0.000841	2.1	16.99	0.36	
STEL2@12	548	11690	21	755	10	0.103	1.8	0.000884	1.96	3	0.000838	1.9	16.94	0.33	0.000859	2.0	17.36	0.34	
STEL2@13	579	10095	17	798	11	0.101	1.8	0.000871	2.26	3	0.000829	2.2	16.75	0.37	0.000844	2.3	17.06	0.39	
STEL2@14	601	10283	17	745	10	0.099	1.8	0.000869	2.15	3	0.000824	2.1	16.65	0.35	0.000843	2.2	17.03	0.37	
STEL2@15	352	19439	55	962	9	0.138	2.0	0.000864	1.83	2	0.000829	1.8	16.75	0.30	0.000848	1.8	17.14	0.31	
STEL2@16	455	10595	23	676	10	0.127	1.8	0.000891	2.06	3	0.000840	2.0	16.96	0.34	0.000861	2.1	17.39	0.36	
STEL2@17	387	8068	21	902	13	0.091	2.2	0.000864	2.03	2	0.000827	2.0	16.71	0.34	0.000846	2.0	17.10	0.35	

STEI2@18	348	11391	33	1180	13	0.101	2.5	0.000846	2.09	1	0.000819	2.1	16.55	0.34	0.000835	2.1	16.87	0.35
STEI2@19	339	12077	36	1048	11	0.095	2.3	0.000876	2.20	1	0.000844	2.2	17.05	0.37	0.000864	2.2	17.45	0.39
STEI2@20	323	7488	23	943	13	0.084	2.6	0.000871	2.04	1	0.000835	2.0	16.87	0.34	0.000858	2.0	17.33	0.35

A	KNOR1@19	149	12269	82	466	7	0.392	3.5	0.000558	2.34	4	0.000527	2.3	10.64	0.24	0.000535	2.3	10.81	0.25
	KNOR1@20	181	9307	52	285	7	0.488	3.2	0.000587	3.28	11	0.000515	3.1	10.41	0.32	0.000522	3.3	10.55	0.35
	KNOR1@21	239	9337	39	642	13	0.400	5.1	0.000604	3.67	5	0.000574	3.6	11.60	0.42	0.000572	3.7	11.56	0.42
	KNOR1@22	172	8289	48	512	9	0.321	4.1	0.000570	2.76	4	0.000537	2.7	10.86	0.29	0.000545	2.8	11.01	0.30
	KNOR1@24	194	7199	37	605	13	0.268	5.3	0.000549	3.18	4	0.000517	3.1	10.44	0.32	0.000529	3.2	10.68	0.34
B	KNOR1@01	32	7767	246	189	5	0.737	2.5	0.000615	2.18	18	0.000498	2.1	10.06	0.21	0.000505	2.2	10.21	0.23
	KNOR1@02	35	6107	175	197	6	0.731	2.9	0.000637	2.60	18	0.000521	2.5	10.53	0.26	0.000524	2.6	10.59	0.28
	KNOR1@03	36	9885	273	115	4	0.784	1.8	0.000767	2.66	32	0.000518	2.3	10.48	0.24	0.000518	2.7	10.47	0.29
	KNOR1@05	27	9535	356	102	3	0.786	1.4	0.000869	2.35	36	0.000560	1.9	11.32	0.22	0.000558	2.4	11.28	0.27
	KNOR1@06	33	9203	277	167	4	0.734	2.1	0.000661	2.18	19	0.000522	2.0	10.54	0.21	0.000533	2.2	10.77	0.24
	KNOR1@07	33	4983	152	112	5	0.726	2.1	0.000768	2.20	31	0.000522	2.2	10.56	0.23	0.000527	2.3	10.64	0.25
	KNOR1@08	36	3783	105	136	6	0.652	2.8	0.000701	2.17	24	0.000516	2.4	10.42	0.25	0.000533	2.3	10.76	0.24
	KNOR1@09	39	5846	149	281	7	0.573	3.4	0.000577	2.30	11	0.000513	2.3	10.37	0.24	0.000514	2.3	10.38	0.24
	KNOR1@04	30	6902	234	95	3	0.759	1.6	0.000920	2.21	37	0.000555	1.9	11.21	0.22	0.000576	2.3	11.63	0.27
C	KNOR1@10	48	5633	118	428	11	0.495	5.2	0.000542	2.37	6	0.000499	2.4	10.07	0.24	0.000508	2.4	10.27	0.24
	KNOR1@11	48	4611	96	444	12	0.478	5.6	0.000560	2.48	6	0.000525	2.6	10.61	0.27	0.000528	2.5	10.67	0.27
	KNOR1@12	57	4583	81	399	11	0.355	5.3	0.000540	2.18	5	0.000498	2.3	10.06	0.23	0.000513	2.2	10.36	0.23
	KNOR1@13	54	4104	77	445	11	0.331	5.0	0.000541	2.29	5	0.000500	2.4	10.10	0.24	0.000513	2.3	10.37	0.24
	KNOR1@14	56	6093	108	729	13	0.285	5.6	0.000516	2.19	3	0.000495	2.2	10.00	0.22	0.000501	2.2	10.12	0.22
	KNOR1@15	76	6847	91	639	11	0.237	5.4	0.000529	2.19	2	0.000508	2.2	10.27	0.23	0.000515	2.2	10.41	0.23
	KNOR1@16	65	5872	91	524	11	0.224	5.8	0.000529	2.17	2	0.000503	2.2	10.17	0.23	0.000517	2.2	10.45	0.23
	KNOR1@18	77	8867	114	628	10	0.141	5.7	0.000559	2.52	1	0.000544	2.6	11.00	0.28	0.000552	2.5	11.15	0.28
KNOR1@17	73	6281	86	585	10	0.191	5.4	0.000590	2.24	2	0.000564	2.3	11.41	0.26	0.000578	2.2	11.68	0.26	

Eastern Tauern Window

	KAIS6@29	12	32285	2726	324	2	0.816	1.1	0.001135	2.68	11	0.001014	2.4	20.48	0.49	0.001015	2.7	20.51	0.55
--	-----------------	----	-------	------	-----	---	-------	-----	----------	------	----	----------	-----	-------	------	----------	-----	--------------	-------------

A	KAIS6@37	10	35152	3587	322	2	0.817	1.1	0.001192	2.71	10	0.001065	2.4	21.51	0.52	0.001072	2.7	21.66	0.59
	KAIS6@38	10	35481	3480	428	3	0.797	1.4	0.001137	2.74	8	0.001046	2.5	21.13	0.54	0.001045	2.8	21.12	0.58
	KAIS6@39	10	31600	3326	316	3	0.820	1.3	0.001154	2.73	11	0.001022	2.4	20.65	0.50	0.001030	2.7	20.81	0.57
	KAIS6@41	8	32642	4280	351	2	0.824	1.2	0.001173	2.74	9	0.001057	2.5	21.36	0.53	0.001063	2.8	21.48	0.59
	KAIS6@42	6	29873	4677	292	2	0.836	1.2	0.001200	2.69	11	0.001054	2.4	21.28	0.51	0.001066	2.7	21.54	0.58
B	KAIS6@15	5	21644	4568	142	2	0.833	0.9	0.001399	2.69	25	0.001031	2.0	20.83	0.43	0.001045	2.8	21.12	0.59
	KAIS6@16	5	22052	4771	161	2	0.831	0.9	0.001329	2.69	23	0.001020	2.1	20.61	0.44	0.001022	2.7	20.65	0.57
	KAIS6@17	5	25100	4752	189	2	0.825	1.0	0.001299	2.73	19	0.001046	2.2	21.12	0.47	0.001049	2.8	21.20	0.59
	KAIS6@18	5	25260	4905	148	2	0.827	0.9	0.001392	2.81	26	0.001040	2.2	21.01	0.45	0.001025	2.9	20.71	0.61
	KAIS6@19	5	23495	5173	148	2	0.825	0.9	0.001390	2.75	24	0.001038	2.1	20.96	0.44	0.001053	2.8	21.28	0.60
	KAIS6@20	5	24260	5377	157	2	0.829	0.9	0.001351	2.83	24	0.001032	2.2	20.85	0.46	0.001033	2.9	20.86	0.61
	KAIS6@21	5	25950	5040	155	2	0.837	0.9	0.001320	2.73	24	0.001003	2.1	20.27	0.43	0.001007	2.8	20.35	0.57
	KAIS6@22	4	20175	4625	134	2	0.813	0.9	0.001424	2.76	27	0.001034	2.1	20.88	0.43	0.001043	2.8	21.07	0.60
	KAIS6@23	3	18427	5349	153	2	0.828	1.0	0.001353	2.82	24	0.001028	2.2	20.76	0.46	0.001027	2.9	20.74	0.60
	KAIS6@24	4	17328	4822	178	2	0.830	1.1	0.001313	2.69	21	0.001045	2.2	21.11	0.46	0.001041	2.7	21.02	0.58
	KAIS6@25	5	17901	3588	154	2	0.833	0.9	0.001366	2.77	24	0.001042	2.2	21.05	0.46	0.001039	2.8	20.98	0.59
	KAIS6@26	4	19477	5281	167	2	0.820	1.0	0.001304	2.75	22	0.001020	2.2	20.60	0.46	0.001017	2.8	20.56	0.58
	KAIS6@27	4	19595	5290	165	2	0.821	1.1	0.001325	2.72	22	0.001030	2.2	20.80	0.45	0.001036	2.8	20.93	0.58
	KAIS6@28	3	17683	5368	162	2	0.817	1.0	0.001354	2.76	23	0.001043	2.2	21.06	0.46	0.001041	2.8	21.02	0.59
	KAIS6@31	3	19464	6314	207	2	0.826	1.2	0.001275	2.67	17	0.001049	2.2	21.19	0.48	0.001059	2.7	21.39	0.58
	KAIS6@32	3	17623	5729	145	2	0.823	1.0	0.001352	2.75	26	0.001007	2.1	20.35	0.43	0.001003	2.8	20.26	0.57
	KAIS6@33	4	23433	5395	191	2	0.819	1.0	0.001257	2.79	18	0.001018	2.3	20.56	0.47	0.001026	2.8	20.73	0.59
	KAIS6@34	3	22517	6923	175	2	0.836	0.9	0.001289	2.73	21	0.001016	2.2	20.52	0.45	0.001015	2.8	20.51	0.57
	KAIS6@35	4	23426	6129	175	2	0.827	0.9	0.001299	2.72	21	0.001025	2.2	20.70	0.45	0.001031	2.8	20.82	0.58
	KAIS6@36	4	24762	6924	169	2	0.821	0.9	0.001316	2.76	21	0.001031	2.2	20.83	0.46	0.001034	2.8	20.89	0.59
	KAIS6@43	4	19511	4948	229	2	0.828	1.2	0.001210	2.76	15	0.001024	2.4	20.68	0.49	0.001023	2.8	20.66	0.58
	KAIS6@44	5	20543	3995	252	3	0.828	1.5	0.001177	2.72	14	0.001007	2.4	20.35	0.48	0.001009	2.8	20.39	0.56
	KAIS6@45	4	17366	4418	225	3	0.834	1.4	0.001269	2.67	15	0.001067	2.3	21.55	0.49	0.001076	2.7	21.73	0.59
	KAIS6@46	4	14595	3614	231	3	0.813	1.5	0.001284	2.70	15	0.001083	2.3	21.88	0.51	0.001094	2.7	22.11	0.61
	KAIS6@01	2	13078	6002	83	2	0.844	0.8	0.001865	2.70	46	0.001011	1.7	20.43	0.34	0.001001	3.1	20.21	0.63
	KAIS6@02	3	14140	4835	97	2	0.823	0.9	0.001682	2.76	40	0.001031	1.9	20.83	0.39	0.001012	3.0	20.44	0.62

C	KAIS6@05	3	10157	2957	96	2	0.837	1.0	0.001672	2.69	38	0.001010	1.9	20.41	0.38	0.001035	3.0	20.91	0.63
	KAIS6@06	4	15227	3566	104	2	0.828	1.0	0.001564	2.84	36	0.000995	2.0	20.11	0.40	0.000994	3.1	20.09	0.63
	KAIS6@09	3	10348	3946	74	1	0.828	0.7	0.002146	2.71	52	0.001030	1.5	20.81	0.32	0.001037	3.7	20.94	0.77
	KAIS6@10	3	12624	4224	90	2	0.828	0.9	0.001795	2.74	42	0.001037	1.8	20.96	0.37	0.001033	3.1	20.87	0.64
	KAIS6@12	3	10457	3171	91	2	0.822	1.0	0.001752	2.68	41	0.001020	1.8	20.61	0.37	0.001039	3.0	20.98	0.63
D	KAIS6@03	4	15947	3922	100	2	0.844	1.0	0.001524	2.91	39	0.000944	2.0	19.07	0.38	0.000924	3.2	18.67	0.59
	KAIS6@04	4	16156	3905	91	2	0.829	1.0	0.001531	3.25	40	0.000890	2.1	17.98	0.38	0.000923	3.5	18.65	0.66
	KAIS6@07	6	11981	2002	89	4	0.843	1.6	0.001562	2.89	44	0.000887	2.3	17.93	0.40	0.000877	3.7	17.71	0.65
	KAIS6@08	3	10466	3145	87	2	0.824	0.8	0.001711	2.68	44	0.000959	1.7	19.37	0.33	0.000956	3.1	19.31	0.59
	KAIS6@11	4	13094	3210	89	2	0.830	1.1	0.001493	2.92	42	0.000846	2.0	17.09	0.33	0.000870	3.3	17.58	0.58
	KAIS6@13	4	13271	3273	88	2	0.842	1.0	0.001621	2.84	41	0.000917	1.9	18.52	0.35	0.000950	3.3	19.19	0.63
	KAIS6@14	9	13459	1568	105	4	0.827	1.7	0.001323	3.57	33	0.000836	2.6	16.89	0.44	0.000881	3.8	17.79	0.68
	KAIS6@30	14	25376	1840	225	2	0.837	1.1	0.001130	2.68	16	0.000950	2.3	19.20	0.44	0.000951	2.7	19.22	0.52
	KAIS6@40	10	32326	3141	301	3	0.800	1.4	0.001094	2.93	12	0.000962	2.6	19.44	0.51	0.000967	3.0	19.53	0.58
	KAIS6@47	9	31411	3692	311	3	0.818	1.3	0.001069	2.68	11	0.000949	2.4	19.16	0.46	0.000955	2.7	19.28	0.52
	<i>KAIS6@48</i>	<i>13</i>	<i>18728</i>	<i>1403</i>	<i>217</i>	<i>3</i>	<i>0.836</i>	<i>1.5</i>	<i>0.001218</i>	<i>2.67</i>	<i>17</i>	<i>0.001014</i>	<i>2.3</i>	<i>20.49</i>	<i>0.47</i>	<i>0.001014</i>	<i>2.7</i>	<i>20.48</i>	<i>0.56</i>
	<i>KAIS6@49</i>	<i>13</i>	<i>18241</i>	<i>1449</i>	<i>248</i>	<i>3</i>	<i>0.813</i>	<i>1.3</i>	<i>0.001252</i>	<i>2.69</i>	<i>14</i>	<i>0.001072</i>	<i>2.3</i>	<i>21.66</i>	<i>0.51</i>	<i>0.001083</i>	<i>2.7</i>	<i>21.87</i>	<i>0.59</i>
	SALZ18@01	11	443	40	428	6	0.642	2.9	0.001001	2.30	8	0.000928	2.2	18.75	0.41	0.000921	2.31	18.61	0.43
	SALZ18@02	19	11907	639	515	6	0.546	3.0	0.000970	2.16	4	0.000914	2.1	18.46	0.39	0.000928	2.17	18.75	0.41
SALZ18@03	23	12452	552	1291	11	0.191	7.3	0.000859	2.25	1	0.000853	2.3	17.23	0.39	0.000854	2.25	17.25	0.39	
SALZ18@04	20	8334	407	800	10	0.246	6.5	0.000943	2.52	1	0.000909	2.5	18.36	0.46	0.000933	2.52	18.84	0.47	
SALZ18@05	28	6912	245	1239	12	0.235	6.6	0.000911	2.20	1	0.000903	2.2	18.24	0.41	0.000902	2.20	18.22	0.40	
SALZ18@06	11	2256	200	1200	13	0.314	7.5	0.000947	2.26	1	0.000941	2.3	19.00	0.44	0.000935	2.26	18.90	0.43	
SALZ18@07	23	9797	429	1862	19	0.208	9.6	0.000863	2.34	1	0.000858	2.4	17.33	0.41	0.000857	2.34	17.31	0.40	
SALZ18@08	20	4607	232	980	14	0.186	10.0	0.000880	2.39	1	0.000856	2.4	17.29	0.42	0.000874	2.39	17.66	0.42	
SALZ18@09	18	3952	224	1353	18	0.180	9.3	0.000942	2.42	1	0.000934	2.5	18.87	0.47	0.000934	2.42	18.88	0.46	
SALZ18@10	19	3681	189	894	18	0.178	10.2	0.000917	2.57	1	0.000889	2.6	17.96	0.47	0.000907	2.57	18.33	0.47	
SALZ18@11	13	1751	134	1123	15	0.312	7.3	0.000979	2.38	2	0.000962	2.4	19.44	0.47	0.000963	2.38	19.46	0.46	
SALZ18@12	17	4555	267	731	19	0.169	10.8	0.000922	2.74	1	0.000881	2.8	17.80	0.50	0.000910	2.74	18.39	0.50	
SALZ18@13	17	1752	106	617	27	0.207	11.1	0.000887	3.43	3	0.000850	3.8	17.18	0.65	0.000860	3.43	17.37	0.60	

SALZ18@14	22	1037	48	975	11	0.270	6.1	0.000953	2.24	1	0.000938	2.3	18.95	0.43	0.000941	2.24	19.01	0.43
SALZ18@15	37	9684	262	1073	14	0.224	7.5	0.000792	2.37	1	0.000781	2.4	15.79	0.38	0.000783	2.37	15.81	0.37
LOHN4@01	14	14552	1076	79	1	0.826	0.7	0.001981	2.96	47	0.001031	1.7	20.84	0.35	0.001059	3.57	21.39	0.76
LOHN4@02	39	25804	662	272	3	0.779	1.4	0.001112	3.21	13	0.000964	2.8	19.47	0.55	0.000969	3.24	19.58	0.63
LOHN4@03	11	12883	1175	151	2	0.805	1.2	0.001356	2.67	24	0.001026	2.1	20.73	0.44	0.001033	2.76	20.86	0.58
LOHN4@04	16	16561	1017	173	2	0.820	1.2	0.001332	2.87	22	0.001051	2.3	21.23	0.49	0.001045	2.96	21.12	0.63
LOHN4@07	34	35456	1048	338	2	0.779	1.1	0.001218	2.68	10	0.001094	2.4	22.11	0.53	0.001097	2.69	22.16	0.60
LOHN4@08	31	32345	1044	312	2	0.782	1.0	0.001208	2.75	11	0.001074	2.5	21.70	0.53	0.001070	2.77	21.62	0.60
LOHN4@09	33	34180	1040	323	2	0.790	1.1	0.001224	2.70	11	0.001094	2.4	22.09	0.54	0.001092	2.71	22.07	0.60
LOHN4@10	33	35690	1072	349	2	0.788	1.1	0.001171	2.68	10	0.001058	2.4	21.38	0.52	0.001060	2.69	21.41	0.57
LOHN4@11	34	29955	888	355	3	0.796	1.3	0.001085	2.67	10	0.000977	2.4	19.75	0.48	0.000977	2.68	19.74	0.53
LOHN4@12	27	29155	1065	366	3	0.776	1.3	0.001185	2.68	9	0.001078	2.5	21.77	0.53	0.001082	2.69	21.86	0.59
LOHN4@13	26	23964	935	97	2	0.823	0.7	0.001750	2.99	39	0.001071	1.9	21.64	0.42	0.001066	3.32	21.54	0.72
LOHN4@14	28	22365	792	156	2	0.806	1.0	0.001418	2.83	23	0.001087	2.2	21.97	0.49	0.001089	2.96	22.01	0.65
LOHN4@15	24	20864	866	523	4	0.742	1.9	0.001109	2.69	6	0.001040	2.5	21.00	0.53	0.001044	2.70	21.09	0.57
LOHN4@16	30	23937	797	575	4	0.728	2.2	0.001062	2.75	5	0.001003	2.6	20.25	0.53	0.001006	2.76	20.33	0.56
LOHN4@19	27	21599	807	299	3	0.788	1.3	0.001221	2.71	12	0.001075	2.4	21.71	0.52	0.001080	2.72	21.82	0.59
LOHN4@20	29	23422	801	350	3	0.785	1.4	0.001156	2.67	10	0.001042	2.4	21.06	0.51	0.001041	2.68	21.02	0.56
LOHN4@21	16	17205	1046	171	2	0.798	1.0	0.001354	2.70	22	0.001064	2.2	21.49	0.47	0.001060	2.76	21.41	0.59
LOHN4@22	17	16983	991	165	2	0.810	1.1	0.001359	2.76	22	0.001055	2.2	21.31	0.47	0.001057	2.82	21.35	0.60
LOHN4@23	16	17269	1091	162	2	0.819	1.0	0.001388	2.79	23	0.001074	2.2	21.70	0.48	0.001065	2.85	21.52	0.61
LOHN4@24	20	21768	1108	176	2	0.810	1.1	0.001258	2.87	22	0.000990	2.3	20.00	0.46	0.000985	2.93	19.90	0.58
LOHN4@25	18	15361	875	174	3	0.823	1.2	0.001232	2.68	21	0.000969	2.2	19.58	0.43	0.000979	2.74	19.77	0.54
LOHN4@26	15	17857	1172	172	2	0.806	1.1	0.001276	2.68	21	0.001001	2.2	20.21	0.44	0.001012	2.73	20.44	0.56
LOHN4@27	27	26405	974	184	2	0.819	0.9	0.001317	2.72	19	0.001056	2.2	21.34	0.47	0.001064	2.76	21.50	0.59
LOHN4@28	28	27181	955	190	2	0.816	0.9	0.001324	2.80	20	0.001068	2.3	21.58	0.49	0.001066	2.84	21.53	0.61
LOHN4@29	27	25484	955	191	2	0.809	1.0	0.001304	2.85	20	0.001051	2.3	21.22	0.50	0.001048	2.90	21.18	0.61
LOHN4@30	27	25099	915	190	2	0.798	0.9	0.001322	2.71	19	0.001067	2.2	21.55	0.48	0.001068	2.75	21.58	0.59
LOHN4@31	30	25226	855	433	3	0.777	1.6	0.001235	2.67	8	0.001139	2.5	23.00	0.57	0.001134	2.68	22.92	0.61
LOHN4@32	36	21812	606	287	4	0.797	1.7	0.001212	2.70	13	0.001061	2.4	21.43	0.52	0.001053	2.73	21.27	0.58

A

	LOHN4@33	27	23182	856	199	2	0.805	1.0	0.001233	2.67	18	0.001002	2.2	20.24	0.45	0.001011	2.71	20.42	0.55
	LOHN4@34	26	24807	948	188	2	0.812	1.0	0.001293	2.71	19	0.001043	2.2	21.06	0.47	0.001044	2.75	21.09	0.58
	LOHN4@35	25	23076	925	174	2	0.812	0.9	0.001327	3.07	21	0.001045	2.5	21.11	0.52	0.001052	3.14	21.26	0.67
	LOHN4@36	26	25326	972	190	2	0.786	0.9	0.001308	2.73	19	0.001052	2.2	21.25	0.47	0.001061	2.77	21.43	0.59
	LOHN4@37	27	26268	980	210	2	0.802	1.0	0.001282	2.78	17	0.001062	2.3	21.45	0.50	0.001061	2.81	21.43	0.60
	LOHN4@38	27	27571	1016	218	2	0.812	1.0	0.001239	2.72	16	0.001033	2.3	20.87	0.48	0.001040	2.75	21.02	0.58
	LOHN4@39	26	25481	988	207	2	0.806	0.9	0.001272	2.69	18	0.001047	2.2	21.16	0.48	0.001044	2.72	21.08	0.57
	LOHN4@40	26	26144	1007	211	2	0.814	1.0	0.001245	2.78	17	0.001029	2.3	20.78	0.48	0.001032	2.81	20.85	0.59
	LOHN4@41	19	24124	1248	221	2	0.800	1.0	0.001271	2.72	17	0.001061	2.3	21.44	0.49	0.001057	2.75	21.35	0.59
	LOHN4@42	19	23602	1235	226	2	0.816	1.1	0.001279	2.74	16	0.001078	2.3	21.78	0.51	0.001076	2.77	21.73	0.60
	LOHN4@43	21	23764	1157	236	2	0.802	1.1	0.001247	2.70	15	0.001057	2.3	21.36	0.49	0.001059	2.72	21.40	0.58
	LOHN4@44	20	23194	1138	231	2	0.803	1.1	0.001254	2.72	15	0.001055	2.3	21.32	0.49	0.001067	2.74	21.56	0.59
	LOHN4@45	20	23831	1188	232	2	0.787	1.0	0.001255	2.70	15	0.001058	2.3	21.37	0.49	0.001065	2.72	21.51	0.58
	LOHN4@46	20	20913	1027	204	2	0.813	1.0	0.001277	2.67	17	0.001047	2.2	21.16	0.47	0.001058	2.70	21.38	0.58
	LOHN4@48	22	23727	1093	262	2	0.808	1.1	0.001210	2.78	14	0.001045	2.4	21.12	0.51	0.001046	2.80	21.13	0.59
	LOHN4@49	22	23546	1065	259	2	0.789	1.1	0.001179	2.73	13	0.001018	2.4	20.56	0.49	0.001022	2.75	20.65	0.57
	LOHN4@50	21	22193	1049	260	2	0.806	1.2	0.001208	2.70	13	0.001045	2.4	21.12	0.50	0.001047	2.72	21.15	0.57
	LOHN4@51	20	22103	1121	259	2	0.800	1.2	0.001179	2.67	14	0.001014	2.3	20.48	0.48	0.001011	2.69	20.43	0.55
	LOHN4@52	20	20091	1023	242	2	0.785	1.2	0.001146	2.68	14	0.000973	2.3	19.66	0.45	0.000987	2.70	19.93	0.54
	LOHN4@53	10	15092	1539	136	2	0.818	1.0	0.001422	2.69	28	0.001029	2.0	20.80	0.42	0.001030	2.79	20.80	0.58
	LOHN4@54	10	13028	1330	137	2	0.812	1.1	0.001350	2.66	26	0.000979	2.0	19.78	0.40	0.000993	2.78	20.07	0.56
	LOHN4@55	10	14821	1515	137	2	0.806	1.0	0.001355	2.67	27	0.000982	2.0	19.83	0.40	0.000983	2.78	19.85	0.55
B	LOHN4@05	19	14990	787	171	4	0.821	1.6	0.001129	3.06	22	0.000882	2.5	17.83	0.45	0.000875	3.15	17.68	0.56
	LOHN4@06	31	9191	298	146	5	0.794	2.3	0.001237	3.80	26	0.000913	3.1	18.45	0.58	0.000912	3.95	18.42	0.73
	LOHN4@17	32	23011	717	714	6	0.732	2.8	0.000980	3.29	5	0.000936	3.2	18.91	0.60	0.000933	3.29	18.85	0.62
	LOHN4@18	39	23334	591	461	5	0.760	2.3	0.001003	3.06	8	0.000927	2.9	18.73	0.54	0.000923	3.07	18.66	0.57
	LOHN4@47	23	19054	816	222	3	0.808	1.2	0.001120	2.66	15	0.000933	2.3	18.85	0.43	0.000946	2.70	19.12	0.52
	LOHN4@56	9	11815	1254	129	2	0.833	1.2	0.001272	2.78	28	0.000895	2.1	18.07	0.38	0.000913	2.90	18.45	0.53
	LOHN4@57	13	11550	862	133	3	0.826	1.5	0.001194	3.44	28	0.000847	2.6	17.12	0.45	0.000855	3.58	17.28	0.62
	ORT1@01	367	5825	16	1263	17	0.084	2.3	0.000945	2.48	2	0.000912	2.5	18.43	0.46	0.000922	2.5	18.63	0.47

ORT1@02	316	4437	14	711	23	0.087	2.4	0.000956	2.43	3	0.000905	2.4	18.27	0.44	0.000930	2.5	18.80	0.46
ORT1@03	277	4950	18	1166	16	0.097	2.5	0.000936	2.26	3	0.000896	2.3	18.10	0.41	0.000911	2.3	18.41	0.42
ORT1@04	356	4831	14	926	16	0.088	2.4	0.000905	2.92	3	0.000861	2.9	17.40	0.50	0.000877	3.0	17.73	0.53
ORT1@05	161	5336	33	930	18	0.139	2.6	0.000970	2.17	3	0.000924	2.2	18.67	0.41	0.000941	2.2	19.01	0.42
ORT1@06	222	3688	17	382	16	0.166	2.1	0.001012	2.99	7	0.000897	3.0	18.12	0.54	0.000938	3.2	18.95	0.61
ORT1@07	219	5005	23	277	13	0.272	1.6	0.001039	2.23	13	0.000893	2.3	18.05	0.41	0.000902	2.4	18.21	0.43
ORT1@08	189	5091	27	422	18	0.220	2.0	0.000979	2.96	8	0.000896	2.9	18.09	0.52	0.000901	3.1	18.21	0.56
ORT1@09	262	6320	24	591	17	0.139	2.3	0.000880	3.78	4	0.000824	3.6	16.65	0.60	0.000841	3.8	16.98	0.65
ORT1@10	199	7415	37	214	11	0.411	1.2	0.001086	2.24	16	0.000892	2.1	18.01	0.38	0.000912	2.4	18.43	0.44
ORT1@11	101	3205	32	655	17	0.172	3.0	0.000981	2.61	4	0.000926	2.7	18.71	0.50	0.000941	2.7	19.01	0.51
ORT1@12	106	3602	34	661	28	0.191	2.9	0.000933	3.58	4	0.000863	3.5	17.44	0.60	0.000895	3.6	18.08	0.66
ORT1@13	95	4969	52	607	18	0.195	2.9	0.000910	2.82	3	0.000855	2.8	17.28	0.48	0.000883	2.9	17.83	0.51
ORT1@14	96	3780	40	628	13	0.183	2.9	0.000960	2.17	4	0.000884	2.3	17.86	0.40	0.000923	2.2	18.65	0.42
<i>ORT1@15</i>	<i>105</i>	<i>4304</i>	<i>41</i>	<i>445</i>	<i>21</i>	<i>0.370</i>	<i>1.9</i>	<i>0.001022</i>	<i>4.60</i>	<i>12</i>	<i>0.000894</i>	<i>4.2</i>	<i>18.06</i>	<i>0.76</i>	<i>0.000903</i>	<i>5.7</i>	<i>18.24</i>	<i>1.04</i>
EUKL2@01	9	296	32	160	3	0.803	1.2	0.001359	2.12	22	0.001043	1.7	21.07	0.37	0.001063	2.21	21.47	0.47
EUKL2@02	14	301	22	209	3	0.803	1.2	0.001317	2.51	18	0.001089	2.1	22.00	0.47	0.001080	2.56	21.81	0.56
EUKL2@03	13	21097	1580	205	2	0.824	1.2	0.001303	2.25	17	0.001072	1.9	21.65	0.41	0.001078	2.30	21.77	0.50
EUKL2@04	14	18352	1313	231	3	0.812	1.5	0.001253	2.08	16	0.001059	1.8	21.39	0.39	0.001048	2.13	21.16	0.45
EUKL2@05	33	52673	1620	345	3	0.782	1.3	0.001194	2.17	10	0.001076	2.0	21.74	0.43	0.001079	2.18	21.79	0.48
EUKL2@06	19	25562	1351	218	2	0.795	1.2	0.001315	2.10	16	0.001097	1.8	22.17	0.40	0.001102	2.14	22.26	0.48
EUKL2@07	19	16767	868	234	3	0.800	1.2	0.001282	2.10	15	0.001085	1.8	21.91	0.40	0.001085	2.14	21.92	0.47
HOAR1@27	148	1591	11	235	13	0.195	2.2	0.001164	1.5	14	0.000973	2.4	19.65	0.48	0.001003	1.6	20.26	0.32
HOAR1@28	100	1383	14	149	11	0.248	2.2	0.001269	1.2	19	0.000940	2.9	19.00	0.55	0.001031	1.3	20.84	0.28
HOAR1@29	95	19676	208	1211	8	0.201	2.5	0.001023	0.8	1	0.000990	0.9	20.00	0.17	0.001013	0.8	20.47	0.17
HOAR1@30	80	650	8	214	19	0.170	3.3	0.001153	3.6	15	0.000946	4.6	19.10	0.88	0.000978	3.7	19.76	0.74
HOAR1@31	124	2725	22	497	14	0.169	2.6	0.001070	0.9	6	0.000987	1.4	19.94	0.28	0.001007	0.9	20.35	0.19
HOAR1@32	316	1076	3	160	12	0.132	2.0	0.001240	3.4	21	0.000950	4.0	19.20	0.76	0.000985	3.5	19.91	0.70
HOAR1@01	50	926	18	322	20	0.244	3.7	0.001121	4.3	9	0.000999	4.6	20.18	0.92	0.001017	4.4	20.55	0.91
HOAR1@02	51	782	15	200	18	0.296	3.5	0.001128	3.5	15	0.000911	4.5	18.40	0.83	0.000954	4.5	19.27	0.87

A

B	HOAR1@03	48	969	20	250	17	0.205	3.5	0.001088	4.7	8	0.000920	4.8	18.59	0.89	0.000997	5.0	20.13	1.00	
	HOAR1@04	71	1075	15	259	18	0.182	3.5	0.001075	4.3	9	0.000926	4.6	18.70	0.85	0.000982	4.5	19.84	0.89	
	HOAR1@05	79	643	8	233	21	0.197	3.4	0.001118	4.2	16	0.000932	4.9	18.84	0.92	0.000940	5.0	18.98	0.94	
	HOAR1@06	118	1676	14	330	15	0.148	2.9	0.001046	2.8	7	0.000924	3.1	18.66	0.57	0.000977	3.0	19.73	0.59	
	HOAR1@07	106	1764	17	448	17	0.162	2.9	0.001065	2.6	7	0.000973	2.8	19.66	0.55	0.000993	2.8	20.07	0.56	
	HOAR1@08	67	1358	20	339	18	0.237	3.2	0.001049	2.8	11	0.000938	3.3	18.94	0.62	0.000938	3.0	18.95	0.57	
	HOAR1@09	62	1579	25	364	16	0.191	3.3	0.001110	3.0	5	0.000992	3.1	20.04	0.63	0.001050	3.2	21.20	0.67	
	HOAR1@10	266	1995	8	433	15	0.097	2.4	0.001076	2.4	5	0.000980	2.6	19.79	0.52	0.001019	2.6	20.59	0.54	
	HOAR1@11	56	6609	117	714	11	0.242	2.7	0.001032	2.2	3	0.000976	2.2	19.71	0.43	0.001005	2.2	20.31	0.45	
	HOAR1@12	104	2748	26	263	10	0.359	1.8	0.001163	2.3	15	0.000992	2.4	20.04	0.49	0.000988	2.4	19.96	0.48	
	HOAR1@13	103	3259	32	679	15	0.171	2.7	0.000998	3.0	4	0.000941	3.0	19.01	0.56	0.000959	3.0	19.37	0.59	
	HOAR1@14	107	1940	18	272	12	0.213	2.3	0.001115	3.9	10	0.000957	3.7	19.33	0.72	0.001005	4.4	20.30	0.88	
	HOAR1@16	145	2711	19	632	16	0.139	2.6	0.001076	2.5	4	0.001010	2.5	20.41	0.51	0.001029	2.5	20.78	0.53	
	HOAR1@17	72	1305	18	263	15	0.211	3.1	0.001059	3.7	8	0.000904	3.9	18.26	0.71	0.000969	3.9	19.58	0.77	
	HOAR1@18	74	1381	19	292	15	0.196	3.1	0.001088	4.2	8	0.000944	4.2	19.07	0.79	0.000998	4.4	20.16	0.89	
	HOAR1@19	60	1129	19	389	19	0.240	3.0	0.001129	3.7	10	0.001026	3.9	20.73	0.81	0.001019	4.0	20.58	0.82	
	HOAR1@20	60	1818	30	499	17	0.206	3.2	0.001035	2.6	5	0.000955	2.7	19.29	0.53	0.000978	2.8	19.76	0.55	
	HOAR1@21	45	1000	22	183	14	0.309	3.0	0.001130	3.8	15	0.000891	4.2	18.01	0.76	0.000964	4.2	19.47	0.82	
	HOAR1@22	49	1540	31	194	12	0.305	2.8	0.001127	2.5	9	0.000909	3.1	18.37	0.57	0.001025	2.9	20.70	0.59	
	HOAR1@23	126	1838	15	824	24	0.119	3.4	0.001015	3.2	5	0.000968	3.2	19.55	0.63	0.000966	3.3	19.52	0.64	
	HOAR1@24	85	1927	23	511	18	0.147	3.3	0.001026	2.6	5	0.000954	2.8	19.27	0.53	0.000974	2.8	19.67	0.54	
	HOAR1@25	53	1330	25	384	19	0.230	3.5	0.001022	2.9	8	0.000919	3.2	18.57	0.60	0.000944	3.0	19.08	0.58	
	HOAR1@26	60	1206	20	343	18	0.197	3.5	0.001023	3.1	8	0.000908	3.5	18.34	0.63	0.000940	3.3	18.99	0.63	
	<i>HOAR1@15</i>	<i>111</i>	<i>2877</i>	<i>26</i>	<i>112</i>	<i>6</i>	<i>0.516</i>	<i>1.2</i>	<i>0.001353</i>	<i>5.1</i>	<i>29</i>	<i>0.000885</i>	<i>3.9</i>	<i>17.88</i>	<i>0.70</i>	<i>0.000964</i>	<i>7.9</i>	<i>19.47</i>	<i>1.53</i>	
		MOKR1@07	307	3840	13	172	11	0.228	2.1	0.001121	3.2	18	0.000876	3.6	17.69	0.64	0.000915	3.3	18.48	0.61
		MOKR1@08	393	5762	15	259	15	0.228	2.8	0.000997	2.7	13	0.000848	3.2	17.13	0.55	0.000869	2.8	17.55	0.48
MOKR1@09		916	5949	6	260	14	0.128	2.3	0.000993	2.6	12	0.000845	3.1	17.08	0.52	0.000879	2.7	17.75	0.48	
MOKR1@10		814	2999	4	166	13	0.134	2.0	0.001143	3.7	22	0.000878	4.1	17.74	0.73	0.000890	3.8	17.99	0.68	
MOKR1@11		1852	2971	2	148	21	0.138	3.2	0.001168	2.9	26	0.000976	6.4	19.71	1.25	0.000859	3.3	17.36	0.57	
MOKR1@12		702	7328	10	245	16	0.224	3.1	0.001029	2.6	13	0.000867	3.4	17.51	0.59	0.000899	2.6	18.15	0.47	

A	MOKR1@20	442	2417	5	255	47	0.062	10.0	0.000754	1.0	5	0.000639	7.2	12.92	0.94	0.000714	1.4	14.42	0.21
	MOKR1@21	473	5279	11	1029	55	0.063	10.2	0.001134	1.0	1	0.001091	2.3	22.05	0.50	0.001124	1.1	22.70	0.24
	MOKR1@22	410	5545	14	2865	95	0.070	11.4	0.001130	1.6	1	0.001115	2.1	22.52	0.46	0.001119	1.7	22.61	0.37
	MOKR1@23	341	2318	7	483	47	0.104	6.6	0.001093	1.3	8	0.001049	4.4	21.18	0.94	0.001011	1.6	20.43	0.32
	MOKR1@24	507	7589	15	3668	67	0.057	6.1	0.001049	1.5	1	0.001038	1.7	20.97	0.35	0.001042	1.5	21.06	0.32
	MOKR1@25	336	4029	12	1546	67	0.087	7.7	0.001041	1.5	3	0.001015	2.2	20.51	0.46	0.001011	1.6	20.43	0.32
	MOKR1@26	220	4084	19	646	39	0.101	6.7	0.001072	1.3	4	0.001008	2.6	20.37	0.53	0.001034	1.3	20.89	0.28
	MOKR1@27	295	3072	10	626	55	0.108	8.3	0.001021	1.3	5	0.000958	3.6	19.35	0.69	0.000969	1.4	19.58	0.28
	MOKR1@28	395	5188	13	1611	67	0.067	9.2	0.001011	1.1	1	0.000987	1.9	19.93	0.39	0.000997	1.2	20.15	0.23
	MOKR1@29	469	3095	7	846	55	0.066	6.5	0.001059	1.0	3	0.001011	2.7	20.42	0.55	0.001025	1.2	20.72	0.25
	MOKR1@30	688	4284	6	802	55	0.062	7.1	0.000922	1.2	3	0.000878	2.9	17.74	0.51	0.000893	1.4	18.03	0.25
MOKR1@31	683	4946	7	2982	95	0.056	7.6	0.001030	1.0	1	0.001017	1.6	20.54	0.33	0.001015	1.1	20.51	0.23	
B	MOKR1@01	132	23439	178	573	9	0.324	2.3	0.000991	2.6	3	0.000924	2.5	18.68	0.46	0.000959	2.6	19.37	0.50
	MOKR1@02	167	21412	128	789	12	0.283	2.7	0.001001	2.6	3	0.000952	2.5	19.23	0.49	0.000970	2.6	19.60	0.51
	MOKR1@03	149	20039	134	694	12	0.307	2.7	0.001011	2.6	3	0.000955	2.6	19.29	0.49	0.000977	2.6	19.73	0.52
	MOKR1@04	162	15315	95	570	12	0.296	2.6	0.001007	2.7	5	0.000943	2.6	19.05	0.50	0.000960	2.7	19.40	0.51
	MOKR1@05	182	11017	61	391	12	0.299	2.6	0.000978	2.6	7	0.000882	2.6	17.81	0.47	0.000913	2.6	18.45	0.48
	MOKR1@06	239	10746	45	355	12	0.242	2.6	0.000993	2.6	6	0.000885	2.6	17.88	0.47	0.000932	2.6	18.83	0.48
	MOKR1@13	127	16222	128	541	10	0.343	2.3	0.001014	2.6	5	0.000942	2.5	19.03	0.47	0.000967	2.6	19.53	0.50
	MOKR1@14	363	17133	47	608	12	0.200	2.4	0.000949	2.6	4	0.000889	2.5	17.95	0.45	0.000908	2.6	18.35	0.47
	MOKR1@15	446	16751	38	468	11	0.191	2.5	0.000948	2.6	4	0.000869	2.5	17.57	0.45	0.000906	2.6	18.30	0.47
	MOKR1@16	517	16572	32	462	12	0.190	2.6	0.000943	2.6	5	0.000864	2.6	17.46	0.45	0.000899	2.6	18.16	0.47
	MOKR1@17	141	16023	113	717	13	0.323	2.6	0.001031	2.6	4	0.000975	2.6	19.70	0.50	0.000986	2.6	19.92	0.52
MOKR1@18	303	8214	27	380	18	0.303	3.2	0.000949	2.7	10	0.000859	3.0	17.35	0.53	0.000851	2.7	17.19	0.46	
	<i>MOKR1@19</i>	263	4051	15	/	0	0.072	7.2	0.001023	1.1	2	0.001023	/	20.67	/	0.001002	1.1	20.24	0.23
	SAND1@01	259	3167	12	125	17	0.337	3.8	0.001114	4.0	21	0.000770	5.9	15.56	0.92	0.000877	4.1	17.72	0.73
	SAND1@02	252	3570	14	175	21	0.430	3.9	0.001104	3.1	24	0.000860	5.2	17.38	0.90	0.000843	3.3	17.03	0.56
	SAND1@04	323	5540	17	184	19	0.441	4.0	0.001150	2.6	17	0.000908	4.4	18.35	0.80	0.000958	2.7	19.34	0.51
	SAND1@05	580	5757	10	203	19	0.331	3.8	0.001106	2.8	15	0.000896	4.2	18.10	0.76	0.000938	2.9	18.96	0.54
	SAND1@06	601	5846	10	216	20	0.328	4.0	0.001123	2.7	15	0.000923	4.2	18.64	0.77	0.000959	2.8	19.38	0.54

A	SAND1@07	272	5768	21	212	12	0.274	2.6	0.001006	2.6	12	0.000829	3.1	16.74	0.52	0.000883	2.6	17.85	0.47	
	SAND1@08	251	6655	27	332	15	0.277	2.9	0.000972	2.6	10	0.000859	2.9	17.35	0.50	0.000879	2.6	17.76	0.46	
	SAND1@21	181	7714	43	2354	55	0.087	8.6	0.001049	1.3	1	0.001032	1.6	20.85	0.33	0.001039	1.3	20.99	0.28	
	SAND1@22	285	6564	23	1186	55	0.096	10.8	0.001045	1.4	1	0.001011	2.3	20.43	0.46	0.001030	1.4	20.80	0.30	
	SAND1@24	289	6472	22	1758	67	0.098	10.4	0.001054	1.2	2	0.001031	1.9	20.82	0.39	0.001036	1.2	20.93	0.26	
	SAND1@25	302	7743	26	2074	67	0.107	10.3	0.001107	1.1	1	0.001086	1.6	21.94	0.36	0.001090	1.1	22.03	0.25	
	SAND1@26	302	7711	26	1385	55	0.140	8.6	0.001117	1.4	3	0.001086	2.1	21.94	0.45	0.001089	1.4	22.01	0.32	
	SAND1@28	468	728	2	513	95	0.066	8.6	0.001116	1.4	10	0.001032	7.3	20.85	1.51	0.001004	3.4	20.28	0.68	
B	SAND1@09	483	2027	4	137	14	0.176	2.2	0.001145	4.2	28	0.000822	4.9	16.61	0.81	0.000820	4.4	16.56	0.72	
	SAND1@10	646	2420	4	109	14	0.176	2.7	0.001136	3.3	26	0.000732	5.5	14.80	0.81	0.000842	3.5	17.01	0.60	
	SAND1@12	729	3802	5	203	16	0.150	2.8	0.001027	2.6	16	0.000831	3.8	16.79	0.63	0.000858	2.7	17.34	0.47	
	SAND1@13	628	2842	5	170	14	0.136	2.3	0.001072	3.0	19	0.000839	3.9	16.95	0.67	0.000873	3.0	17.63	0.54	
	SAND1@14	966	3518	4	124	16	0.194	3.1	0.001118	2.6	23	0.000771	5.2	15.57	0.81	0.000862	2.8	17.41	0.48	
	SAND1@18	278	1247	4	67	14	0.309	2.9	0.001372	5.0	43	0.000578	8.4	11.67	0.97	0.000783	5.5	15.81	0.88	
	SAND1@19	277	811	3	70	16	0.321	3.0	0.001620	5.1	55	0.000731	9.2	14.77	1.36	0.000725	6.5	14.66	0.96	
	SAND1@11	659	2325	4	92	16	0.217	3.1	0.001572	8.4	35	0.000909	8.5	18.36	1.56	0.001021	8.6	20.62	1.78	
	SAND1@15	189	964	5	49	11	0.307	2.4	0.001476	6.1	49	0.000322	8.3	6.51	0.54	0.000751	6.7	15.17	1.01	
	SAND1@16	228	601	3	59	15	0.307	2.8	0.001752	6.7	62	0.000612	10.1	12.36	1.25	0.000664	8.7	13.41	1.17	
	SAND1@17	202	401	2	46	15	0.312	2.9	0.002061	8.4	73	0.000324	12.4	6.56	0.81	0.000559	13.0	11.30	1.47	
	SAND1@20	233	376	2	54	17	0.305	3.0	0.002238	7.9	74	0.000741	12.4	14.98	1.86	0.000578	13.8	11.68	1.61	
	SAND1@29	493	448	1	112	67	0.056	11.1	0.001114	2.4	9	0.000729	23.3	14.72	3.43	0.001014	6.8	20.49	1.39	
	SAND1@30	640	398	1	186	95	0.060	11.3	0.001180	3.8	14	0.000935	20.0	18.88	3.78	0.001019	9.3	20.59	1.91	
	SAND1@31	636	404	1	95	67	0.061	10.6	0.001085	3.4	21	0.001505	38.9	30.39	11.80	0.000856	10.2	17.30	1.76	
	SAND1@23	299	5895	20	/	0	0.112	10.5	0.000878	1.2	3	0.000878	/	17.73	/	0.000855	1.2	17.27	0.21	
	SAND1@27	284	679	2	/	0	0.069	7.7	0.001130	1.0	9	0.001130	/	22.84	/	0.001027	2.8	20.74	0.58	
	SAND1@32	573	501	1	33	96	0.017	17.8	0.000118	15.8	89	/	/	-0.43	-0.49	0.000013	251	0.26	0.66	
	SAND1@33	919	304	0	/	0	0.035	18.9	0.000222	13.7	184	0.000222	/	4.49	/	/	-76	-3.76	2.86	
	SAND1@35	1160	691	1	/	0	0.057	12.0	0.001323	2.2	8	0.001323	/	26.73	/	0.001215	5.7	24.54	1.39	
	SAND1@36	935	512	1	/	0	0.067	11.3	0.001293	1.9	20	0.001293	/	26.11	/	0.001037	8.8	20.95	1.84	
		REIS1@27	166	541	3	188	25	0.088	4.1	0.000926	2.32	13	0.000762	5.7	15.39	0.88	0.000806	2.7	16.28	0.44

A	REIS1@28	288	1516	5	601	30	0.077	3.8	0.000836	2.25	6	0.000783	2.8	15.81	0.45	0.000788	2.3	15.93	0.37
	REIS1@29	185	697	4	530	42	0.093	4.6	0.000853	2.24	11	0.000791	3.7	15.99	0.59	0.000760	2.5	15.36	0.39
	REIS1@31	141	763	5	226	42	0.121	3.8	0.000977	2.60	20	0.000810	7.6	16.37	1.24	0.000779	4.2	15.74	0.66
	REIS1@32	306	2964	10	260	26	0.059	3.6	0.000893	2.48	15	0.000760	4.4	15.36	0.68	0.000759	2.8	15.33	0.42
	REIS1@33	762	737	1	874	24	0.050	2.7	0.000877	2.56	2	0.000839	2.7	16.94	0.45	0.000863	2.6	17.44	0.45
	REIS1@35	195	618	3	290	32	0.083	4.3	0.000966	2.95	10	0.000865	5.2	17.48	0.90	0.000865	3.2	17.48	0.56
	REIS1@36	153	668	4	222	27	0.125	4.0	0.000963	2.87	18	0.000796	5.3	16.08	0.86	0.000794	3.2	16.05	0.52
	REIS1@23	236	324	1	326	47	0.053	5.0	0.000821	2.56	8	0.000771	6.7	15.57	1.04	0.000756	3.8	15.27	0.58
	REIS1@17	437	738	2	515	33	0.055	2.9	0.000903	2.26	7	0.000852	3.4	17.21	0.59	0.000842	2.7	17.01	0.45
	REIS1@19	384	454	1	318	33	0.062	3.2	0.000932	2.69	15	0.000819	4.7	16.54	0.78	0.000793	3.8	16.03	0.61
	REIS1@20	353	562	2	1500	67	0.062	3.3	0.000894	2.24	11	0.000870	2.8	17.59	0.49	0.000798	2.9	16.13	0.46
REIS1@21	288	433	2	336	36	0.060	3.4	0.000981	2.54	10	0.000868	4.7	17.54	0.82	0.000881	3.6	17.81	0.63	
B	REIS1@18	328	486	1	467	42	0.061	3.3	0.000802	2.96	18	0.000736	4.4	14.87	0.66	0.000657	4.1	13.27	0.55
	REIS1@24	218	398	2	689	67	0.064	4.9	0.000791	3.13	14	0.000747	4.8	15.08	0.72	0.000679	4.1	13.71	0.56
	REIS1@25	189	225	1	321	55	0.061	5.0	0.000851	3.74	17	0.000748	7.4	15.12	1.11	0.000705	6.1	14.25	0.87
	REIS1@30	297	441	1	778	47	0.083	5.2	0.000749	3.54	10	0.000712	4.1	14.38	0.59	0.000676	4.6	13.66	0.63
	REIS1@34	560	505	1	437	47	0.044	3.3	0.000773	3.93	14	0.000738	6.0	14.90	0.89	0.000666	6.2	13.45	0.84
	<i>REIS1@22</i>	881	386	0	229	32	<i>0.051</i>	2.3	<i>0.000979</i>	2.77	25	<i>0.000814</i>	5.8	<i>16.45</i>	<i>0.95</i>	<i>0.000736</i>	<i>34.6</i>	<i>14.88</i>	<i>5.15</i>
	<i>REIS1@26</i>	201	197	1	199	47	<i>0.075</i>	4.5	<i>0.000867</i>	3.41	41	<i>0.000781</i>	10.7	<i>15.79</i>	<i>1.69</i>	<i>0.000508</i>	<i>11.6</i>	<i>10.26</i>	<i>1.19</i>

Table 4. Summary of weighted mean ages of monazite growth domains and spot age ranges of each grain from the TW.

Sample domain	ID N°	Figure	Table	Zoning of the grains	Weighted mean domain $^{208}\text{Pb}/^{232}\text{Th}$ ages (Ma, $\pm 1\sigma$)	MSWD	Number of analyses	Spot $^{208}\text{Pb}/^{232}\text{Th}$ age range of entire grain (Ma, $\pm 1\sigma$)	Reference
<i>Western Tauern Window</i>									
INNBI	1	3a	3	Regular	-	-	-	11.5 \pm 0.2 - 10.4 \pm 0.2	this study
ZEI1 - A	2	3b	3	Regular	10.0 \pm 0.2	1.8	20	10.8 \pm 0.3 - 7.2 \pm 0.2	this study
SCHR1 - A	3	3c	4	Regular	20.9 \pm 0.6	1.7	6	21.9 \pm 0.5 - 19.3 \pm 0.5	this study
SCHR1 - B					20.3 \pm 0.2	0.98	16		
SCHR1 - C					19.7 \pm 0.4	1.00	6		
MAYR4	4	3d	3	Regular	-	-	-	11.8 \pm 0.2 - 8.9 \pm 0.2	this study
PFIT1 - A	5	3e	4	Patchy core	17.3 \pm 0.3	1.2	9	17.8 \pm 0.4 - 12.9 \pm 0.3	this study
PFIT1 - B					13.2 \pm 0.3	0.38	5		
BURG2	6	3f	3	Regular	-	-	-	17.1 \pm 0.4 - 12.1 \pm 0.3	this study
PLAN1 - A	7	3g	3	Patchy core	11.9 \pm 0.2	2.2	37	12.6 \pm 0.3 - 7.8 \pm 0.2	this study
<i>Central Tauern Window</i>									
SCEI1 - A	8	4a	3	Regular	18.3 \pm 1.1	2.0	4	18.9 \pm 0.5 - 15.9 \pm 0.4	this study
SCEI1 - B					17.4 \pm 0.4	1.5	5		
SCEI1 - C					16.6 \pm 0.2	1.9	23		
HOPF2 - B	9	4b	4	Regular	12.2 \pm 0.4	2.6	8	13.7 \pm 0.4 - 11.0 \pm 0.3	this study
HOPF2 - C					12.2 \pm 0.5	2.9	6		
GART1 - A	10	4c	3	Regular	16.3 \pm 0.2	0.69	10	16.9 \pm 0.3 - 14.5 \pm 0.4	this study
NOWA3 - B	11	4d	3	Regular	15.8 \pm 0.5	0.27	5	17.0 \pm 0.2 - 13.8 \pm 0.8	this study
NOWA3 - C					14.9 \pm 1.1	2.4	5		
GART3 - B	12	4e	3	Regular	15.0 \pm 0.5	2.3	11	16.1 \pm 0.4 - 12.0 \pm 0.4	this study
STEI2	13	4f	3	Regular / Patchy tail	17.2 \pm 0.2	0.24	20	17.5 \pm 0.4 - 16.8 \pm 0.4	this study
KNOR1 - A	14	4g	4	Regular	10.8 \pm 0.3	1.02	5	11.6 \pm 0.4 - 10.8 \pm 0.3	this study
KNOR1 - B					10.6 \pm 0.3	1.6	8		
KNOR1 - C					10.4 \pm 0.2	1.4	8		

Eastern Tauern Window

KAIS6 - A					21.2 ± 0.5	0.64	6		
KAIS6 - B	15	5a	4	Patchy border	20.9 ± 0.2	0.53	24	$22.1 \pm 0.6 - 17.6 \pm 0.6$	this study
KAIS6 - C					20.6 ± 0.5	0.34	7		
KAIS6 - D					18.8 ± 0.5	1.5	10		
SALZ18-A	16a	5b	4	Regular	18.3 ± 0.4	2.6	14	$19.5 \pm 0.5 - 15.8 \pm 0.4$	this study
T3	16b			<i>Regular</i>	18.1 ± 0.4	<i>0.51</i>	4	$18.5 \pm 0.4 - 14.8 \pm 0.4$	<i>Gnos et al., 2015</i>
					17.2 ± 0.5	<i>3.4</i>	10		
					16.0 ± 0.3	<i>0.51</i>	8		
					15.5 ± 0.2	<i>0.74</i>	24		
LOHN4 - A	17	5c	4	Patchy core	21.1 ± 0.2	1.4	50	$22.9 \pm 0.6 - 17.3 \pm 0.6$	this study
LOHN4 - B					18.4 ± 0.6	1.3	7		
ORT1	18	5d	3	Regular	18.4 ± 0.3	1.07	13	$19.0 \pm 0.6 - 17.0 \pm 0.7$	this study
EUKL2	19a	5e	4	Regular	21.7 ± 0.4	0.56	7	$22.3 \pm 0.5 - 21.2 \pm 0.5$	this study
T2	19b		-	<i>Patchy</i>	15.1 ± 0.5	<i>0.26</i>	4	$15.4 \pm 0.4 - 15.0 \pm 0.7$	<i>Gnos et al., 2015</i>
HOAR1-A	20	5f	3	Patchy	20.4 ± 0.2	0.80	6	$21.2 \pm 0.7 - 19.0 \pm 0.9$	this study
HOAR1-B					19.9 ± 0.3	0.95	25		
T1	21			<i>Regular</i>	19.0 ± 0.5	<i>0.51</i>	5	$19.2 \pm 0.5 - 14.3 \pm 0.5$	<i>Gnos et al., 2015</i>
					17.6 ± 0.6	<i>1.6</i>	8		
					16.3 ± 0.6	<i>3.0</i>	12		
					15.0 ± 0.5	<i>1.7</i>	8		
T4	22		-	<i>Patchy</i>	15.6 ± 0.7	<i>9.1</i>	21	$18.3 \pm 1.1 - 13.1 \pm 0.8$	<i>Gnos et al., 2015</i>
MOKR1 - B	23	5g	3	Regular	18.8 ± 0.5	2.9	12	$22.6 \pm 0.4 - 14.4 \pm 0.2$	this study
SAND1 - B	24	5h	3	Regular	17.0 ± 0.8	1.8	7	$22.0 \pm 0.3 - 14.7 \pm 1.0$	this study
REIS1 - A	25	5i	3	Regular	16.2 ± 0.5	2.9	13	$17.8 \pm 0.6 - 13.5 \pm 0.8$	this study
REIS1 - B					13.6 ± 0.6	0.25	5		